Master's thesis
Master's Programme in Atmospheric Sciences

Evaluation of selected CMIP6 models' simulation on Arctic sea ice

Xinfang Zhang

September 22, 2022

Supervisor(s): Professor Jari Haapala and Professor Petteri Uotila

Examiner(s): Professor Petteri Uotila

University of Helsinki
Faculty of Science

P. O. Box 68 (Pietari Kalmin katu 5)
00014 University of Helsinki

HELSINGIN YLIOPISTO — HELSINGFORS UNIVERSITET — UNIVERSITY OF HELSINKI

Tiedekunta — Fakultet — Faculty	Koulutusohjelma — Utbildningsprogram — Degree programme
Faculty of Science	Master's Programme in Atmospheric Sciences

Tekijä — Författare — Author

Xinfang Zhang

Työn nimi — Arbetets titel — Title

Evaluation of selected CMIP6 models' simulation on Arctic sea ice

Työn laji — Arbetets art — Level	Aika — Datum — Month and year	Sivumäärä — Sidantal — Number of pages
Master's thesis	September 22, 2022	95

Tiivistelmä — Referat — Abstract

To evaluate whether CMIP6 models provide good simulation in Arctic sea-ice extent, thickness, and motion, selected 6 CMIP6 models are EC-Earth3, ACCESS-CM2, BCC-CSM2-MR, GFDL-ESM4, MPI-ESM1-2-HR, NORESM2-LM. For CMIP6 models and observations, seasonal cycle and the annual variation from 1979-2014 of sea-ice extent were studied, for sea-ice thickness and sea-ice motion, the Arctic is separated into three regions, geographical distribution, inter-annual variation from 1979-2014, seasonal cycle, and trend were studied. Then student t-test is used to evaluate whether the model output has a significant difference from observation, to select the best model(s). For sea-ice extent, EC-Earth3 is overestimating sea-ice extent, especially in winter, BCC-CSM2-MR model underestimates sea-ice extent, ACCESS-CM2, MPI-ESM1-2-HR, NorESM2-LM models perform the best. For sea-ice thickness, BCC-CSM2-MR underestimates sea-ice thickness, EC-Earth3, ACCESS-CM2, and NORESM2-LM models are overestimating sea-ice thickness. GFDL-ESM4 and MPI-ESM1-2-HR have the best performance at sea-ice thickness simulation. For sea-ice motion, the MPI-ESM1-2-HR model overestimates sea-ice drifting speed all year round, ACCESS-CM2 model tends to overestimate sea-ice drifting speed in summer for region1 and region2, in region3 ACCESS-CM2 model mostly overestimate sea-ice motion except winter months. NorESM2-LM model has the best performance overall, and ACCESS-CM2 has the second-best simulation for region1 and region2. EC-Earth3 also has a satisfactory simulation for sea-ice motion. Models and observation also agree on common results for sea-ice properties: Maximum sea-ice extent occurs in March, and minimum sea-ice extent occurs in September. There's a decreasing trend of sea-ice extent. The Central Arctic and Canadian Archipelago always have the thickest sea ice, followed by the East Siberian Sea, Laptev Sea, and Chukchi Sea, Beaufort Sea. East Greenland Sea, Barents Sea, Buffin Bay, and the Kara Sea always have the thinnest sea ice. There's a decreasing trend for sea-ice thickness according to models, sea-ice is thicker in the Chukchi Sea and the Beaufort Sea than in Laptev and East Siberian seas. Winter sea-ice thickness is higher than in summer, and sea-ice thickness has a more rapid decreasing rate in summer than in winter. Laptev and the East Siberian Sea have the most rapidly sea-ice thinning process. Sea-ice thickness has seasonal cycle that maximum usually occurs in May, and minimum sea-ice thickness happens in October. For sea-ice motion, there's an increasing trend of sea-ice motion, and summer sea-ice motion has faster sea-ice motion than winter, Chukchi Sea, and the Beaufort Sea has faster sea-ice motion than Laptev and the East Siberian Sea. Corresponding with the comparatively faster-thinning in the Laptev and the East Siberian Seas simulated by models, there's also a faster increasing rate in the Laptev and the East Siberian Sea.

Avainsanat — Nyckelord — Keywords

Arctic sea ice, CMIP6, sea ice extent, sea-ice thickness, sea motion, IABP

Säilytyspaikka — Förvaringsställe — Where deposited

Muita tietoja — Övriga uppgifter — Additional information

Contents

1. Introduction

1.1 Observed changes in sea-ice extent

The sea-ice extent in the Arctic region has changed significantly after 2002, which is an iconic indicator of climate change (Perovich et al., 2020). Sea ice coverage varies by season, reaches its maximum mostly in March, and reaches its minimum extent in September. The smallest declining trend happens in March, and the largest decreasing trend happens in September from 1981-2010. Forsstrom et al., 2011, reveals that September has the steepest decline that the rate of decline range in -12.8% $\pm$2.3 per decade in 1979-2018 (Mingle, 2020).

The decline in Arctic summer sea-ice extent has accelerated in the first decade of the 21st century, and the retreating rate of sea ice is faster than the IPCC model projected. Over the past few decades, summer Arctic sea-ice extent has declined over 30% (Meier et al., 2014). Summer sea-ice extent has been at or near record low level every year since 2001, the extremely low state of sea-ice extent begins in 2002. Before 2001, the decreasing trend of sea-ice extent is primarily in summer while not statistically significant in winter, from 2002 onward winter decreasing trend becomes statistically significant because of sea-ice albedo feedback (Mingle, 2020).

From 21 century, the periodical signal has disappeared and the rate of decline has increased (Mingle, 2020). In the case of sea-ice extent variation in different Arctic regions, in Beaufort, Chukchi, and Siberian Seas, there's steepest summer sea-ice extent decreasing trend. The Central Arctic have months with a zero trend because they are completely ice-covered during the month in all years despite thinning happened, other regions and months which do have significant trend are all negative. The sharp decrease of sea-ice extent is related to atmospheric circulation (Arctic Oscillation) and air temperature (Meier et al., 2007), Arctic surface air temperature has increased by almost 4 times the global average over the last two decades, with feed-backs from loss of sea ice and snow cover contributing to the amplified warming. And even though the main process of Arctic sea-ice loss is melting, ice drift through the Fram strait is also causing Arctic sea-ice loss (Smedsrud et al., 2011). Sea-ice extent decrease is induced by human activities too, causing above mentioned changes in physical processes.

1.2 Observed changes in sea-ice thickness

Change in sea-ice thickness distribution is dominated by thermodynamical and dynamic processes. In the dynamic process, the divergence of sea ice turn to lead opening, where thin ice grows afterward, and the convergence of sea ice is forming pressure ridges. The thermal dynamic process is the growth and melting of sea ice (Haas, 2017).

New satellite missions extended sea-ice thickness information, but long-term records are sparse and short. Sea ice thickness uncertainties arises when satellites measurement are used in sea-ice thickness derivation (Forsstrom et al., 2011) and ice density (Zygmuntowska et al., 2014). There's a strong need to lower the uncertainties of sea-ice thickness data while integrating data from different measurement methods faces difficulties (Meier et al., 2014). Satellite indicated a 40 % decline in sea ice thickness in the last few decades and sea ice decrease has big inter-annual variability (Meier et al., 2014). Mean Sea ice thickness has a seasonal cycle, the maximum occurs in May, and the minimum in September. The amplitude of the seasonal cycle is (1.8±0.8) meters. according to moored upward-looking sonar data (Hansen et al., 2013), after $2005 - 2006$, there's a strong decrease in sea-ice thickness. Sea-ice thickness distribution also has a regional difference, dynamic processes like ridging and lead formation play an important role in sea-ice thickness evolution.

The sea-ice type has huge variation in recent decades: There's substantial thinning in multi-year ice but little change in first-year ice (Forsstrom et al., 2011), according to submarine sonar measurements on sea-ice draft, multiyear thick ice portion decreased in recent decades and seasonal thin sea-ice become dominate at the end of the 21^{st} century, especially in spring (Meier et al., 2014; Oikkonen and Haapala, 2011). Sea-ice is under further thinning process due to a continued increase in melt season length (Laxon et al., 2003). Thinner sea ice leads to decreased mechanical strength, increasing surface strength which leads to faster sea-ice drifting speed (Meier et al., 2014). Sea-ice thinning results in the lead opening. There's also negative feedback of sea-ice loss that larger open water area which leads to efficient new ice growth in winter (Smedsrud et al., 2011).

1.3 Observed changes in sea-ice motion

IABP (International Arctic Buoy Program) buoy trajectory data shows Arctic sea-ice drifting speed has seasonal dependence, maximum in October and minimum in April (Rampal et al., 2007). The positive trend of sea ice drifting speed is prevailing in

most regions of the Arctic, and it is associated the decreasing trend of multi-year ice coverage. Kwok et al., 2013 and Rampal et al., 2009a pointed out that the sea ice mean speed and deformation rate has increased (17% per decade for winter,8.5% for summer) more likely because of sea ice kinematics (increasing sea-ice strain rate), large deformation rates affected the Arctic sea ice extent that sea-ice cover is shrinking which is mentioned in the last paragraph. Kwok et al., 2013 indicates that sea-ice drifting speed has a small decreasing trend in the last two decades of 20^{th} century, while in the first decade of the 21st century, sea-ice drifting speed variation rate is +23.6%/decade in winter and +17.7%/decade in summer, this is associated to the decline of AO index. It is still not clear if the trend is associated with the sparse sampling of buoy recording (Zhang et al., 2022).

From 1979-2019, all seasons have a significant sea-ice drifting speed increase in the Arctic region, while the increasing trend in autumn and winter is higher than that of spring and summer. The rate of increase in sea-ice drifting speed also has a regional difference. Peripheral seas in the Pacific sector, the Beaufort, Chukchi, and East Siberian Seas have a higher increasing rate of drifting speed than the Central Arctic and the peripheral seas in the Atlantic sector and the Kara and Laptev Seas (Zhang et al., 2022). The change of sea-ice drifting speed is related to regional winds, multiyear sea ice coverage, ice export, ice thinning, rate of change of sea-ice drifting speed (Kwok et al., 2013), Arctic Oscillation, air pressure, and North Atlantic Oscillation are also factors influencing arctic sea-ice drifting (Zhang et al., 2022). Zhang et al., 2022 also indicates that possible reason for the increasing Arctic sea-ice drifting speed is: the increase of the speed of extreme wind events, reduced ice-thickness and ice-pack strength, and increased ice mobility and deformation while wind forcing is unable to completely account for the drift speed increase. The reason for using IABP(International Arctic Buoy Program) data in study for observation of sea-ice motion is: The response of ice kinematic to synoptic processes is instantaneous and highly intermittent, and that's why buoy data is being used, to have access to accurate, high temporal resolution sea-ice velocity information. Problem unsolved in the previous study which is going to be solved in the thesis: Spatial variation of the seasonality of sea ice is still waiting to be examined.

1.4 Equation of sea-ice drifting motions

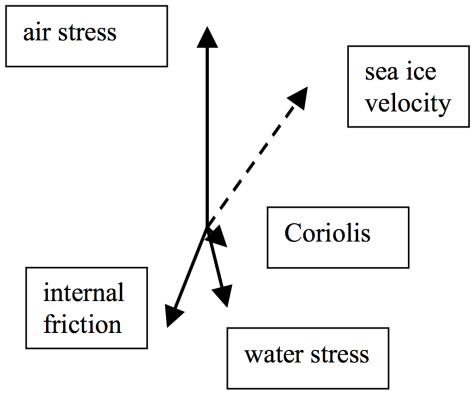

Figure 1.1: A typical diagram of major forces in drifting sea ice (northern hemisphere) (Lepparanta, 2011)

Major forces in drifting sea-ice shown in Figure 1.1 are Air stress, Water stress, Coriolis force, and internal Friction force. Sea-ice drifting motion on the sea surface plane follows the following equations:
$\rho h(\frac{\partial \mathbf{u}}{\partial t} + \mathbf{u} \cdot \bigtriangledown \mathbf{u} + \mathit{f}\mathbf{k} \times \mathbf{u}) = \bigtriangledown \cdot \sigma + \tau_a + \tau_w - \rho g h \beta - h \bigtriangledown p_a$
$\frac{\partial \mathbf{u}}{\partial t}$ is the local acceleration term, $\mathbf{u} \cdot \bigtriangledown \mathbf{u}$ is the advective acceleration term, the Coriolis acceleration term in horizontal plane is $\mathit{f}\mathbf{k} \times \mathbf{u}$, where $f = 2\Omega \sin \Phi$ is the Coriolis Parameter, $\Omega = 7.292 \cdot 10^5 s^{-1}$ is the angular velocity of the Earth and Φ is the latitude. σ is the internal ice stress, and $\bigtriangledown \cdot \sigma$ is the divergence of the stress tensor, which is the total net force per unit area due to the interaction between ice floes. τ_a is the atmosphere drag force and τ_w is the water drag force. $\rho g h \beta$ is the sea surface tilt, this term can be expressed in terms of the surface geostrophic current. $h \bigtriangledown p_a$ is the air pressure gradient term (Lepparanta, 2011).

1.5 Model development and projection for Arctic sea-ice

Sea-ice properties changes are closely related to dynamic and thermal dynamic processes, and models for this have been developed (Vihma and Haapala, 2009). Projecting the future state of the Arctic sea ice requires a physical model. Coupled Model Intercomparison Project (CMIP) which began in 1995 provides century-scale sea-ice projections and it contributes to Intergovernmental Panel on Climate Change(IPCC) report (Meier et al., 2014), it is under the ship of the World Climate Research Programme (WCRP), CMIP collects the output of the experiments that the models performed. CMIP provides projections for WCRP activities to help communities worldwide to un-

derstand past, present, and future climate change. Coupled models are computer-based models which make different climate parameters(such as ocean, land, atmosphere, and ice) coupled together. CMIP models have varied performance compared with historical observation records, so a subset of the model ensemble needs to be selected to make better future projections. The subset of CMIP5 models overestimates the thickness of thin ice while underestimating total sea-ice thickness and early autumn ice growth rate. The model also indicates ice-free conditions in the 21 century, while different studies have a different estimates on the exact decade. CMIP5 indicate an overestimate of sea extent. The latest phase of CMIP is CMIP6. CMIP6 is the coupled model inter-comparison project phase 6, there are currently already 23 CMIP6-Endorsed MIPs, involving 33 modeling groups in 16 countries. (Notz and Community, 2020 indicates CMIP6 has a widespread model output covering observation results, and it better than CMIP5 simulates the sensitivity of September sea-ice area to Greenhouse gases emissions, while it still fails to simulate the correct evolution of the sea-ice area. Compared with CMIP5, CMIP6 improved the simulation of sea-ice mean state and trend over the period of satellite observation. In CMIP6 sea-ice areas also decline faster than in CMIP5, leading to more open water. In the thesis, we are going to study sea-ice extent, thickness, and motion in CMIP6 climate models and figure out CMIP6 performance in simulating sea-ice properties compared with observations. In CMIP6 models we adopt the historical experiment only, and six models are Representative for projecting Arctic sea-ice evolution that we select based on previous study experience. They are ACCESS-CM2, BCC-CSM2-MR, EC-EARTH3, GFDL-ESM4, MPI-ESM1-2-HR, and NORESM2-LM.

2. Data availability

2.1 Observational data

Ananicheva et al., 2011 introduced measurement method of sea-ice extent: satellite-based Passive microwave remote sensing instruments provide near complete record of sea-ice extent after late 1978, that's also the reason why studying period in the thesis of sea-ice start from 1979. For the sea-ice extent study, the observational sea-ice concentration of the Arctic region and its corresponding grid cell area is obtained from the dataset *Gridded Monthly Sea Ice Extent and Concentration*, provided by the National snow and ice data center (NSIDC) (Walsh et al., 2017). Time series is from 1979-2014, time resolution is monthly, spatial resolution is 0.25 degree $\times$ 0.25 degree in latitude-longitude grid, the spatial range used in sea-ice extent analysis is from $40°N - 90°N$. For the sea-ice thickness study, satellite derived sea ice data was used. Dataset is *Sea Ice Thickness Climate Data Record (CDR)* (ECMWF, 2015) provided by Copernicus Climate Change Services (C3S) project, its spatial resolution is 25.0 km, range from $50°N - 81.45°N$. Time series is from 2002-10-01 to 2015-04-01. Time resolution is monthly, but Northern hemisphere sea ice thickness coverage is limited to the winter months between October and April due to the effect that satellite echoes are weak when ice is warm and wet. Variables used in the dataset are sea-ice thickness and uncertainties. Dataset is based on Envisat and CryoSat-2 satellite mission.
For the sea-ice motion study, we use IABP dataset (Rigor, 2017). Buoy data are different from gridded data, data points are distributed unevenly in the Arctic regions, so there's not fixed spatial resolution. The spatial coverage selected in the study is $50°N - 90°N$. Time resolution is daily, and temporal coverage is 1979-2014. In the IABP dataset, there are 7 columns of variables which are respectively: buoy identification number, day of the year, latitude, longitude, ice velocity x-component, ice velocity y-component, and magnitude of ice velocity which is sea-ice drifting speed. The buoys are deployed on sea ice and drift according to the sea-ice motion. (Rampal et al., 2007). Different type of positioning system embarked on the buoy leads to uncertainties ranging from 100-300 meters (Thomas, 1999).

Table 2.1: Modeling data properties

Model name	experiment	spatial resolution	variant label
$EC-Earth3$	historical	100km	r10i1p1f1
$ACCESS-CM2$	historical	250km	r5i1p1f1
$BCC-CSM2-MR$	historical	100km	r3i1p1f1
$GFDL-ESM4$	historical	50km	r1i1p1f1
$MPI-ESM1-2-HR$	historical	50km	r10i1p1f1
$NorESM-LM$	historical	100km	r3i1p1f1

2.2 Modelling data

All the modeling data used for sea-ice extent, sea-ice thickness, and sea-ice motion studies are CMIP6(coulped model inter-comparison project phase 6) data, which is available at Earth System Grid Federation (ESGF, 2022). The six models selected are ACCESS-CM2, BCC-CSM2-MR, EC-EARTH3, GFDL-ESM4, MPI-ESM1-2-HR, and NORESM2-LM. For all sea-ice properties, the realization number chosen in a certain CMIP6 model needs to be the same, but different CMIP6 models don't need to have the same realization number, because it is not practical.

For sea-ice extent, variables used are sea-ice concentration and grid cell area for ocean variables, temporal resolution is monthly and spatial coverage is $40°N-90°N$. For sea-ice thickness, the variable used is sea ice thickness, temporal resolution is monthly and spatial coverage is $50°N-90°N$. For sea-ice motion, variables used are X-Component of Sea-Ice Velocity and Y-Component of Sea-Ice Velocity, temporal resolution is daily because IABP data is daily data, we need to capture observed and model sea-ice motion of the same temporal scale. Spatial coverage is $50°N-90°N$.

Table 2.1 shows some common properties of modeling data. (Parodi-Perdomo, 2019, Dix et al., 2019, Krasting et al., 2018, Wu et al., 2018, Jungclaus et al., 2019, Seland et al., 2019)

3. Analysis method

To examine if these six CMIP6 models selected for this study function well in simulating Arctic sea-ice evolution, we inspect sea ice extent, sea-ice drifting speed, and sea-ice thickness. Among the three sea-ice properties, only sea-ice thickness data can be used without pretreatment. In ACCESS-CM2, NORESM2-LM, and EC-EARTH3 models, sea-ice drifting speed is provided as a scalar quantity, in BCC-CSM2-MR, MPI-ESM1-2-HR models, sea-ice velocity data is provided as vectors which have two parameters: x component of sea-ice velocity and y component of sea-ice velocity, so sea-ice drifting speed is calculated based on following equations.

$$seaicespeed = \sqrt{EW\ component\ of\ sea\ ice\ velocity^2 + NS\ component\ of\ sea\ ice\ velocity^2}$$

We unify the scale of analysis to monthly, so daily data of sea-ice drifting speed need to be converted to monthly data. For CMIP6 model data, it is much easier, since the longitude and latitude coordinate doesn't change throughout the whole period. While for buoy data, since there is a substantial amount of buoys in each day's observation, different buoy follows different drifting routes which makes sea-ice drifting speed information distribute unevenly in the spatial and temporal case. To solve this problem, we define a longitude and latitude grid which is $1° \times 1°$, then for each grid cell, we sum up all the value of data points that fall into this grid cell, and divide the summation by the total number of the data points, when there are at least two data points. To be further noted, those values which are above $0.5m/s$ are not taken into account. This is a threshold that we set by ourselves which might not be completely accurate, but plausible. Sea ice speed usually doesn't exceed $0.5m/s$, unexpected values might be caused by misplacement of buoys. The region selected is $50°N - 90°N, 0 - 360°$. We convert sea-ice drifting speed CMIP6 modeling daily data to monthly data by averaging data in each months. Different CMIP6 model data has different spatial resolution, but it does not need to be unified.

Sea-ice extent is calculated based on sea-ice concentration data and grid cell area, no matter the observation data or CMIP6 model data. Kern et al., 2019 showed that the Arctic sea-ice extent(SIE) is computed as the total area of all grid cells where the sea-ice area fraction exceeds 15%.

To calculate the trend of sea-ice properties, sea-ice drifting speed and sea-ice thickness

need to have regional average values for each month, in this case, all the values in the region in which we concerned need to make an average. For sea-ice drifting speed, it is fair enough to simply make an average of all values in the concerned region. While for regional average sea-ice thickness, sea-ice concentration needs to be taken into account, since in each grid cell, the sea-ice area is different. Regional mean sea-ice thickness is calculated based on the equation:

$$average\ sea\ ice\ thickness\ = \frac{\sum sea\ ice\ concentration\ \times ocean\ grid\ cell\ area \times sea\ ice\ thickness}{\sum sea\ ice\ concentration \times ocean\ grid\ cell\ area}$$

which means total sea-ice volume divided by total sea-ice area. According to the definition of sea ice extent, a grid cell where sea-ice concentration is lower than 15% is not taken into account when doing summation.

As Zhang et al., 2022 stated, peripheral seas in the Pacific sector have a higher increasing rate of sea-ice drifting speed than the Central Arctic and the peripheral seas in the Atlantic sector, the inspection of regional difference for sea-ice drifting speed is essential. According to Maeda et al., 2020 who defined three Arctic regions to do Arctic ice drift analysis, we similarly divide the Arctic into three regions. region1 $(70°N - 80°N, 120°W - 180°W)$ include Chukchi Sea and Beaufort Sea, region2 $(70°N - 80°N, 100°E - 180°E)$ include the Laptev sea and East Siberian, region3 $(80°N - 90°N)$ is central Arctic region. This region segmentation certainly applies to the study of sea-ice drifting speed, and since the redistribution of sea-ice thickness has a close relation to sea-ice drifting and deformation, we also study Arctic sea-ice thickness in the three regions above and compare them. Our statistic method is an independent samples t-test.

We first create a null hypothesis:

$H_O : \mu_1 = \mu_2$

The alternative hypothesis is:

$H_O : \mu_1 \neq \mu_2$

First, calculate the average of the variances for the two groups: $S_P = S_1^2 + S_2^2$

Then Calculate the test statistic:

$t = \frac{\overline{x_1} - \overline{x_2}}{s_P \sqrt{1/n_1 + 1/n_2}}$

Then calculate the degree of freedom:

$d_f = n_1 + n_2$

x_1 represent group 1, which in this study refers to monthly averaged model data, x_2 represent group 2, which in this study refers to monthly averaged observation data, n_1, n_2 means the number of data points in group 1 and group 2 respectively. Select significance level as 0.05, then compare calculated t with $t_{0.05,d_f}$

If the test statistic is lower than $t_{0.05,d_f}$, we fail to reject the null hypothesis, if it is higher than $t_{0.05,d_f}$ we can reject.

4. CMIP-6 models

Basic information of CMIP6 model is in Table 4.1

4.1 EC-Earth3

EC-Earth is a modular Earth system model (ESM) that is collaboratively developed by the European consortium with the same name. The current generation of the model, EC-Earth3, was developed after CMIP5, and CMIP6 experiments are using version 3.3 (Döscher et al., 2022a). The Sea ice component of the EC-Earth3 model is version 3.6 of the Louvain-La-Neuve ice model. A set of variables (ice concentration, volume per unit area, ice and snow enthalpy, and salt content) is characterized five ice categories. It uses the sea ice thickness distribution framework, conservation of horizontal momentum(vertical sea-ice motion neglected), and elastic-viscous-plastic rheology. Thermodynamics it is following energy-conserving halo-thermodynamics. Model resolution is $1.0° \times 1.0°$ (Döscher et al., 2022b).

4.1.1 Sea ice extent

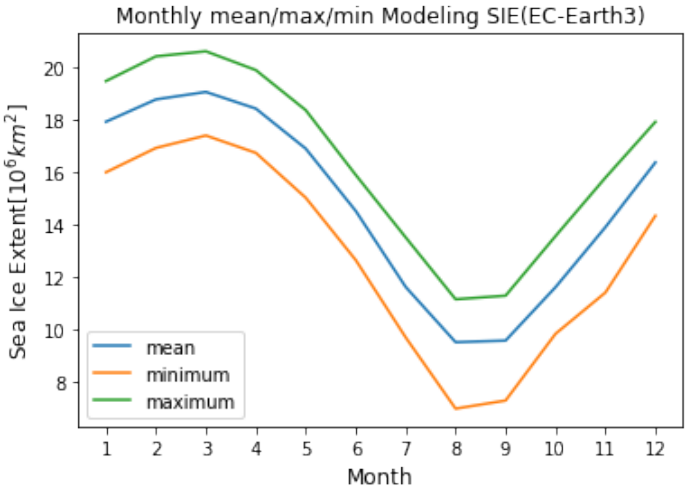

Table 4.1: Thermodynamical model, ice dynamic, ice category, and resolution of CMIP6 models(* an extra open water layer; ** 720 zonal×576 meridional points; *** Resolution 1/4 ° meridionally at the equator, gradually approaching more isotropic grid cells at higher latitudes; **** SIS: sea ice simulator)

Models	Thermodynamical model	Ice categories	Ice dynamics	Resolution (°, lat × lon)
$EC-Earth3$	Energy Conserving Halo thermodynamics	5	ITD frame work EVP dynamics	1.0 × 1.0
$ACCESS-CM2$	CICE5.1.2, Multilayer thermal dynamics, albedo scheme	5+1*	LANL CICE5.1, EVP dynamics, incremental linear remapping	1.258 lat × 1.876 lon
$BCC-CSM2-MR$	SIS4, Semtner's thermodynamic process	4+1*	SIS4****, EVP dynamics, MOM4 L40	1.0 × 1.0
$GFDL-ESM4$	SIS2, energy-conserving model	5	EVP dynamics, Modified Upwind scheme	0.5 × 0.5 nominally**
$MPI-ESM1-2-HR$	zero-layer Thermodynamic model,	1	viscoplastic rheology	0.4 × 0.4
$NorESM-LM$	Mushy layer thermodynamics	5	EVP dynamics	1 × 1/4-1 ***

Figure 4.1: EC-Earth3 output sea-ice extent mean, maximum and minimum, the X-axis is the month, Y-axis is sea ice extent, the green line is the maximum sea ice extent of all 36 years from 1979-2014, the blue line is the mean sea ice extent, and the orange line is the minimum sea ice extent.

Figure 4.1 shows the seasonal cycle of monthly sea-ice extent in the EC-Earth3 model simulation. Maximum, mean, and mean sea ice extent follow a similar seasonal cycle. The maximum sea ice extent month happens in March when sea ice extent can reach up to $20.61 \times 10^6 km^2$, and the minimum sea ice extent happens in August when minimum sea ice extent can reach down to $6.98 \times 10^6 km^2$. sea ice extent in September pretty much approach August. There is a slight difference between August and September in the maximum and mean sea ice extent lines, but sea ice extent recovers rapidly after September. Similarly, sea ice extent declines rapidly after April. The seasonal cycle amplitude (estimated from mean sea ice extent) is approximately $4.77 \times 10^6 km^2$.

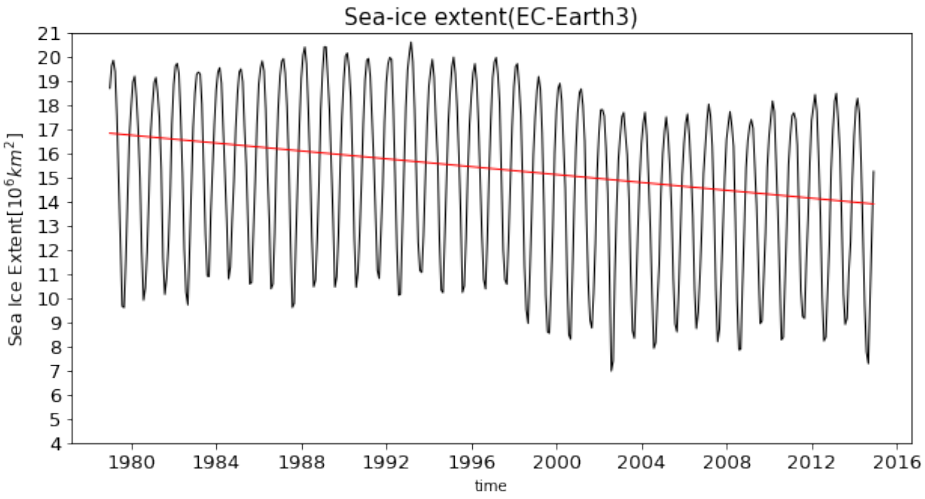

Figure 4.2: EC-Earth3 output sea ice extent trend.

Figure 4.2 shows the annual variation of EC-Earth output sea-ice extent between 1979-2014. The black line is the variation of sea-ice extent; the red line is the linear regression trend of sea-ice extent. It shows that sea-ice extent overall has a decreasing trend in 36 years, it decreased by 17.41%.

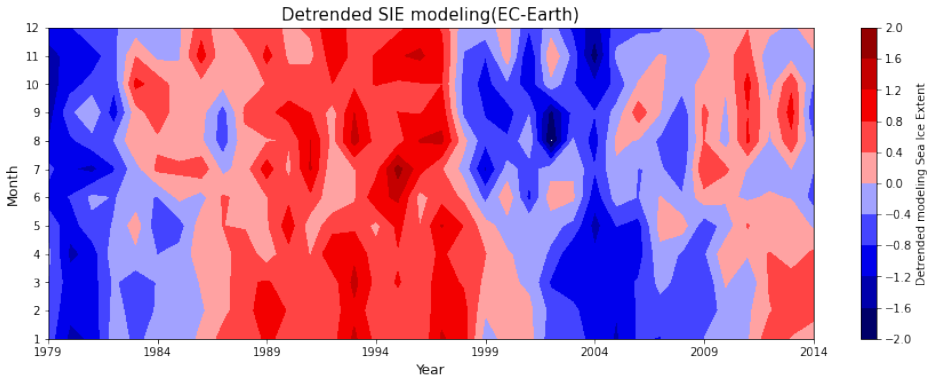

Figure 4.3: EC-Earth3 output detrended sea ice extent

Detrended sea ice extent is shown in Figure 4.3, where the red color indicates a positive phase of sea ice extent, blue color indicates a negative phase of sea ice extent. There's decadal variation of sea-ice extent.

4.1.2 Sea-ice thickness

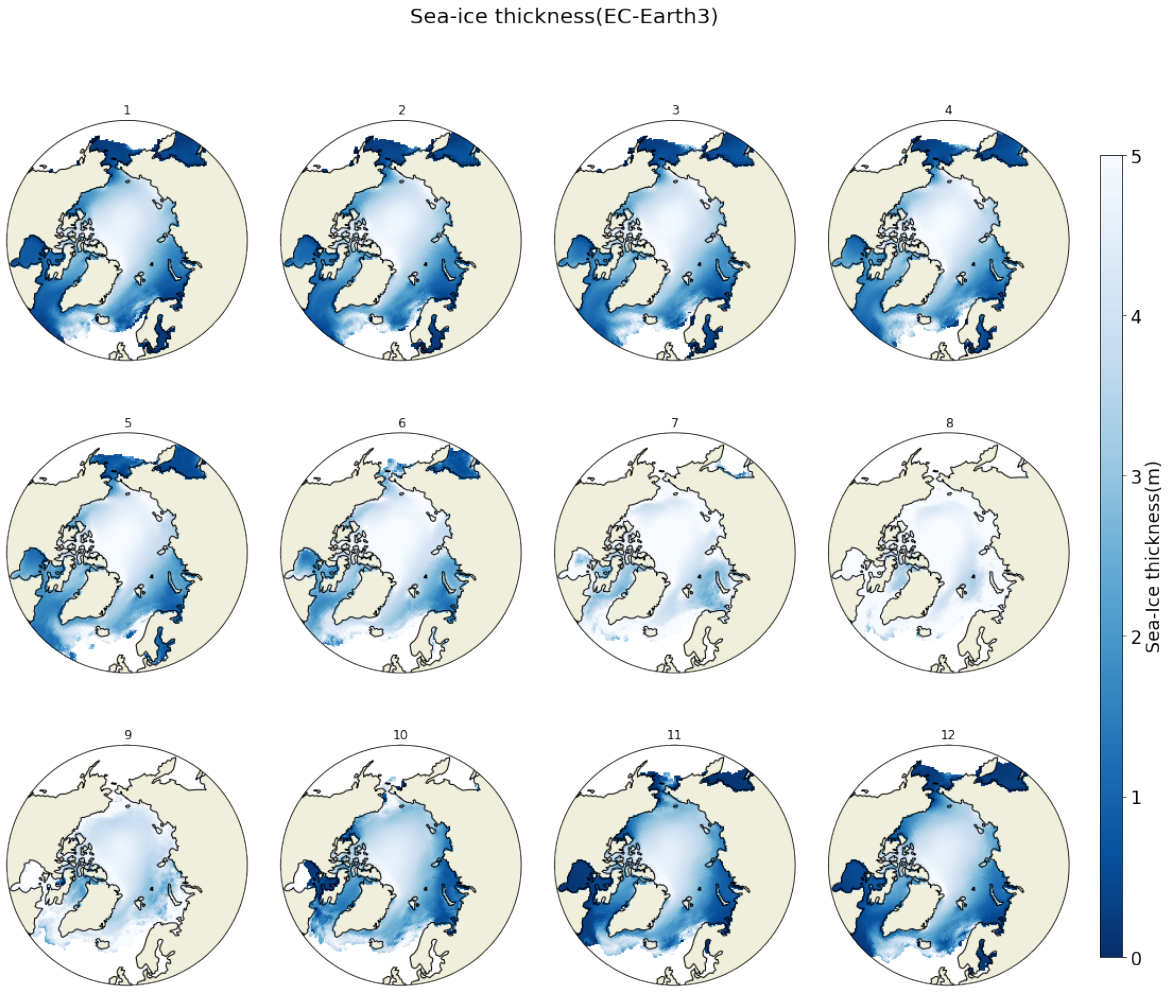

Figure 4.4: EC-Earth3 output monthly average sea-ice thickness distribution from 1979-2014

Figure 4.4 shows the seasonal distribution of sea-ice thickness. August has the maximum sea-ice thickness, while December has the minimum. Concerning regional differences, the whole year round, the central arctic and Canadian archipelago always have the thickest sea ice, followed by Sea East Siberian sea, the Laptev sea and, the Chukchi Sea and the Beaufort Sea. East Greenland sea, Barents sea, and the Kara Sea have comparatively low sea-ice thickness.

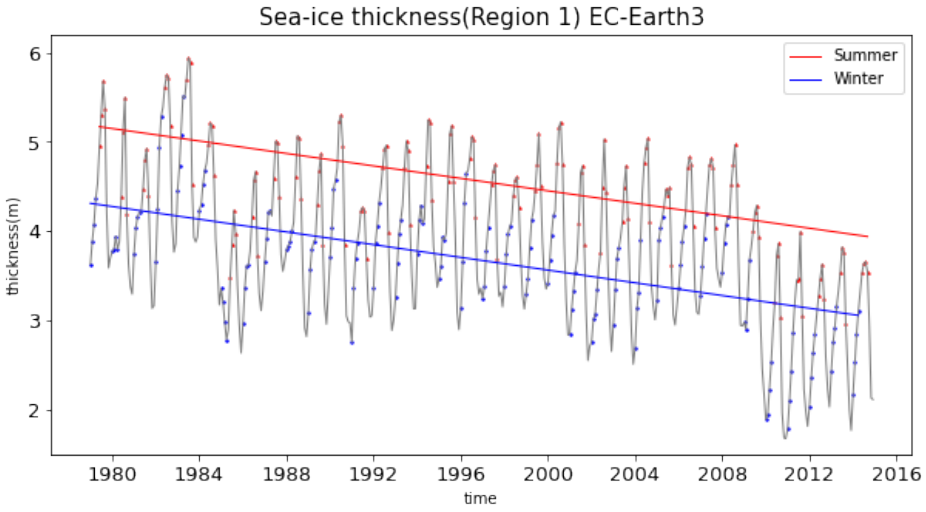

Figure 4.5: EC-Earth3 output time series of sea ice thickness from 1979-2014 in region 1

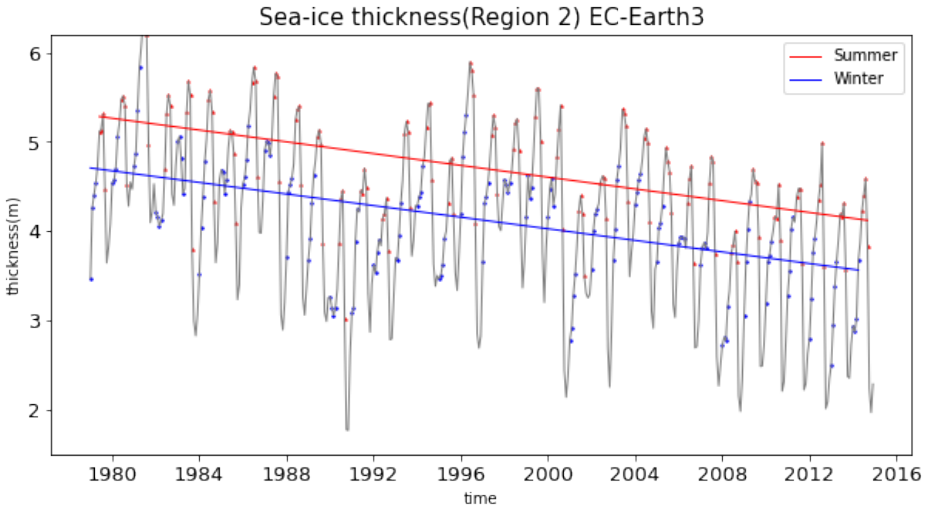

Figure 4.6: EC-Earth3 output time series of sea ice thickness from 1979-2014 in region 2

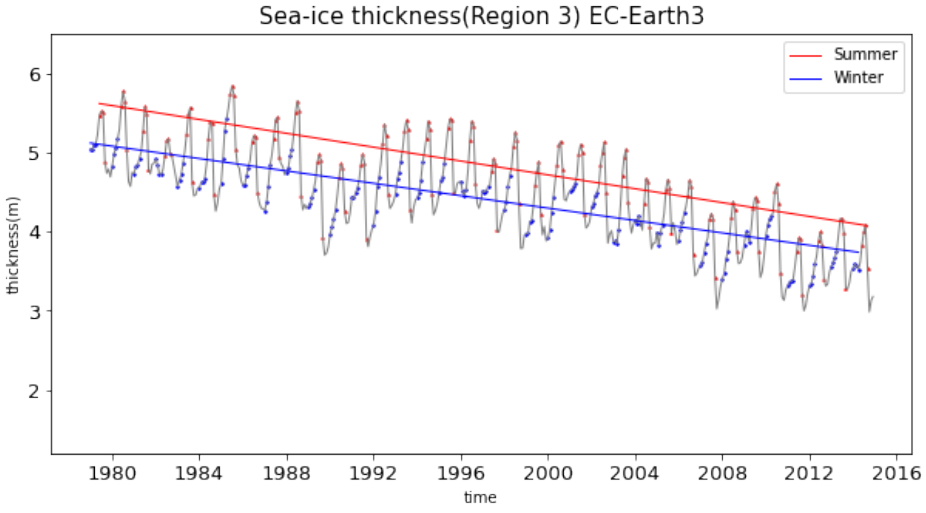

Figure 4.7: EC-Earth3 output time series of sea ice thickness from 1979-2014 in region 3

Figures 4.5-4.7 show the variation trend of sea-ice thickness between 1979-2014

in three different regions. The X-axis is the year, Y-axis is thickness, the red line is the summer trend, and the blue line is the winter trend. In all three regions, summer sea-ice thickness is higher than winter. Region1 has the largest summer-winter difference, region2 is the second, and region 3 has the smallest seasonal difference. Region 3 generally has higher sea-ice thickness than the other two regions, and Region 2 has a higher sea-ice thickness magnitude than region 1. In Region 1, in summer seasons, sea-ice thickness decreased by 23.79%; in winter seasons, sea-ice thickness decreased by 29.10%. In region 2, in summer seasons,sea-ice thickness decreased by 22.00%; in winter seasons, sea-ice thickness decreased by 24.28%. In region 3, summer sea-ice thickness decreased by 27.45%, and in winter seasons, sea-ice thickness decreased by 26.94%. Overall, sea-ice thickness has a faster decreasing rate in winter in regions1, and 2, while it has a faster-decreasing rate in summer in region3.

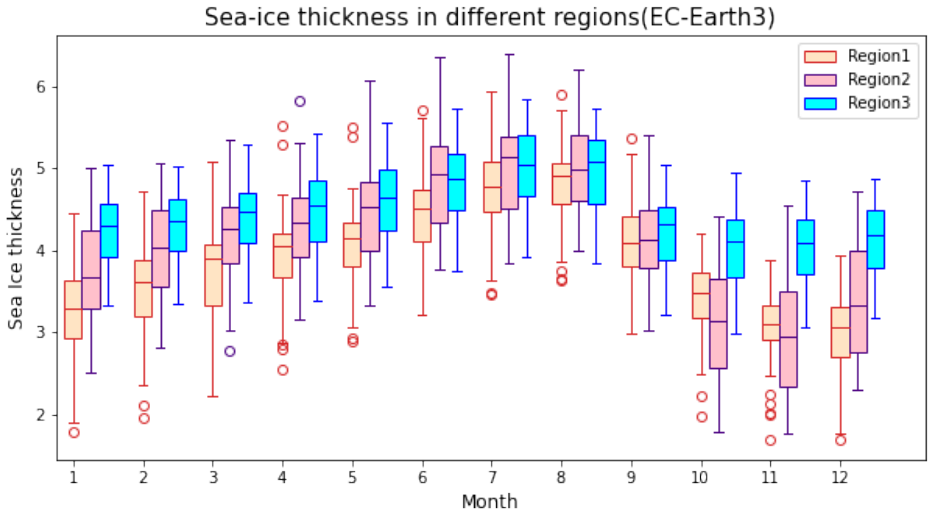

Figure 4.8: Regional comparison of EC-Earth3 output sea-ice thickness

In Figure 4.8, we compared sea-ice thickness within three Arctic regions. The x-axis is the month; y-axis is sea ice; the bar represents the range of sea-ice thickness among all time. The orange box represents Region1, the pink box represents Region2, and the blue box represents Region3. We can see that Region 3 has the most stable sea-ice thickness all year round, while region1 and region2 have considerable seasonal fluctuation of sea-ice thickness. In region1, sea-ice thickness reaches its maximum in August and its minimum in December; Region2 has the maximum sea-ice thickness in July and the minimum in November. Region 3 has its maximum sea-ice thickness in August and its minimum sea-ice thickness in November. When the sea-ice thickness is low, like in October, November, December, and January February, sea-ice thickness has a considerable regional variation; in other seasons, when sea-ice is thicker, there is minor regional variation. From December to May, sea-ice is thickest in region 3, followed by region 2, and region 1 has the thinnest sea ice. In October and November,

region 2 became the region with the thinnest sea ice. In June and July, region 2 has the thickest sea ice. In August and September, sea-ice thickness in all three regions is similar. Regarding annual variation, region 2 has the most comprehensive range of sea-ice thickness, demonstrated by taller boxes.

4.1.3 Sea-ice motion

Arctic sea-ice motion is illustrated by sea-ice drifting speed. Like sea-ice thickness, sea-ice motion is also studied in three Arctic regions.

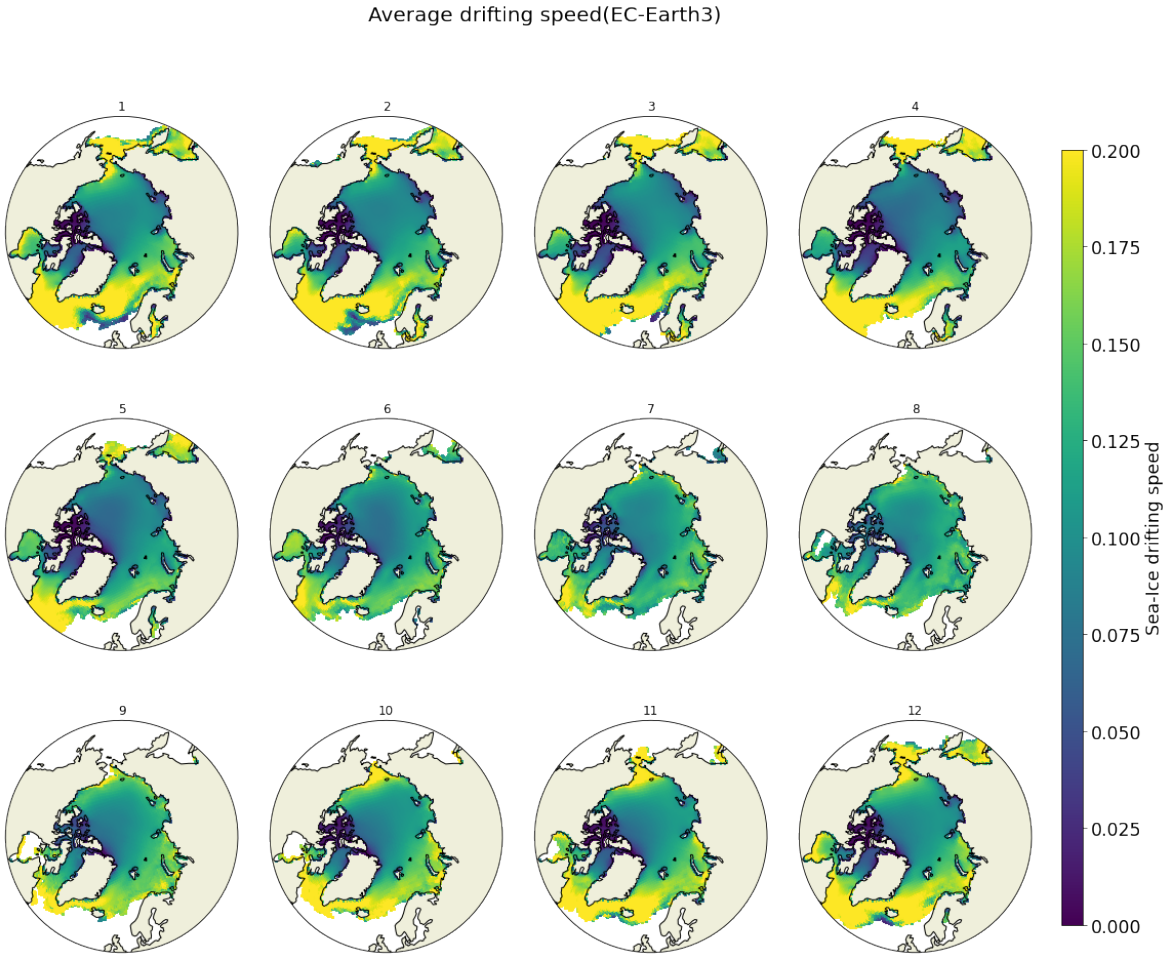

Figure 4.9: EC-Earth3 output monthly average sea-ice drifting speed distribution from 1979-2014

Figure 4.9 shows the monthly average sea-ice drifting speed from 1979-2014, which tightly coped with sea-ice thickness distribution shown in 4.4. Sea-ice drifting speed distribution has regional and seasonal differences. The region and month with the slowest sea-ice motion correspond with the region and month with the thickest sea-ice. Canadian archipelago has the slowest sea-ice motion, followed by North Baffin Bay and the central Arctic region. High sea-ice drifting speeds are mostly concentrated in Peripheral ice regions, such as the Barents sea, Kara sea, and Chukchi sea. Some marginal Arctic area has high drifting speed due to model simulating error.

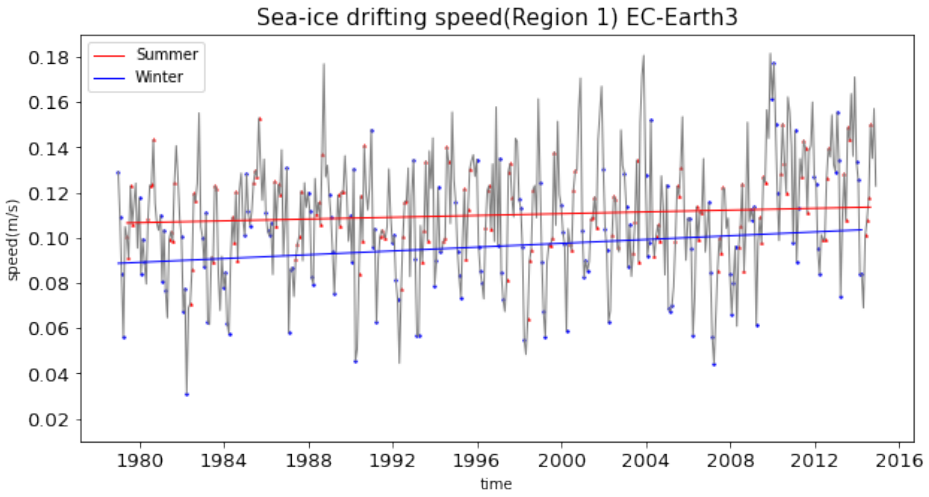

Figure 4.10: EC-Earth3 time series drifting speed from 1979-2014 in region 1

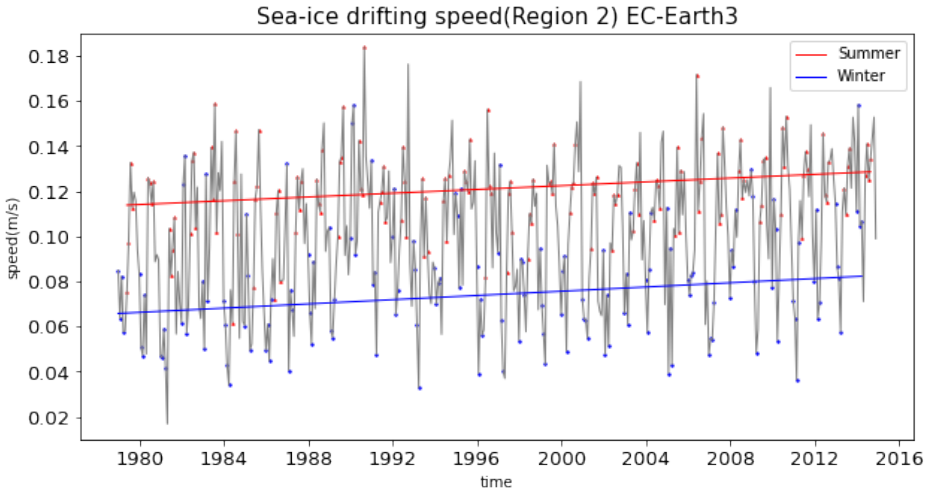

Figure 4.11: EC-Earth3 output time series of sea ice drifting speed from 1979-2014 in region 2

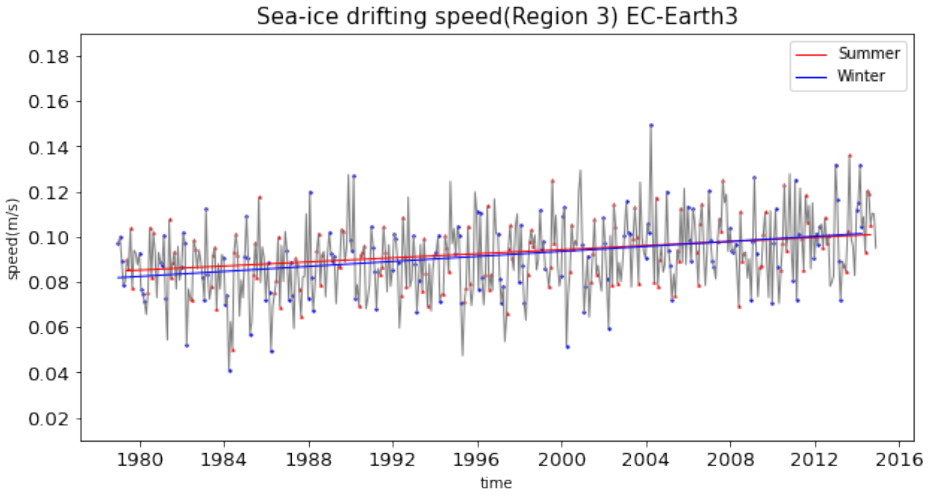

Figure 4.12: EC-Earth3 output time series of sea ice drifting speed from 1979-2014 in region 3

Figure 4.10-4.12 shows the annual variation and summer, winter trend of sea-

ice drifting speed in region 1,2 and 3 respectively. There is a positive trend in three regions, summer and winter. It is tightly coped with the decline of sea-ice thickness. In EC-Earth3 model output, in region 1, summer sea-ice drifting speed increased by 6.55%, and winter sea-ice drifting speed increased by 16.71%. In region 2, summer sea-ice drifting speed increased by 12.94%, and winter sea-ice drifting speed increased by 25.05%. In region 3, summer sea-ice drifting speed increased by 18.76%, and winter sea-ice drifting speed increased by 23.81%. Generally, wintertime sea-ice speed has a faster acceleration. In region1 and region2, the summer month sea-ice drifting speed is significantly higher than that in the winter month, and in region 2, the seasonal difference is the biggest seasonal difference. In region 3, before the 21st century, summer sea-ice drifting speed is slightly higher than that in winter, but after the 21st century, summer and winter trend lines pretty much approach each other.

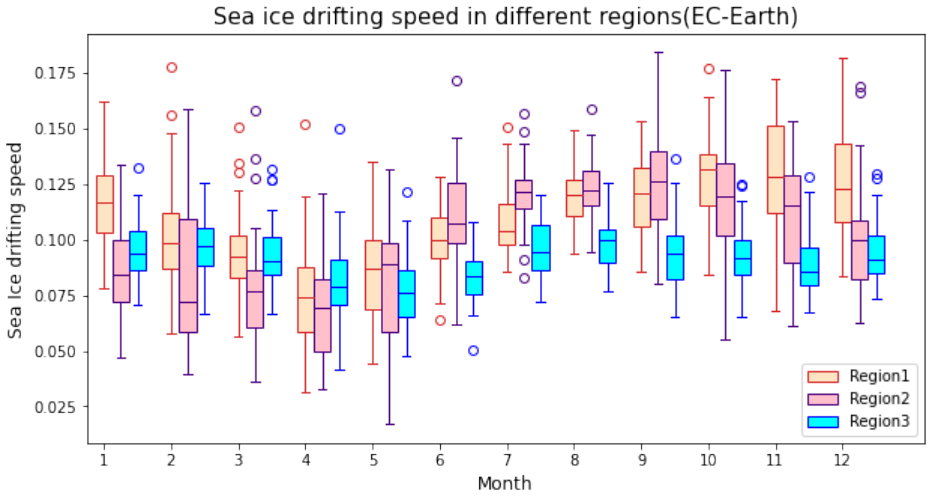

Figure 4.13: Regional comparison of EC-Earth3 output sea-ice drifting speed

In Figure 4.13 box plots compare sea-ice drifting speed in regions 1,2 and 3 in each season. The orange box is region 1, the pink box is region2, and the blue box is region 3. The seasonal cycle is clearly shown in the figure. In region 1, minimum sea-ice drifting speed occurs in April, and maximum sea-ice drifting speed occurs in October. In region 2, minimum sea-ice drifting speed occurs in April and maximum in September. In region 3, the minimum sea-ice drifting speed happens in May, and the maximum happens in August. Region 3 has the smallest seasonal fluctuation compared with regions 1 and 2. Region1 and region2 have similar seasonal cycle amplitude. In summer seasons, from May to September, region 2 has the highest sea-ice drifting speed in the whole arctic, while in winter seasons, from October to March, region 1 has the fasted sea-ice drifting speed. Generally, there is the slowest sea-ice motion all year round, but the sea-ice drifting speed in region3 can still exceed at least drifting speed in the region2 from January to April, and in April, region 3 has the highest sea-ice drifting speed. The regional difference is large when sea-ice drifting speed is high like

in winter months, and when sea-ice motion has a comparatively stable state like April and May, there is a less regional difference.

4.2 ACCESS-CM2

ACCESS is the Australian Community Climate and Earth System Simulator. ACCESS-CM2 comprises the UKMO UM atmospheric model, the CABLE land surface model, the GFDL MOM5 ocean model at 1-degree resolution, the LANL CICE5.1 sea ice model, and the OASIS-MCT coupler. ACCESS-CM2 implemented the 2012 release of MOM model version 5 as the ocean component. The sea ice model CICE version 5.1.2 is the sea ice component (Bi et al., 2020). The model has an ice thickness distribution that divides the ice into categories that evolve throughout the simulation due to thermodynamic growth and melt and mechanical redistribution/ridging of the ice. The ice thickness distribution is represented by five ice thickness categories and an open water ice-free area. Multi-layer thermal dynamics are implemented in CICE5. CICE5 also uses an albedo scheme. Spatial resolution is 1.258 latitude by 1.8758 longitude CICE5 uses an elastic-viscous-plastic dynamical scheme (III, 1979) for the internal ice stress, and an incremental linear remapping for the ice advection term.

4.2.1 SIE

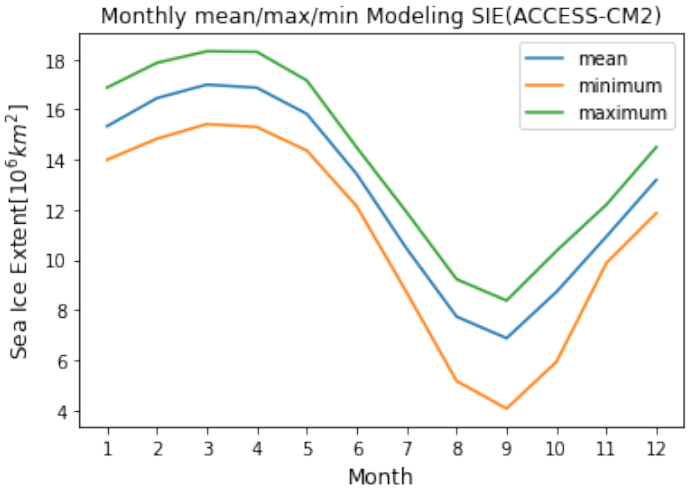

Figure 4.14: ACCESS-CM2 output sea-ice extent mean, maximum and minimum

Figure 4.14 shows the seasonal cycle of sea-ice extent in ACCESS-CM2 model output, legends are same as Figure 4.1. sea-ice extent reaches the maximum in March up to $18.32 \times 10^6 km^2$ and minimum in September down to $4.07 \times 10^6 km^2$. The seasonal cycle of sea-ice extent amplitude is approximately $5.06 \times 10^6 km^2$. The sea-ice extent has a rapid decrease from May on; after it reaches a minimum in September, it recovers

rapidly.

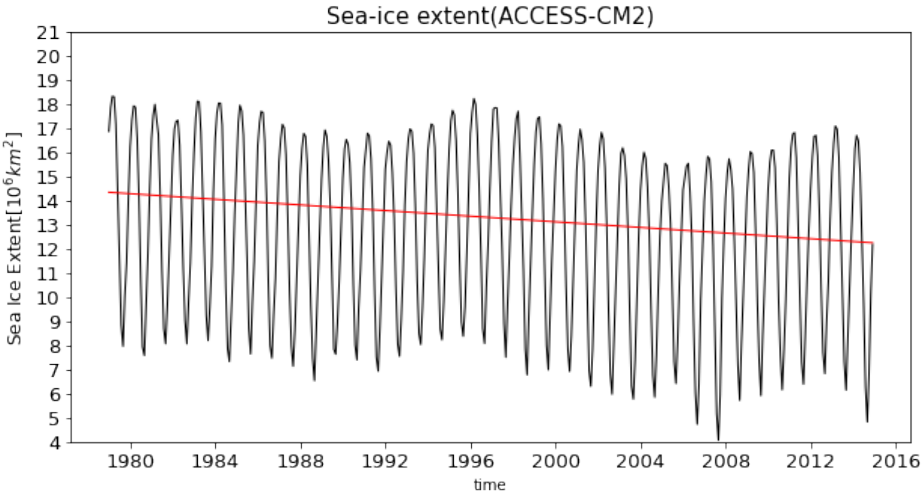

Figure 4.15: ACCESS-CM2 output sea ice extent trend

Figure 4.15 shows the annual variation between 1979-2014 and the overall trend. It clearly shows that the Arctic sea-ice extent has a seasonal cycle, as demonstrated in Figure 4.14, and sea-ice extends decreasing in the 36 years, and it decreased by 14.60%. However, sea-ice extent still has an annual cycle, the sea-ice extent decreasing from 1979-1990, and after that, there is a recovery period between 1990 and 1996, after 1996 sea-ice extent starts to decrease again, until 2004, from 2004-2014 is another sea-ice recovery period.

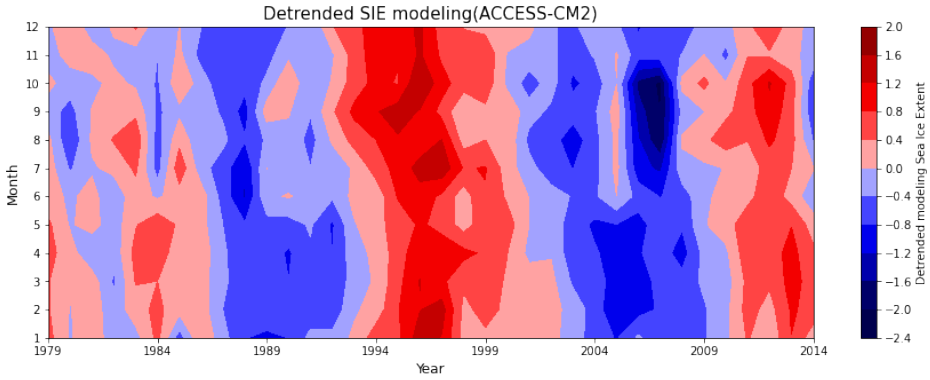

Figure 4.16: ACCESS-CM2 output detrended sea ice extent

Figure 4.16 shows the detrended sea-ice extent for all the seasons from 1979-2014. There's decadal variation.

4.2.2 Sea-ice thickness

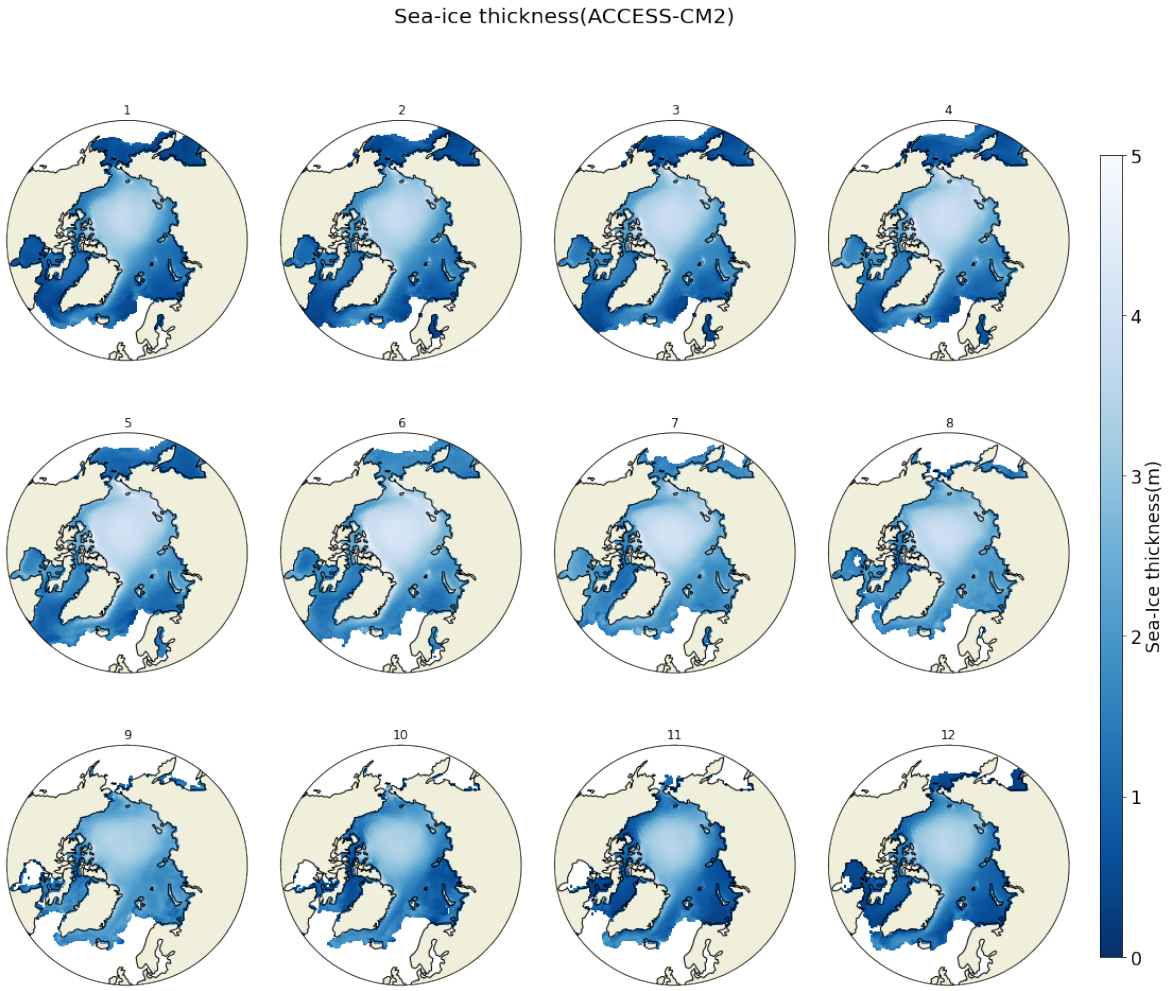

Figure 4.17: ACCESS-CM2 output monthly average sea-ice thickness distribution from 1979-2014

Figure 4.17 shows the monthly average sea-ice thickness distribution of the ACCESS-CM2 model's output. Even though there are seasonal variations, the regional distribution in each month are pretty similar. Thin ice is mainly distributed in the Peripheral Arctic, especially in the Kara Sea, Barents Sea, and the eastern Greenland Sea. The thickest sea ice is concentrated on the north part of Beaufort Sea, Chukchi Sea, East Siberian Sea, Laptev Sea, central Arctic region, and east coast of Greenland.

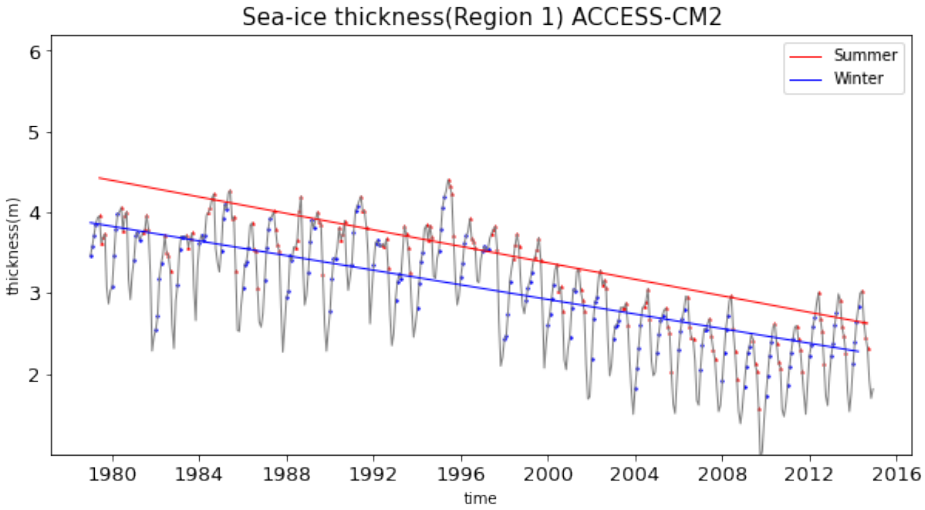

Figure 4.18: ACCESS-CM2 output inter-annual variability of regional average sea-ice thickness from 1979-2014 in region 1

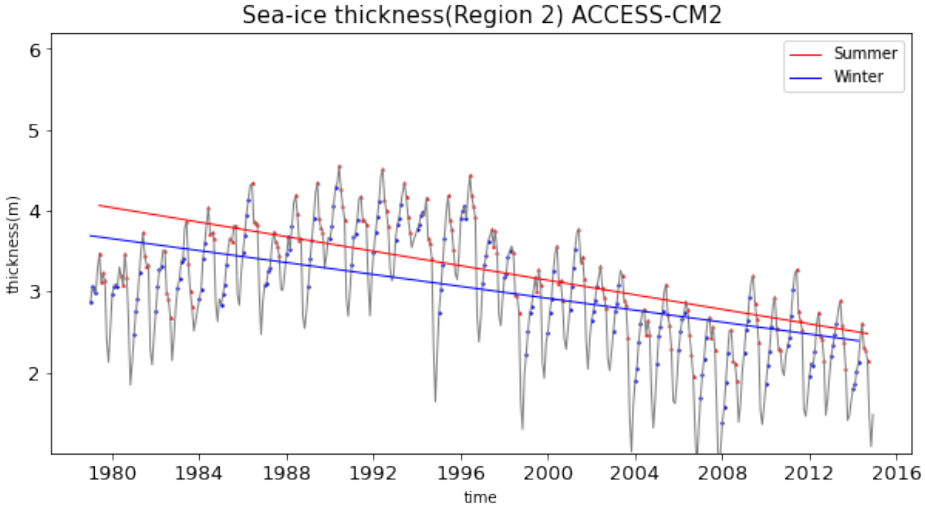

Figure 4.19: ACCESS-CM2 output inter-annual variability of regional average sea-ice thickness from 1979-2014 in region 2

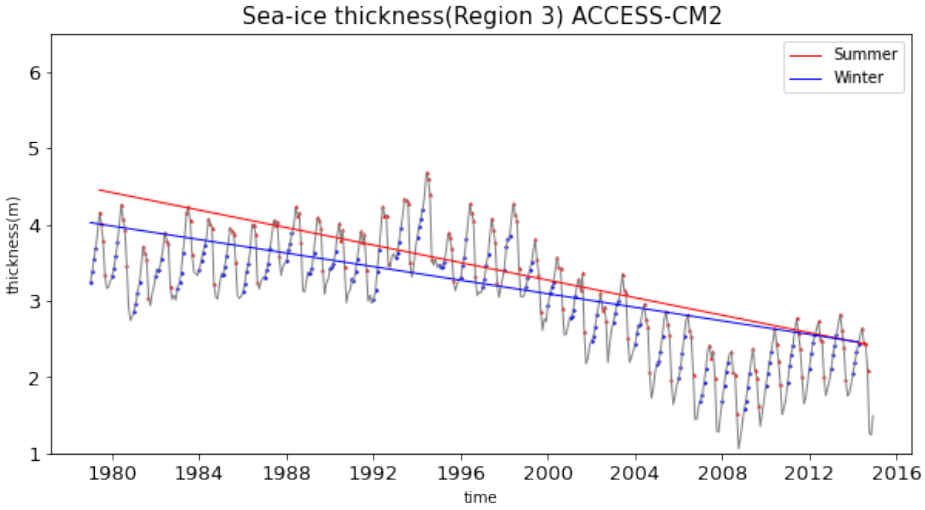

Figure 4.20: ACCESS-CM2 output inter-annual variability of regional average sea-ice thickness from 1979-2014 in region 3

Figure 4.18-4.20 show the variation trend of sea-ice thickness between 1979-2014 in three different regions. During the whole time, especially after 1996, all regions sharply decreased sea-ice thickness in both summer and winter. In region 1, summer sea-ice thickness decreased by 40.68%; winter sea-ice thickness decreased by 41.22%. In region 2, summer sea-ice thickness decreased by 38.98%; winter sea-ice thickness decreased by 35.20%. In region 3, summer sea-ice thickness decreased by 45.43%, and winter sea-ice thickness decreased by 38.88%. In all the regions, summer sea ice is thicker than winter sea ice. However, since summer sea-ice thickness has a more rapid decreasing rate, the seasonal difference in sea-ice thickness is greatly reduced by the end of the studying period.

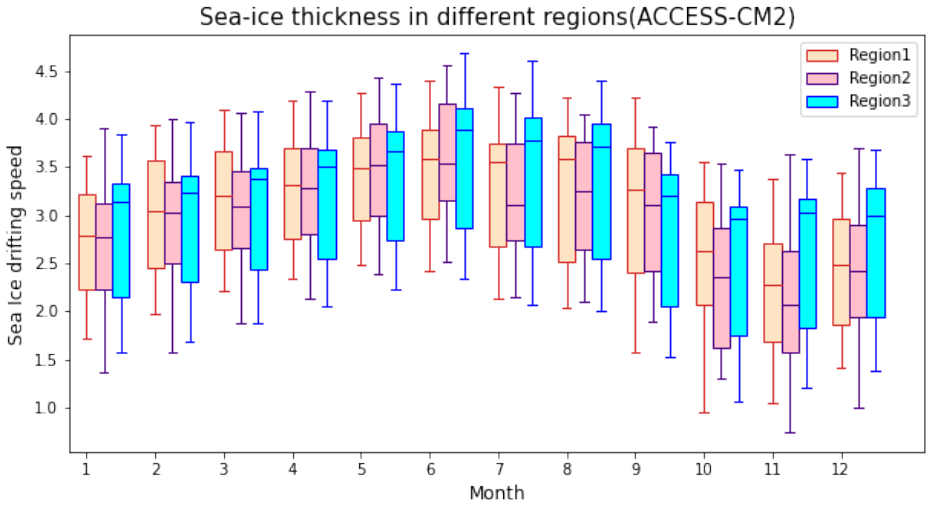

Figure 4.21: Regional comparison of ACCESS-CM2 output sea-ice thickness

Figure 4.21 shows the box plot comparing sea-ice thickness in three regions each month. The ACCESS-CM2 model output sea-ice thickness results in three regions are considerably unified. In June, sea-ice thickness in regions 1,2, and 3 reaches the maximum. Region 1 and Region2 have the thinnest sea ice in November, while Region 3 has the thinnest sea ice in October. Except for September, sea-ice thickness is higher in the central Arctic than in the other two regions.

4.2.3 Sea-ice motion

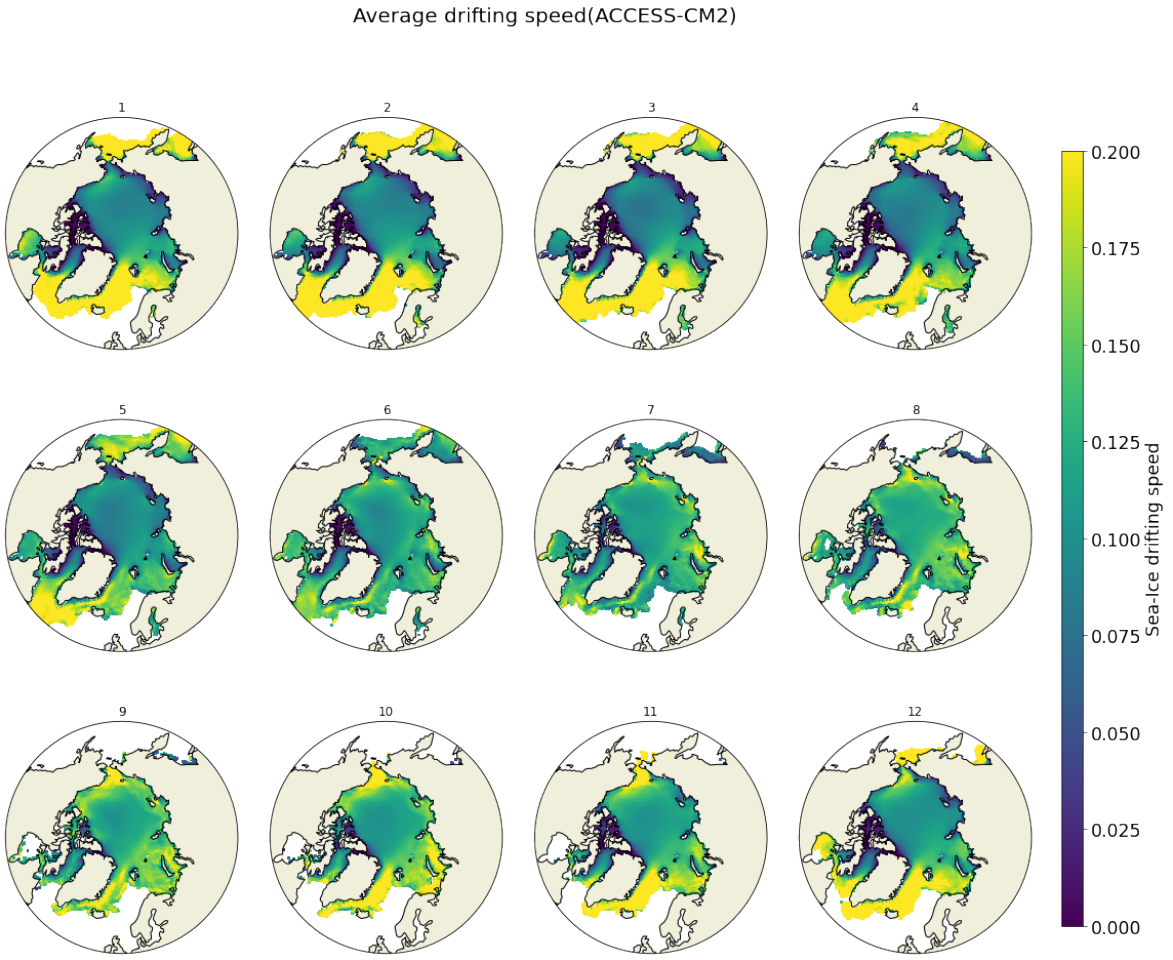

Figure 4.22: ACCESS-CM2 output monthly average sea-ice drifting speed distribution from 1979-2014

Figure 4.22 shows the monthly average sea-ice drifting distribution from 1979-2014. Synchronized with sea-ice thickness output by the ACCESS-CM2 model, the Arctic region with thin ice coverage tends to have fast sea-ice drifting speeds. From January to May, the Chukchi sea has comparatively low sea ice drifting speed; from June to August, the drifting speed of the Chukchi Sea gradually increases, and from September to December, it maintains a fast sea-ice motion in the Chukchi Sea. All year round, compared with other regions, the Greenland Sea, Barents Sea, and the Laptev Sea always have a higher sea-ice drifting speed, and Central Arctic and Canadian Archipelago have slow sea-ice motions. The Greenland Sea has the biggest seasonal variation.

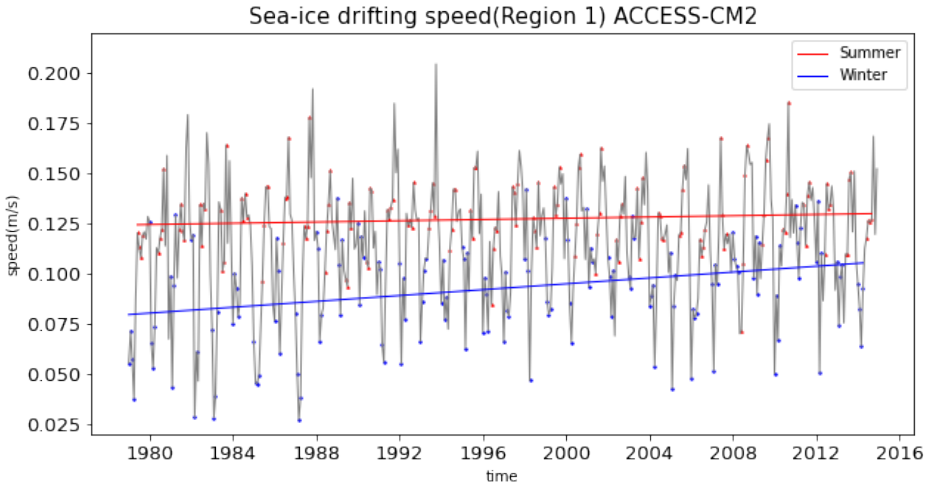

Figure 4.23: ACCESS-CM2 output time series of sea ice drifting speed from 1979-2014 in region 1

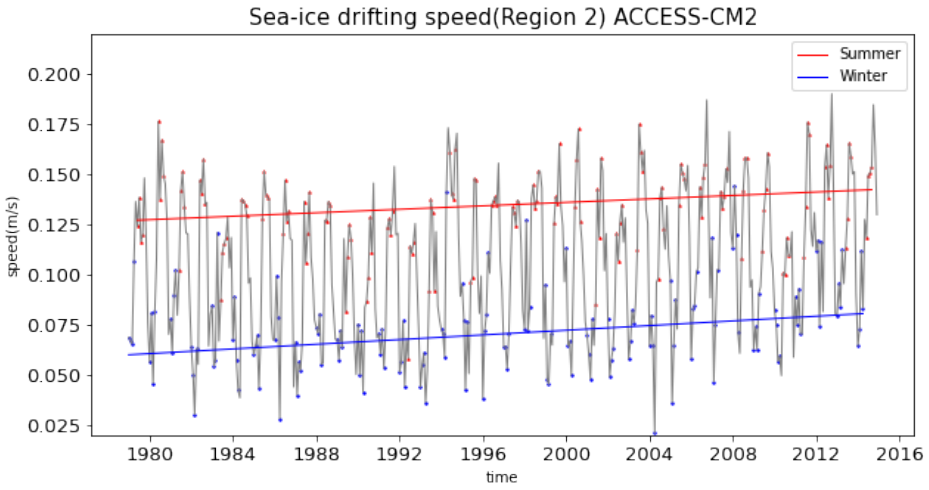

Figure 4.24: ACCESS-CM2 output time series of sea ice drifting speed from 1979-2014 in region 2

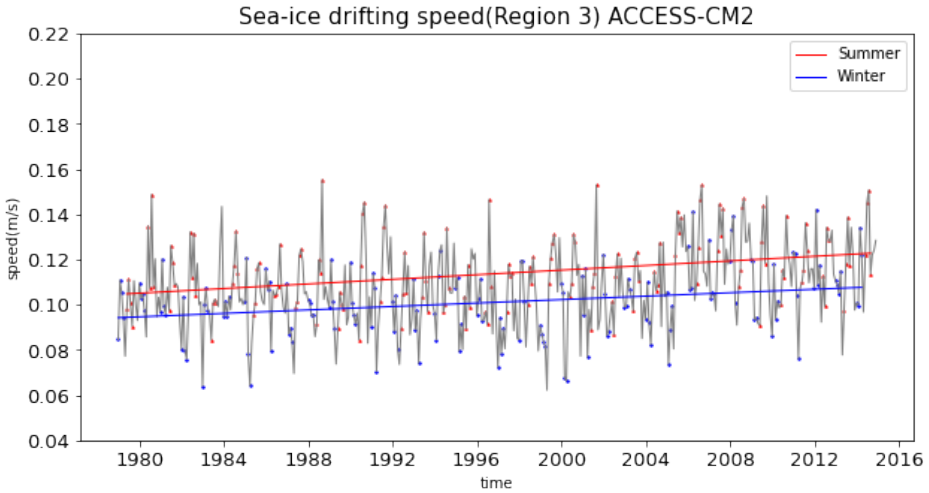

Figure 4.25: ACCESS-CM2 output time series of sea ice drifting speed from 1979-2014 in region 3

Figure 4.23-4.25 shows the annual variation and summer, winter trend of ACCESS-CM2 output sea-ice drifting speed in region 1,2 and 3 respectively. In the

Arctic region, the ACCESS-CM2 model provided a positive trend result of sea-ice drifting speed both in summer and winter, and summer sea-ice motion is faster than in winter. Region2 has the biggest seasonal variation of sea-ice drifting speed, followed by regions1 and region3. Even though region3 has the smallest seasonal variation, it still has more seasonal variability than EC-Earth3 output. In region 1, in summer, sea-ice drifting speed increased by 4.44%, and winter increased by 32.32%. In region 2, in summer, sea-ice drifting speed increased by 11.96%, and winter increased by 34.16%. In region 3, in summer, sea-ice drifting speed increased by 17.15%, and winter increased by 14.25%. There is a rapid increase in sea-ice motion in region1 and 2 in winter, much higher than in summer. Only in region3 does sea-ice motion have a slightly faster increasing rate in summer than in winter.

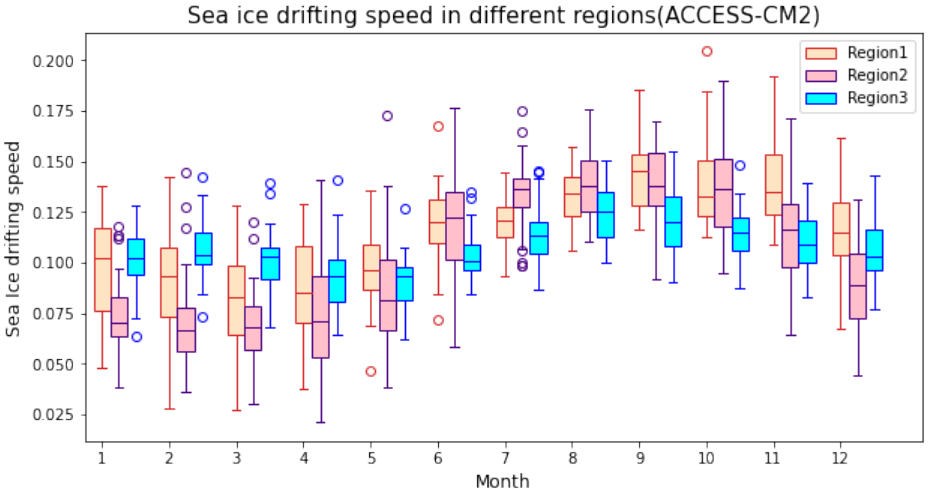

Figure 4.26: Regional comparison of ACCESS-CM2 output sea-ice drifting speed

Figure 4.26 compares sea-ice drifting speed between three regions for each month. It shows that Region 2 has the most significant seasonal cycle amplitude, and region 3 has the slightest seasonal fluctuation. In region1 and region2, sea-ice drifting speed reaches the minimum in March and maximum in September. In region 3, sea-ice drifting speed reaches the minimum in May and the Maximum in August. From January to April, region 3 has the fastest sea-ice motion; In May, September, November, and December, Region 1 has the fastest sea-ice drifting speed. In June, July, August, and October, region 2 has the highest sea-ice drifting speed. From December to May, region 2 has the slowest sea-ice motion; from June to November, region 3 has the slowest sea-ice motion. There is a prominent regional difference in most of the seasons.

4.3 BCC-CSM2-MR

BCC-CSM2-MR is a medium-resolution version of the Beijing Climate Center (BCC) Climate System Model, and its resolution is 1 latitude × 1 longitude with a tri-pole grid BCC-CSM2-MR performed under CMIP6-prescribed historical forcing. BCC-CSM2-MR well captures observed global warming trends of surface air temperature from 1950 to 2014. Its thermal dynamical model is SIS4, including Elastic-viscous-plastic dynamical processes and Semtner's thermodynamic processes. Snow albedo 0.8, ice albedo 0.5826 sea-ice components are presented by Modular Ocean Model version4(MOM4) and Sea Ice Simulator version 4 (SIS4), and five categories of sea ice (including open water) are considered. Dynamics: MOM4 L40 adopts some mature parameterization schemes, including Sweby's tracer-based third-order advection scheme, the isopycnal tracer mixing and diffusion scheme, the Laplace horizontal friction scheme, the KPP vertical mixing scheme, the complete convection scheme, the overflow scheme of topographic processing of sea bottom boundary/steep slopes, and the shortwave penetration schemes based on the spatial distribution of the chlorophyll concentration (Döscher et al., 2022b).

4.3.1 Sea ice extent

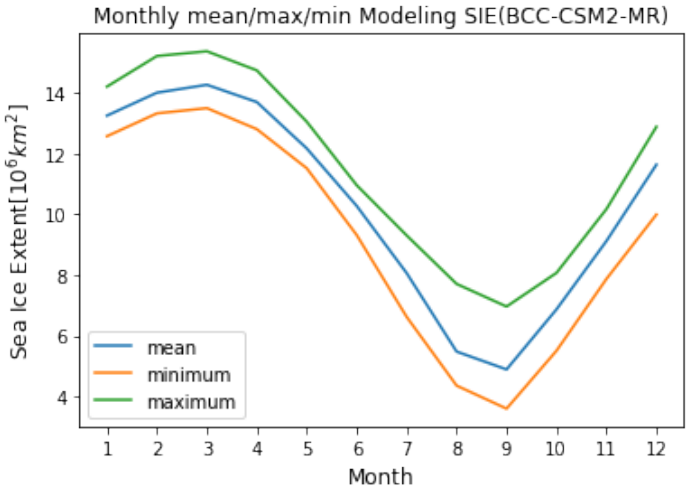

Figure 4.27: BCC-CSM2-MR output sea-ice extent mean, maximum and minimum

Figure 4.27 shows the seasonal cycle of sea-ice extent in the BCC-CSM2-MR model projection. Sea-ice extent reaches the maximum in March, up to $15.36 \times 10^6 km^2$, minimum in September down to $3.60 \times 10^6 km^2$. Sea-ice extent decreases rapidly after April; after it reaches the minimum in September, sea-ice extent recovers quickly. Seasonal cycle amplitude is approximately $4.68 \times 10^6 km^2$.

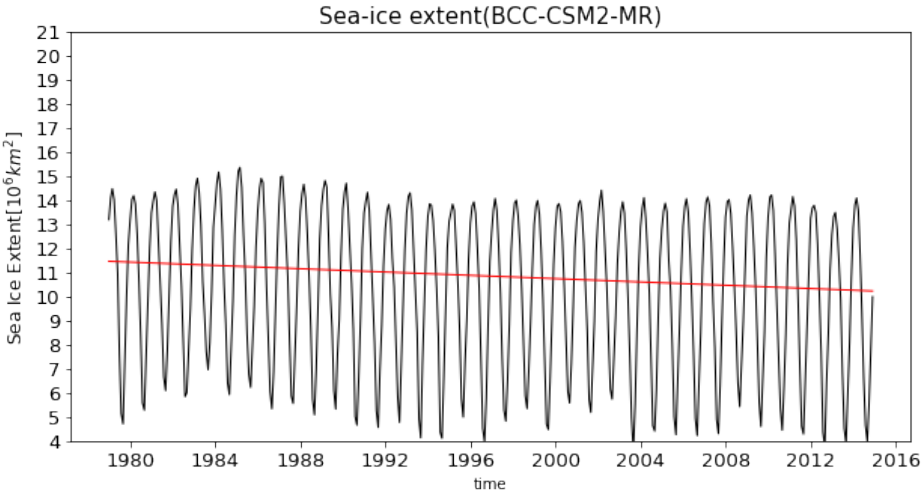

Figure 4.28: BCC-CSM2-MR output sea ice extent trend

Figure 4.28 shows the annual variation and trend between 1979-2014. Overall there is a negative trend in sea-ice. However, there are fluctuations in the variation of sea-ice extent, which means a smaller period of sea-ice recovery also exists. Over the 36 years, sea-ice extends decreased by 10.76%.

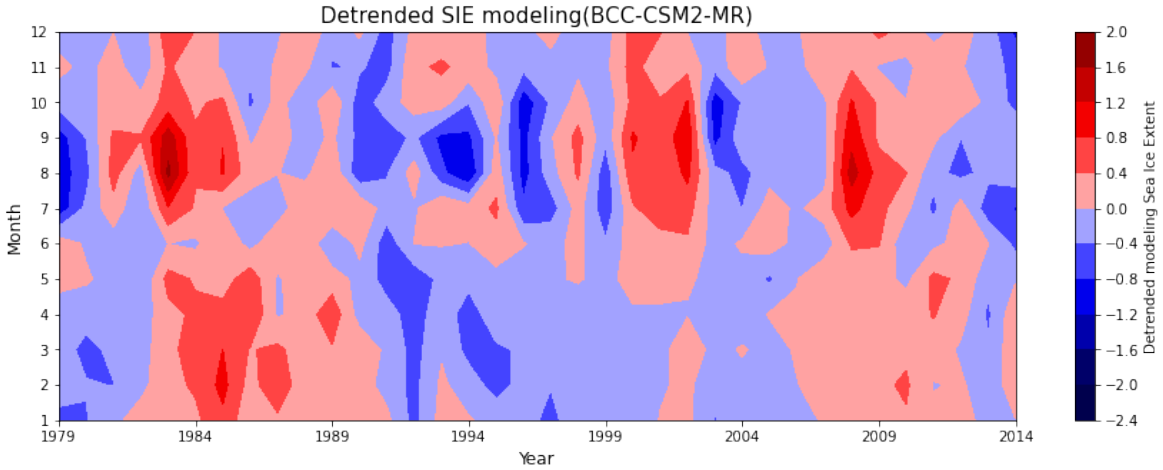

Figure 4.29: BCC-CSM2-MR output detrended sea ice extent

Detrended sea ice extent is shown in Figure 4.29. In the summer seasons, there is an alternation between the positive and negative phases, but Figure 4.29 doesn't show a clear variation in winter. It means summer has more variation of a sea-ice extent than winter.

4.3.2 sea-ice thickness

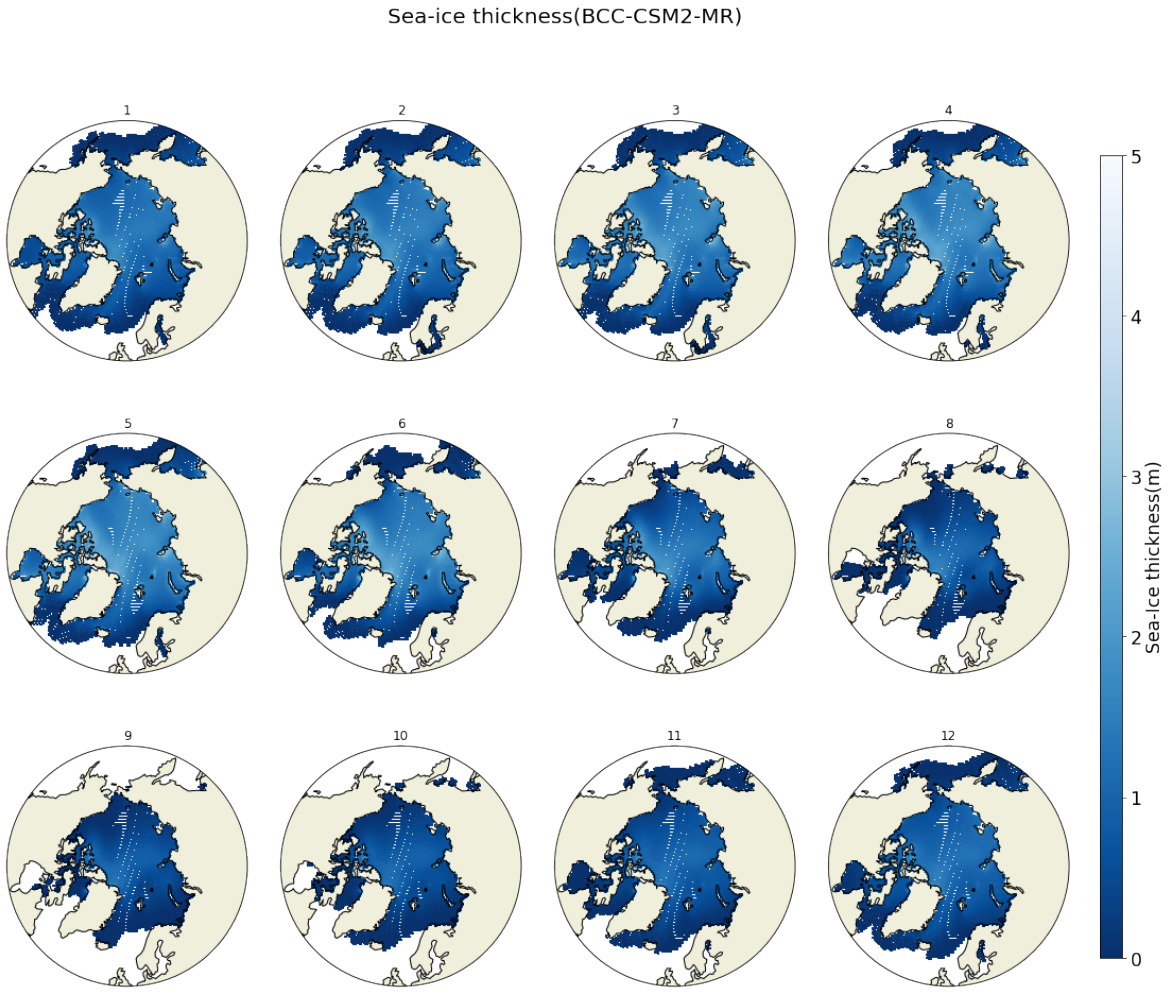

Figure 4.30: BCC-CSM2-MR output monthly average sea-ice thickness distribution from 1979-2014

Figure 4.30 shows the monthly average sea-ice thickness distribution of the BCC-CSM2-MR model's output. BCC-CSM2-MR projected a thin sea-ice thickness in the Arctic region compared with other model projection results. In summer, only the central Arctic and Canadian Archipelago have marginally thicker sea ice; in winter, other than the two regions listed above, Beaufort Sea, Chukchi Sea, East Siberian Sea, Laptev Sea, and the Kara Sea have enhanced sea-ice thickness.

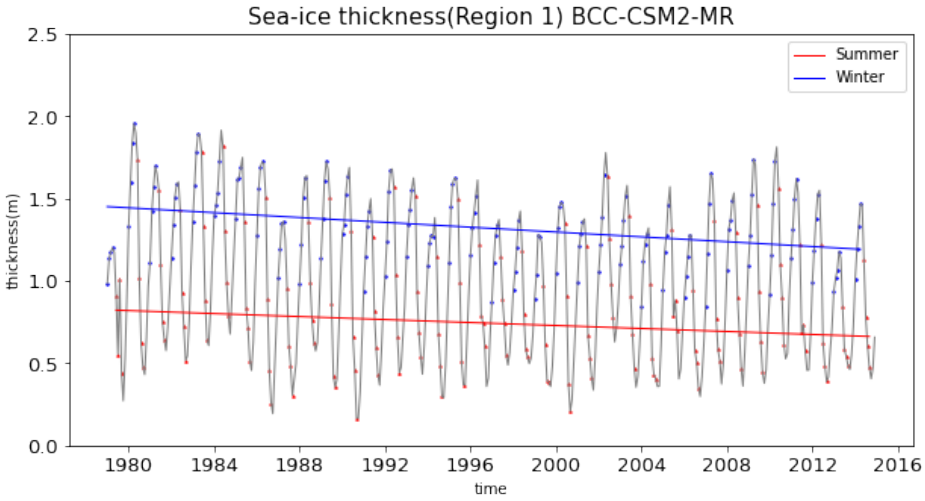

Figure 4.31: BCC-CSM2-MR output inter-annual variability of regional average sea-ice thickness from 1979-2014 in region 1

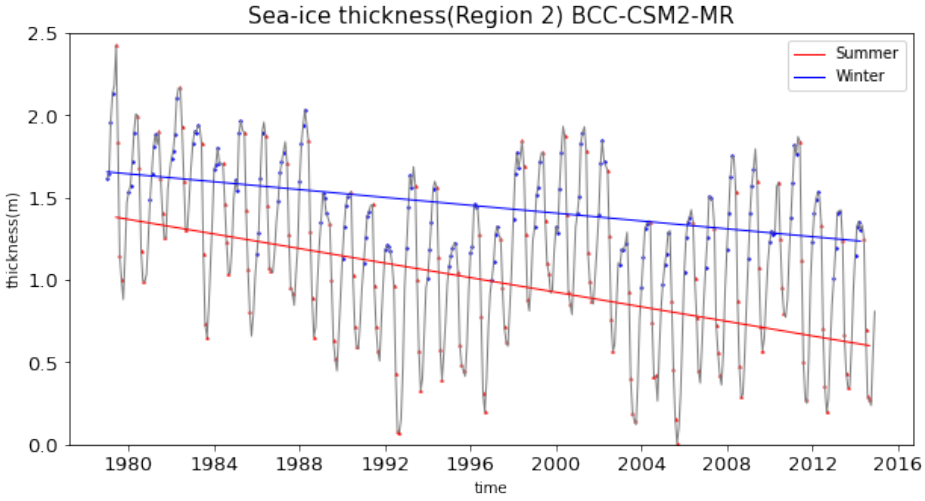

Figure 4.32: BCC-CSM2-MR output inter-annual variability of regional average sea-ice thickness from 1979-2014 in region 2

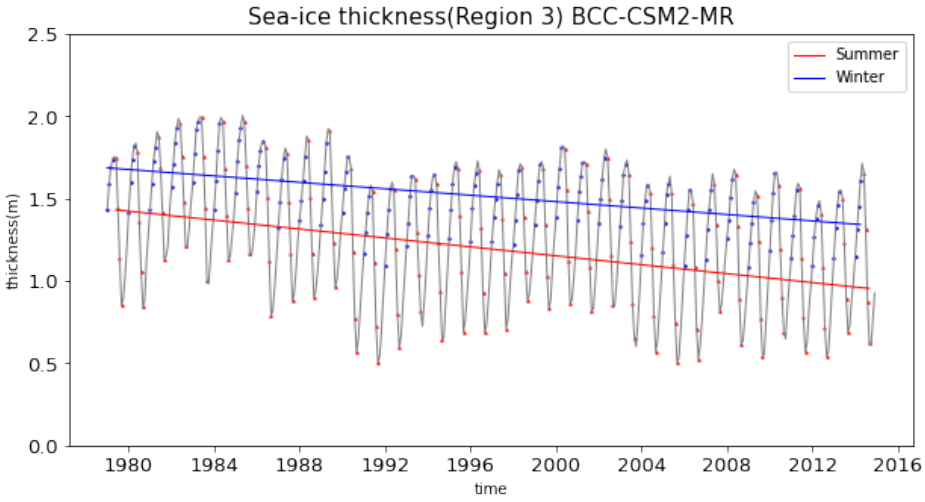

Figure 4.33: BCC-CSM2-MR output inter-annual variability of regional average sea-ice thickness from 1979-2014 in region 3

Figure 4.31-4.33 show the variation trend of sea-ice thickness between 1979-2014 in three different regions. Different from EC-Earth3 and ACCESS-CM2 model results, in BCC-CSM2-MR model projection results, in the whole Arctic region, winter sea-ice thickness is higher than summer sea-ice thickness. Almost every year, the thinnest sea-ice thickness occurs in one of the summer months. In general, there is a decreasing trend for sea-ice thickness. In region 1, summer sea-ice thickness decreased by 19.41%; winter sea-ice thickness decreased by 17.85%. In region 2, summer sea-ice thickness decreased by 56.46%; winter sea-ice thickness decreased by 25.37%. In region 3, summer sea-ice thickness decreased by 33.37%; winter sea-ice thickness decreased by 20.4%. Sea-ice thinning happens more robustly in summer than in winter, especially in region2 and region3. The sharpest sea-ice thinning happens in the summer season in region 2, where sea-ice thickness decreases by more than half. The Arctic region has a significant seasonal variation of sea-ice thickness.

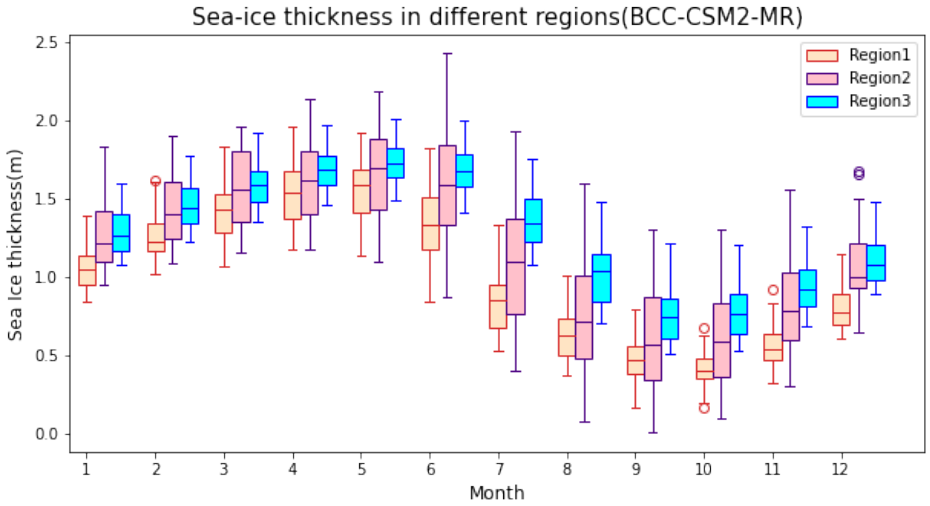

Figure 4.34: Regional comparison of BCC-CSM2-MR output sea-ice thickness

Figure 4.34 compares three regions each month for BCC-CSM2-MR output sea-ice thickness. Seasonal variation appears to be very synchronized in regions 1,2, and 3. The thickest sea-ice condition happens in May, and the thinnest sea ice occurs in October for region1 and in September for regions 2 and 3. Region 3 always has the thickest sea ice, and region 1 has the thinnest sea ice. Among all the three regions, region 2 has the biggest annual variation.

4.3.3 sea-ice motion

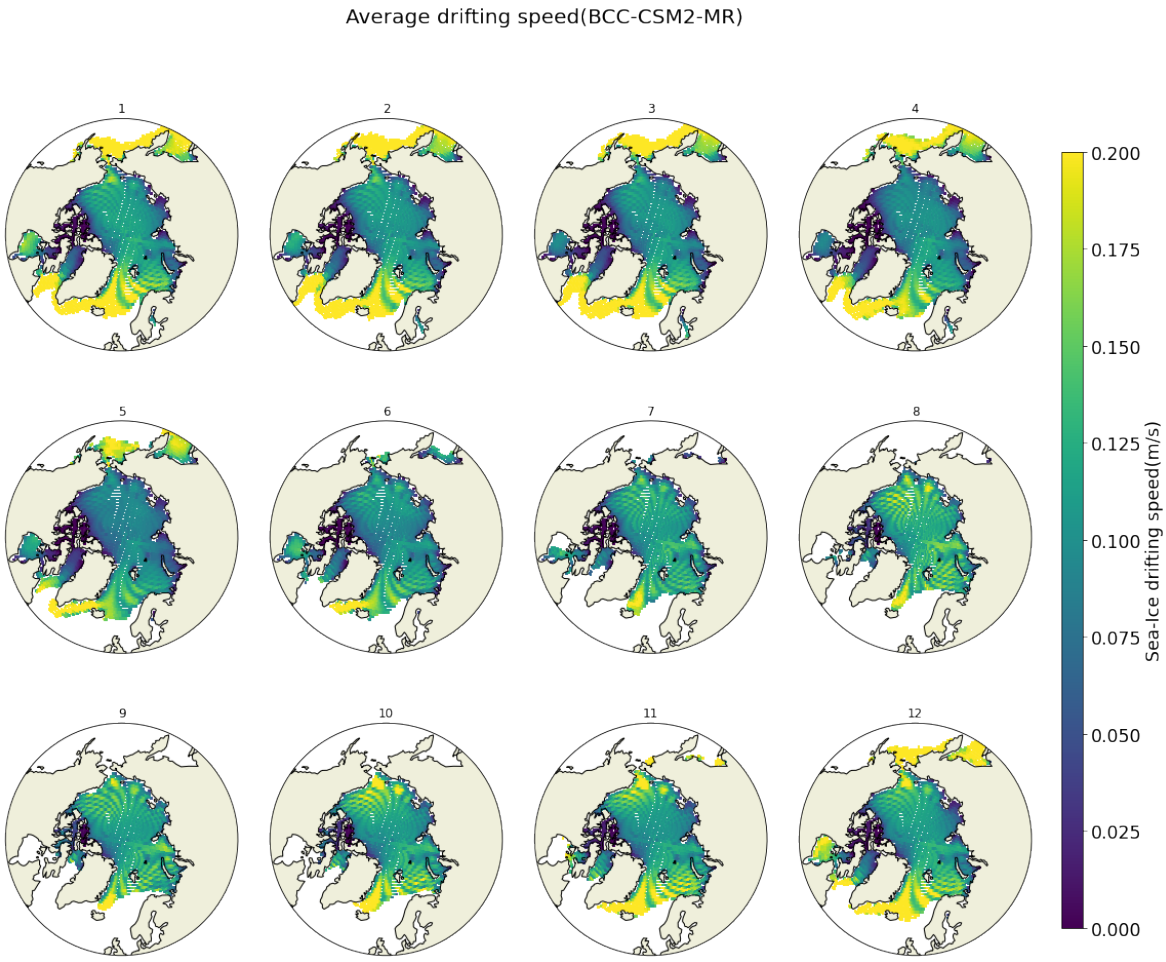

Figure 4.35: BCC-CSM2-MR output monthly average sea-ice drifting speed distribution from 1979-2014

Figure 4.35 shows the monthly average sea-ice drifting speed from 1979-2014. There is a vast regional difference, particularly in the winter months. The high sea-ice drifting speed area is concentrated in the Greenland Sea and the Barents Sea. From November to February, high sea-ice drifting speed also occurs in the Chukchi Sea. Low values in the marginal sea are likely to be algorithm errors.

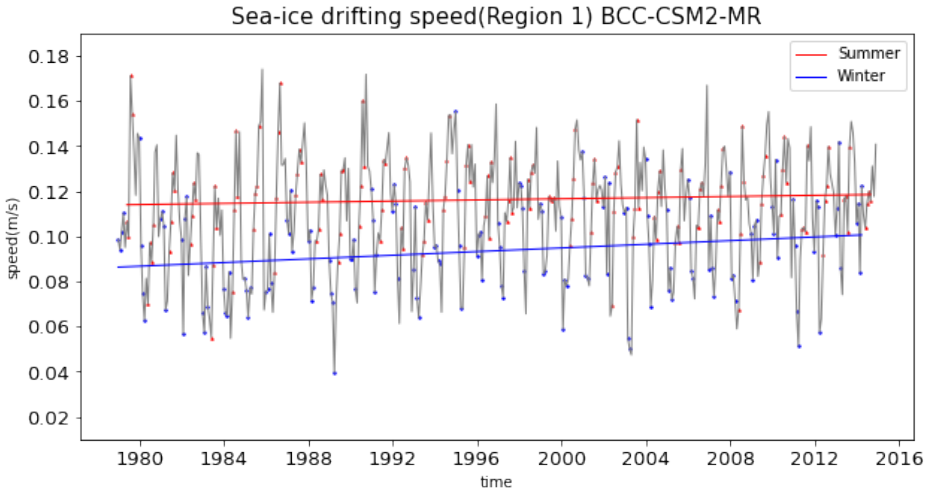

Figure 4.36: BCC-CSM2-MR output time series of sea ice drifting speed from 1979-2014 in region 1

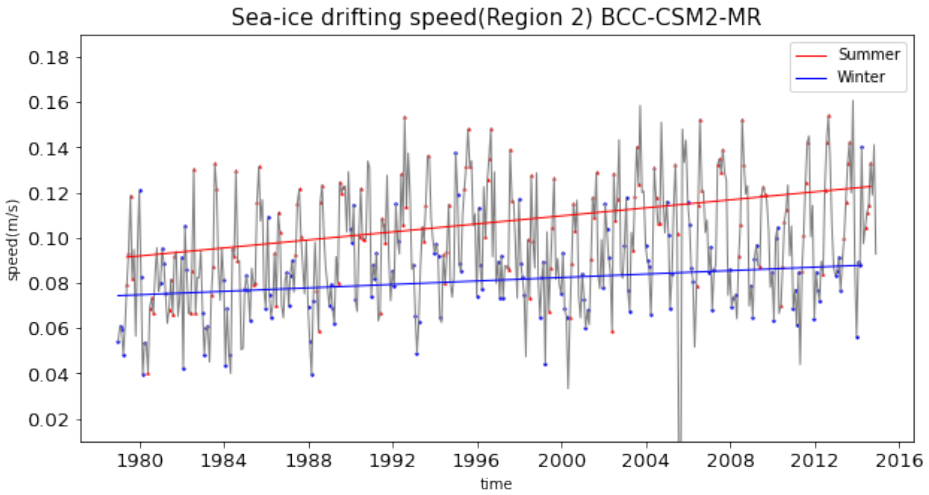

Figure 4.37: BCC-CSM2-MR output time series of sea ice drifting speed from 1979-2014 in region 2

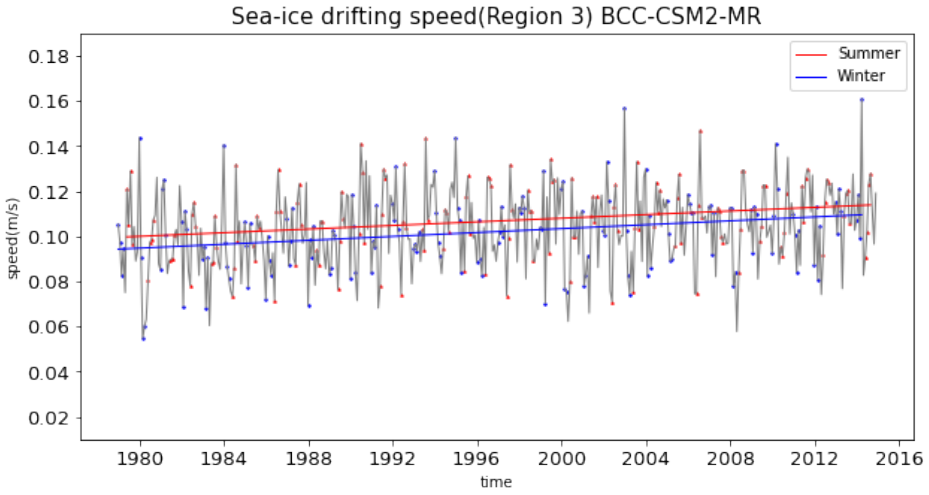

Figure 4.38: BCC-CSM2-MR output time series of sea ice drifting speed from 1979-2014 in region 3

Figure 4.36-4.38 shows the annual variation and summer, winter trend of BCC-CSM2-MR output sea-ice drifting speed in region 1,2 and 3 respectively. In the Arctic,

Summer has faster sea-ice motion than winter. Sea-ice drifting speed is increasing. In region 1 in summer, sea-ice drifting speed increased by 3.9%, in winter increased by 16.51%, and at the end of the studying period, winter speed slightly exceeded summer speed. In region 2, in summer, sea-ice drifting speed increased by 34.18%, and winter increased by 18.09%. In region 3, in summer, sea-ice drifting speed increased by 14.52%, and winter increased by 16.14%. There is no sharp increase in sea-ice motion except summer in region2. According to BCC-CSM2-MR model projection, annual variation and seasonal variation are not as big as in other models. In region1, there is the biggest seasonal variation and sea ice motion is constantly faster than region 2; in region3 summer trend line and winter trend line approach each other, which means a small seasonal variation.

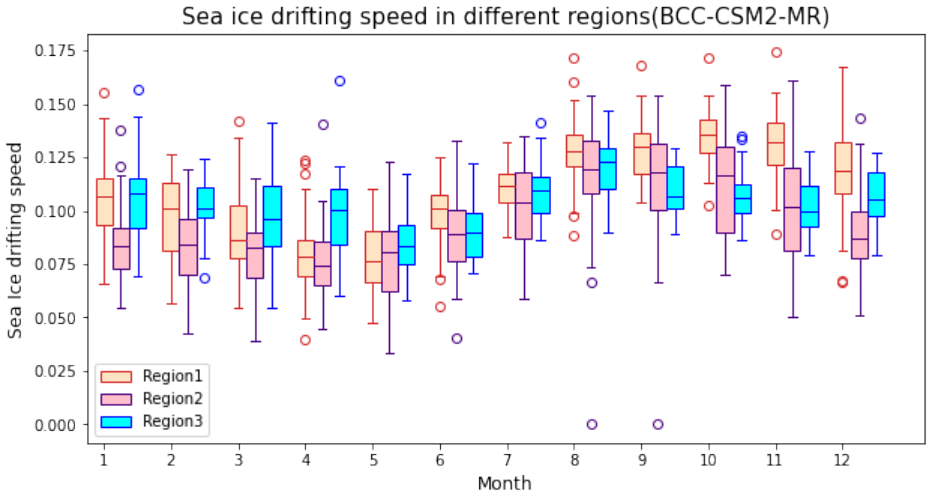

Figure 4.39: Regional comparison of BCC-CSM2-MR output sea-ice drifting speed

Figure 4.39 compares the BCC-CSM2-MR output sea-ice drifting speed between three regions for each month. There is a slight seasonal fluctuation in the Arctic region, which corresponds with the above result. Region 1 has the slowest sea-ice motion in May and the fastest sea-ice motion in November when it far exceeds the other two regions. Region 2 has the slowest sea-ice motion in April and the fastest sea-ice motion in August. Region 3 has the slowest sea-ice motion in May and the fastest sea-ice motion in August. From December to March, sea-ice drifting speed in region 2 is exceedingly lower than in other regions. From February to August(Except June), region 3 has the highest sea-ice drifting speed. From October to December, region 1 has the highest sea-ice drifting speed.

4.4 GFDL-ESM4

GFDL-ESM4 is 4^{th} generation of a new coupled chemistry-carbon-climate Earth system model developed in the Geophysical Fluid Dynamics Laboratory, contributing to

CMIP6. This model focus on climate means patterns and variability. Resolution 0.5 nominally(720 zonal points and 576 meridional points). Physical ocean model is based on MOM6 and SIS2. Five sea ice thickness categories are managed according to a Lagrangian scheme. The separating thickness boundaries for the five thickness levels are 0.1, 0.3, 0.7, and 1.1 m. SIS2 and MOM6 use Arakawa C-grid horizontal stencil. Dynamics is the elastic-viscous-plastic rheology. Thermodynamic model is An energy-conserving thermodynamic which is included in SIS2, model of sea ice. Ice and snow thicknesses are advected with a modified upwind scheme. Tracer advection uses a third-order piecewise parabolic method (Adcroft et al., 2019).

4.4.1 Sea ice extent

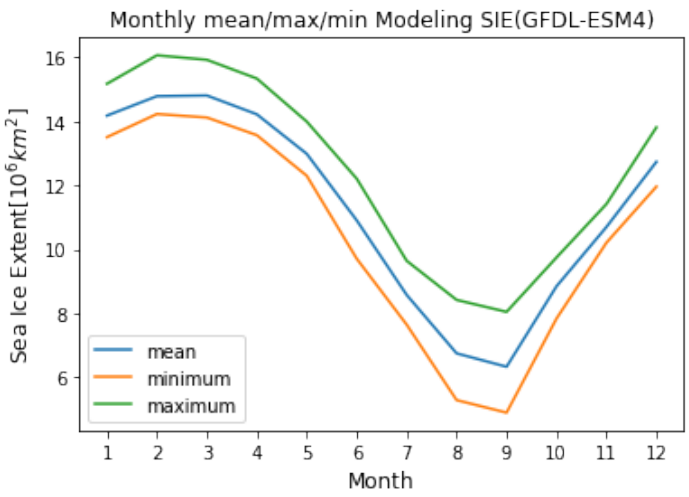

Figure 4.40: GFDL-ESM4 output sea-ice extent mean, maximum and minimum

Figure 4.40 shows the seasonal cycle of sea-ice extent in GFDL-ESM4 model output. It shows sea-ice extent reaches a maximum during February up to $16.06 \times 10^6 km^2$, and minimum during September down to $4.90 \times 10^6 km^2$. Seasonal cycle amplitude of GFDL-ESM4 model output sea-ice extent is $4.24 \times 10^6 km^2$. Maximum sea-ice extent occurs one month earlier than other models. Sea ice shrinks rapidly from May to August and recovers fast from September.

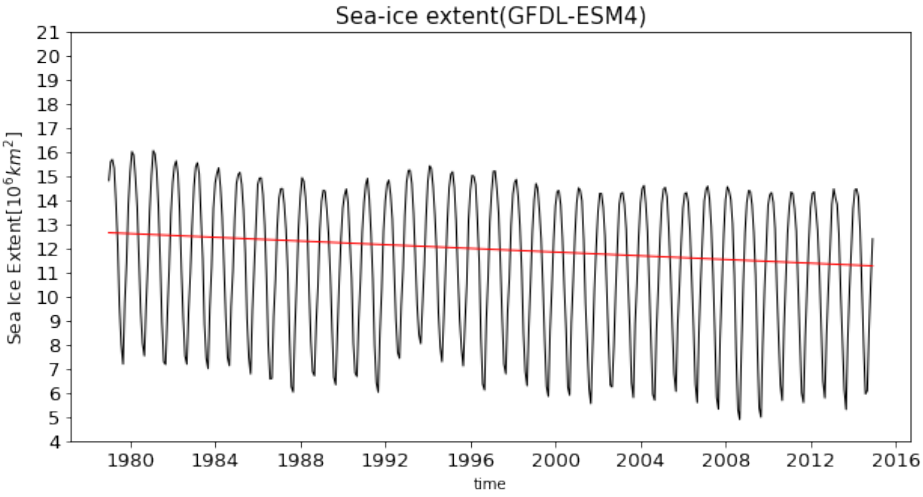

Figure 4.41: GFDL-ESM4 output sea ice extent trend

Figure 4.41 shows the annual variation and trend between 1979-2014 by GFDL-ESM4 model output. There is a decreasing trend of sea-ice extent in general. Sea-ice extent decreased by 10.90%. As in other models, the GFDL output sea-ice extent also has periodical features. From 1979-1990, sea-ice extent has a decreasing period. From 1990-1994 there is a short, increasing period, flowed by decreasing period from 1994-2000. After 1994 sea-ice extent entered a steady state.

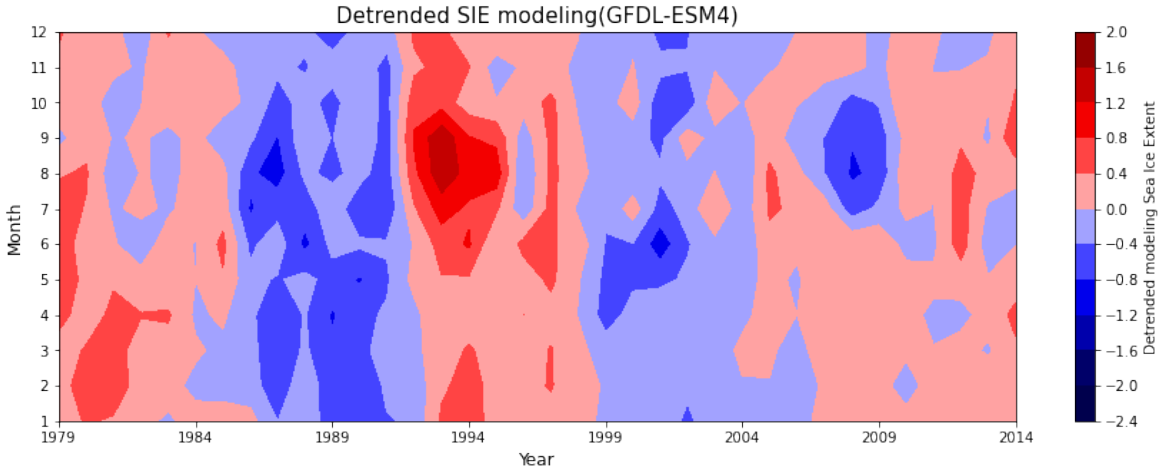

Figure 4.42: GFDL-ESM4 output detrended sea ice extent

Detrended sea ice extent by GFDL-ESM4 output is shown in Figure 4.42. There's decadal variation.

4.4.2 sea-ice thickness

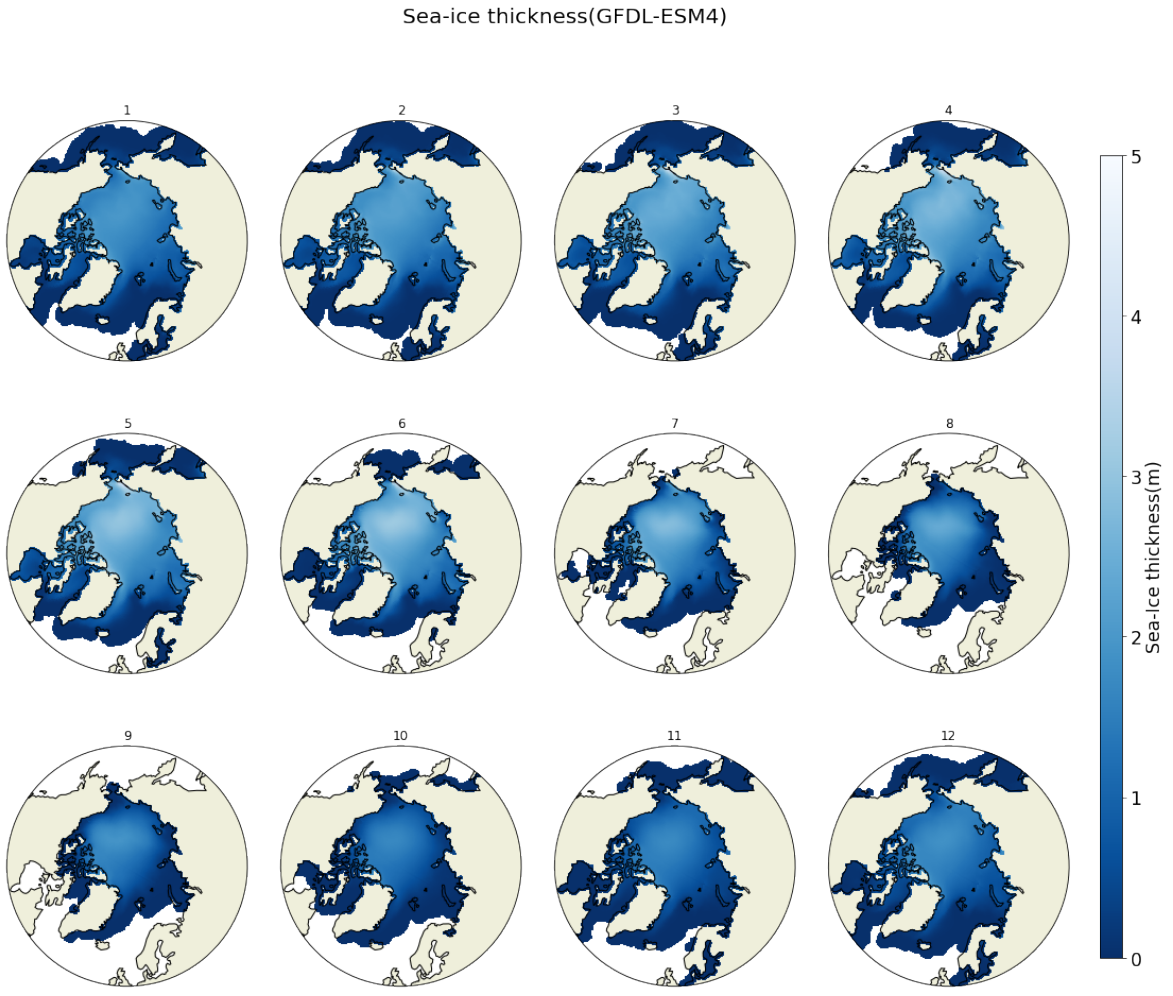

Figure 4.43: GFDL-ESM4 output monthly average sea-ice thickness distribution from 1979-2014

Figure 4.43 shows the monthly average sea-ice thickness distribution of the GFDL-ESM4 model's output. In GFDL-ESM4 model output, there is generally thin ice in the Arctic region compared with other models. Only the central and Peripheral Arctic on the Pacific side have slightly thicker sea ice.

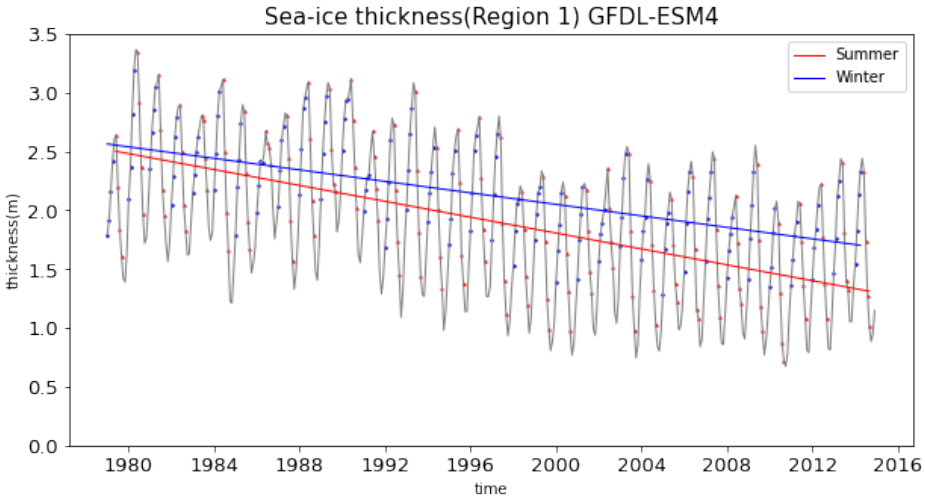

Figure 4.44: GFDL-ESM4 output inter-annual variability of regional average sea-ice thickness from 1979-2014 in region 1

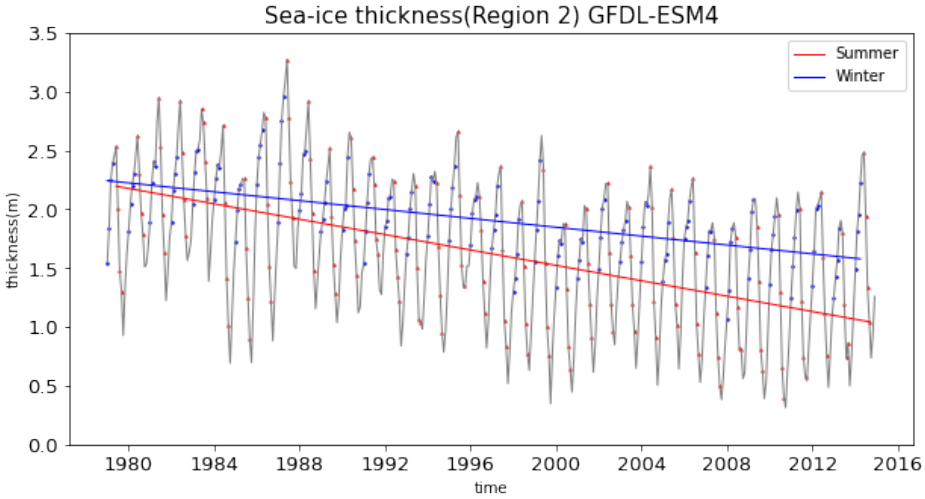

Figure 4.45: GFDL-ESM4 output inter-annual variability of regional average sea-ice thickness from 1979-2014 in region 2

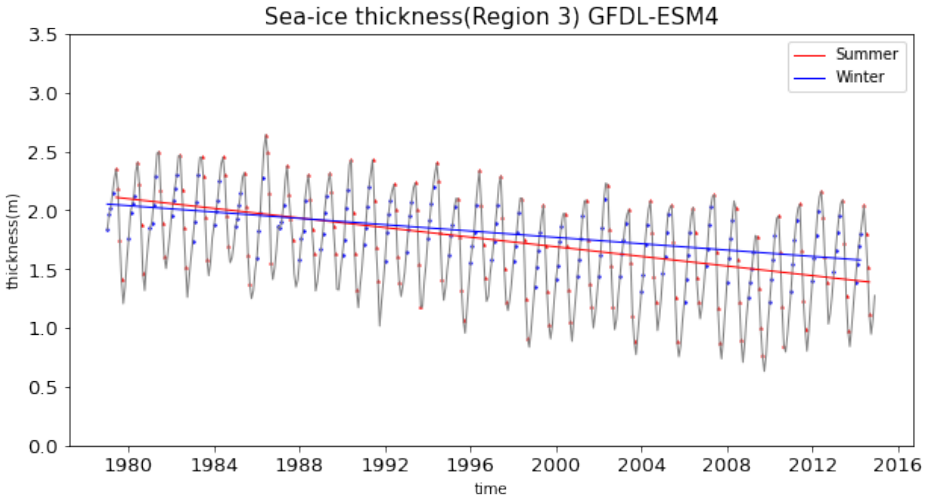

Figure 4.46: GFDL-ESM4 output inter-annual variability of regional average sea-ice thickness from 1979-2014 in region 3

Figure 4.44-4.46 show annual variation and trend of sea-ice thickness by GFDL-ESM4 model projection in summer and winter seasons in three different regions, respectively. The GFDL-ESM4 model projection result shows a decreasing trend in sea-ice thickness. In region 1, in summer, sea-ice thickness decreased by 47.56%, and winter decreased by 33.59%. In region 2, in summer,sea-ice thickness decreased by 52.47%, and winter decreased by 29.61%. In region3, summer sea-ice thickness decreased by 34.10%, and winter sea-ice thickness decreased by 23.14%. In winter, sea ice is thicker than in summer, except in the early 1980s in region 3. In the GFDL-ESM4 model projection result, the thinning effect of sea ice in summer is much stronger than in winter. At the beginning of the studied period, there is barely a seasonal difference in sea-ice thickness; as time goes by due to the much faster summer sea. Ice thinning, the seasonal difference in sea-ice thickness becomes larger. The Central Arctic region still has the slightest seasonal difference among all the regions.

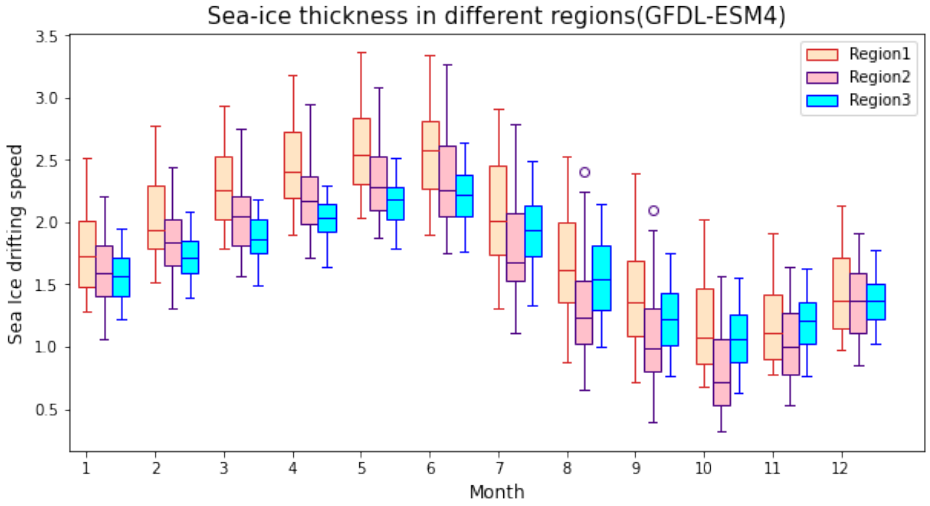

Figure 4.47: Regional comparison of GFDL-ESM4 output sea-ice thickness

Figure 4.47 compares three regions each month for GFDL-ESM4 output sea-ice thickness. The GFDL-ESM4 model result shows a precise and simultaneous seasonal cycle. Sea-ice thickness reaches the highest during May and June and thinnest during October. Region 1 has the thickest sea ice all year round except in November and December. From January to June, region 2 has thicker sea ice than region 3. From July to November, region 3 has thicker sea ice than region 2. November is the only month when region 3 has the thickest sea ice. In December, the sea-ice thickness was almost evenly distributed in regions 1,2, and 3. Region 1 has the most considerable sea-ice thickness annual variation; region 3 has the smallest.

4.4.3 sea-ice motion

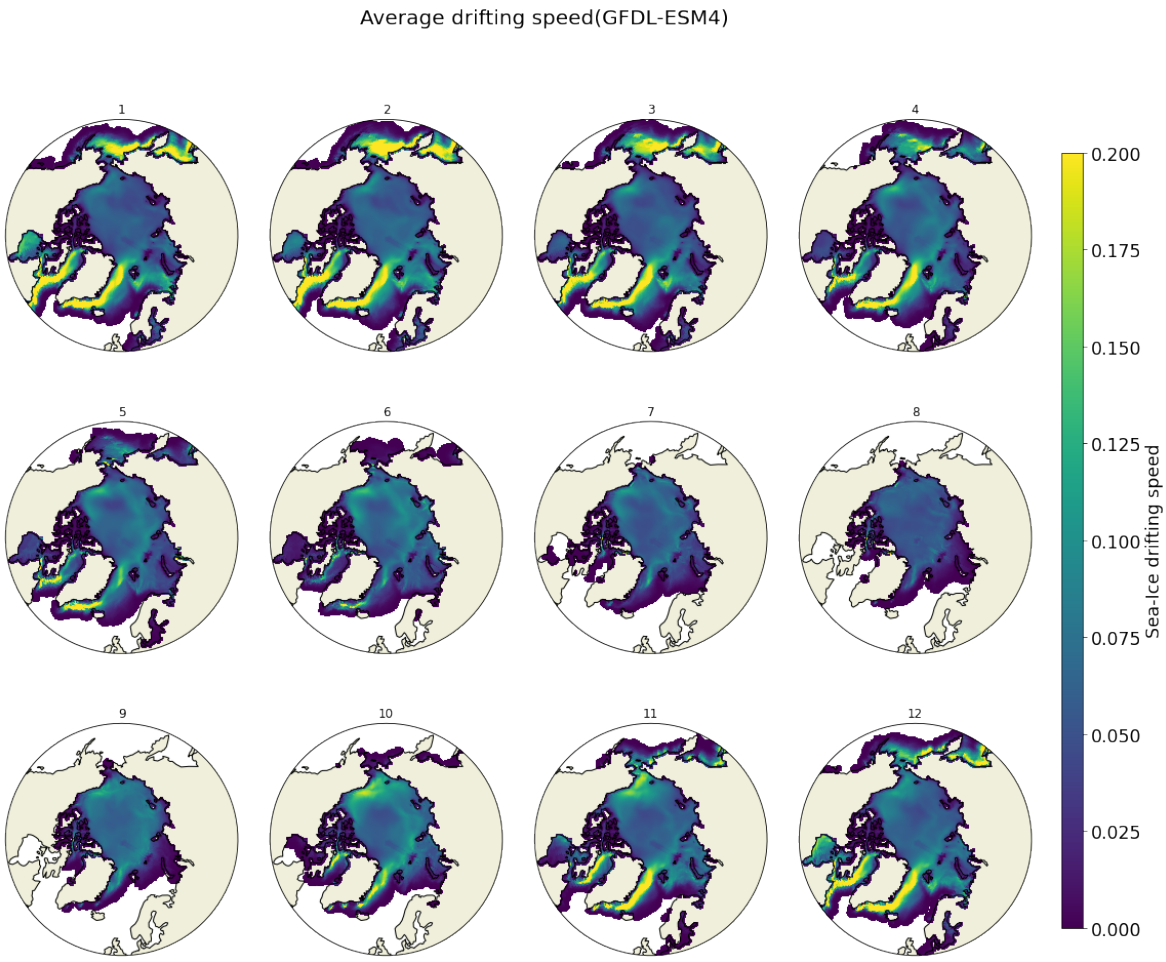

Figure 4.48: GFDL-ESM4 output monthly average sea-ice drifting speed distribution from 1979-2014

Figure 4.48 shows the monthly average sea-ice drifting speed from GFDL-ESM4 output from 1979-2014, and there is apparent regional and seasonal variation. From November to April Greenland sea, the Baffin Bay, and the Labrador sea has active sea-ice motion. The Chukchi Sea has a higher sea-ice drifting speed in October and November. The Bering Sea has a higher sea-ice drifting speed from December to March. The Central Arctic region has low sea-ice drifting speed all year round.

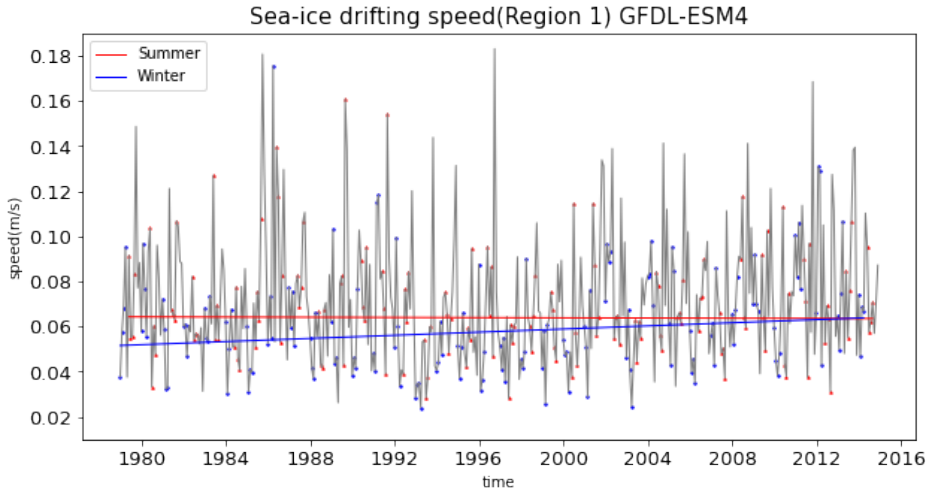

Figure 4.49: GFDL-ESM4 output time series of sea ice drifting speed from 1979-2014 in region 1

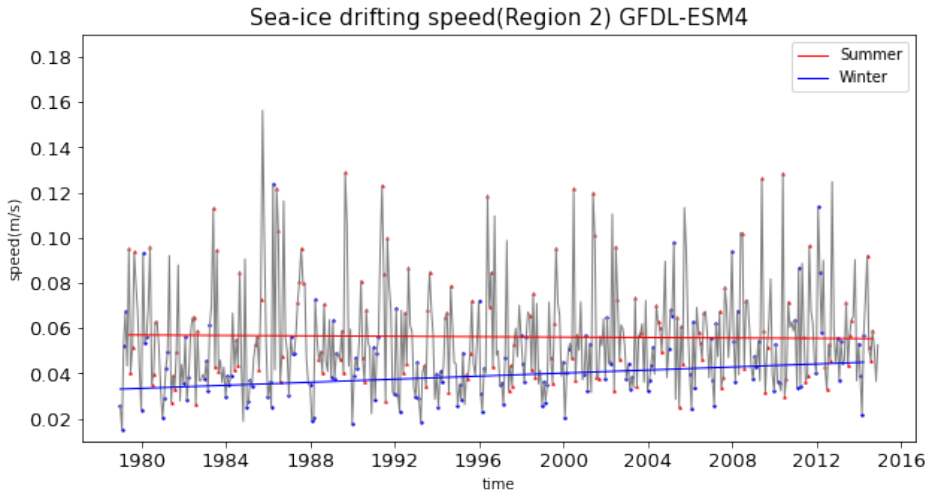

Figure 4.50: GFDL-ESM4 output time series of sea ice drifting speed from 1979-2014 in region 2

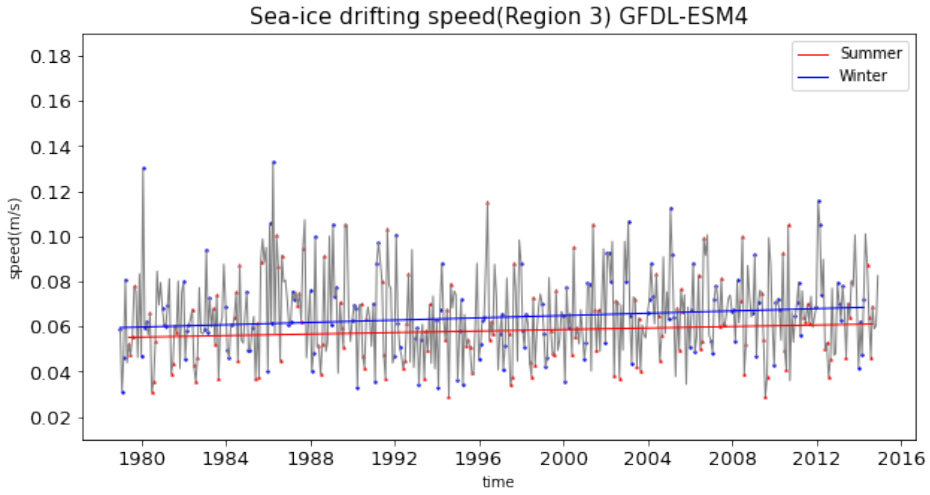

Figure 4.51: GFDL-ESM4 output time series of sea ice drifting speed from 1979-2014 in region 3

Figure 4.49-4.51 show annual variation and trend of sea-ice drifting speed by GFDL-ESM4 model projection in summer and winter seasons in three different regions,

respectively. For sea-ice drifting speed data, the daily data is not available as in other models, so the sea-ice drifting speed value has a lower deviation because monthly drops much detail of sea-ice drifting speed. So GFDL-ESM4 model output sea-ice motion cannot be considered when making an inter-model and model-observation comparison. However, the trend of sea-ice drifting speed can still be considered. GFDL result shows a slowly increasing rate in sea-ice motion; in winter, sea-ice motion increases faster than in summer. In regions 1 and 2, sea-ice motion in summer is faster than in winter, and in region3, it is the opposite. Seasonal variation is not entirely noticeable.

4.5 MPI-ESM1-2-HR

MPI-ESM1-2-HR is Max Planck Institute Earth System Model high resolution. Ocean resolution is 0.4(40km) (Gutjahr et al., 2019a). For sea ice dynamics, MPI-ESM1.2 uses viscoplastic rheology following III, 1979. The sea ice model consists of code both in MPIOM and in ECHAM. In ECHAM, a simplified thermodynamic sea ice model is incorporated to provide a physically consistent surface temperature in ice-covered regions at each atmospheric step. This part of the sea ice model contains a melt-pond scheme, which divides the sea ice surface into the snow, bare ice, and melt pond, with each their albedo (Pedersen et al., 2009). In MPI-ESM1.2, these melt ponds are now fully activated. The thermodynamic model of sea ice is based on a simple zero-layer, a mono-category formulation with only three variables: snow thickness, ice thickness, and surface temperature (Semtner Jr, 1976). Amplitude and phase of seasonal variation of sea-ice thickness are somewhat distorted but have reasonable values for mean annual thickness. There is one ice category.

4.5.1 Sea-extent

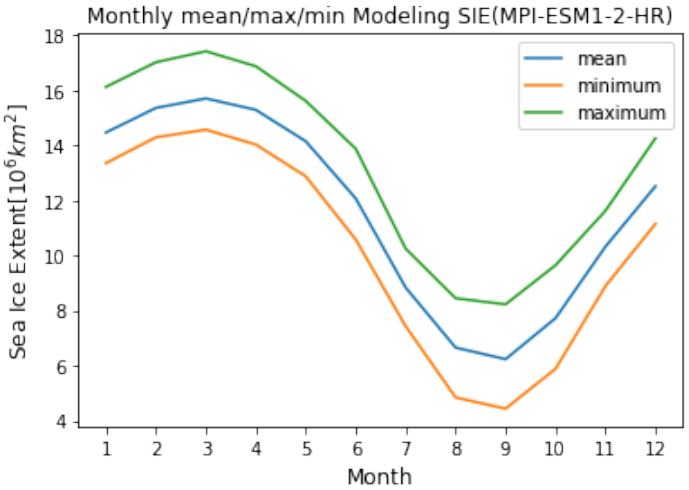

Figure 4.52: MPI-ESM1-2-HR output sea-ice extent mean, maximum and minimum

Figure 4.52 shows the seasonal cycle of sea-ice extent in the MPI-ESM1-2-HR model projection. In MPI-ESM1-2-HR model output, March has the maximum sea-ice extent up to $17.41 \times 10^6 km^2$, and September has the minimum sea-ice extent down to $4.44 \times 10^6 km^2$. The amplitude of the seasonal cycle is approximately $4.73 \times 10^6 km^2$. From May to August, sea-ice extent rapidly decreases; after September, sea-ice extent recovers quickly.

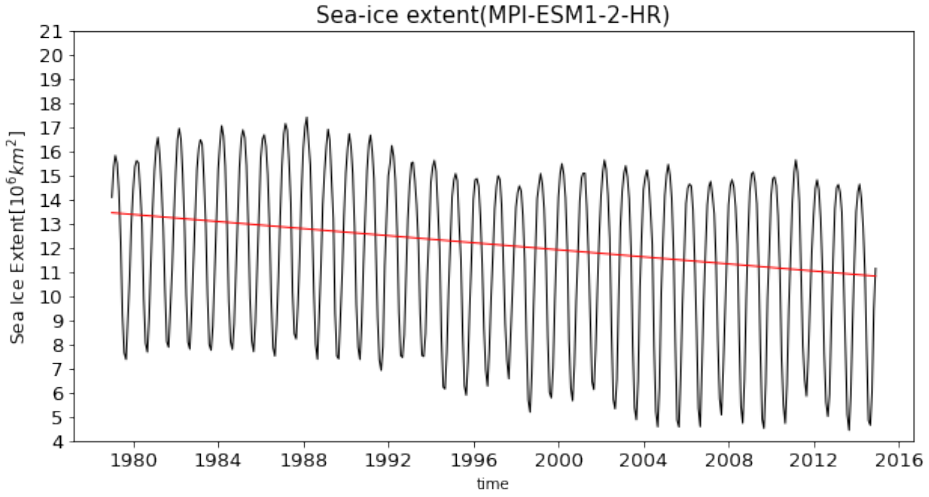

Figure 4.53: MPI-ESM1-2-HR output sea ice extent trend

Figure 4.53 shows the annual variation and trend between 1979-2014 by MPI-ESM1-2-HR model output. There is a decreasing trend in sea-ice extent from 1979-2014. Sea-ice extent decreased by 19.54%. The sea-ice extent has a small increasing period from 1979-1989, and the decreasing period from 1989-1997, which then entered a steady state.

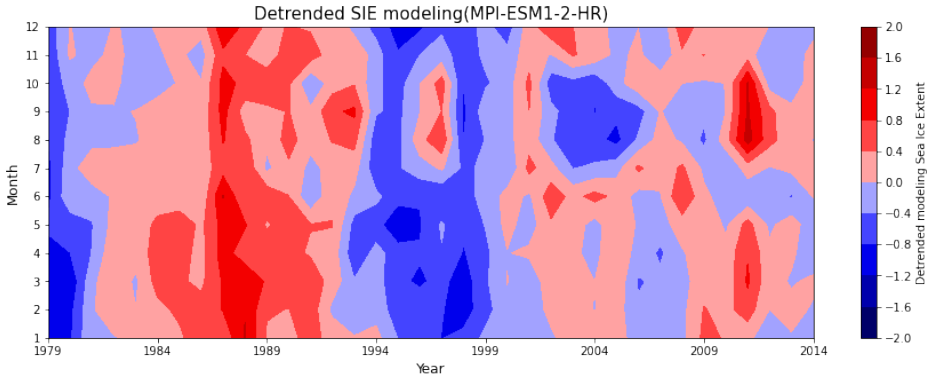

Figure 4.54: MPI-ESM1-2-HR output detrended sea ice extent

Figure 4.54 shows the detrended sea-ice extent for each month between 1979-2014. There decadal variation of sea-ice extent.

4.5.2 Sea-ice thickness

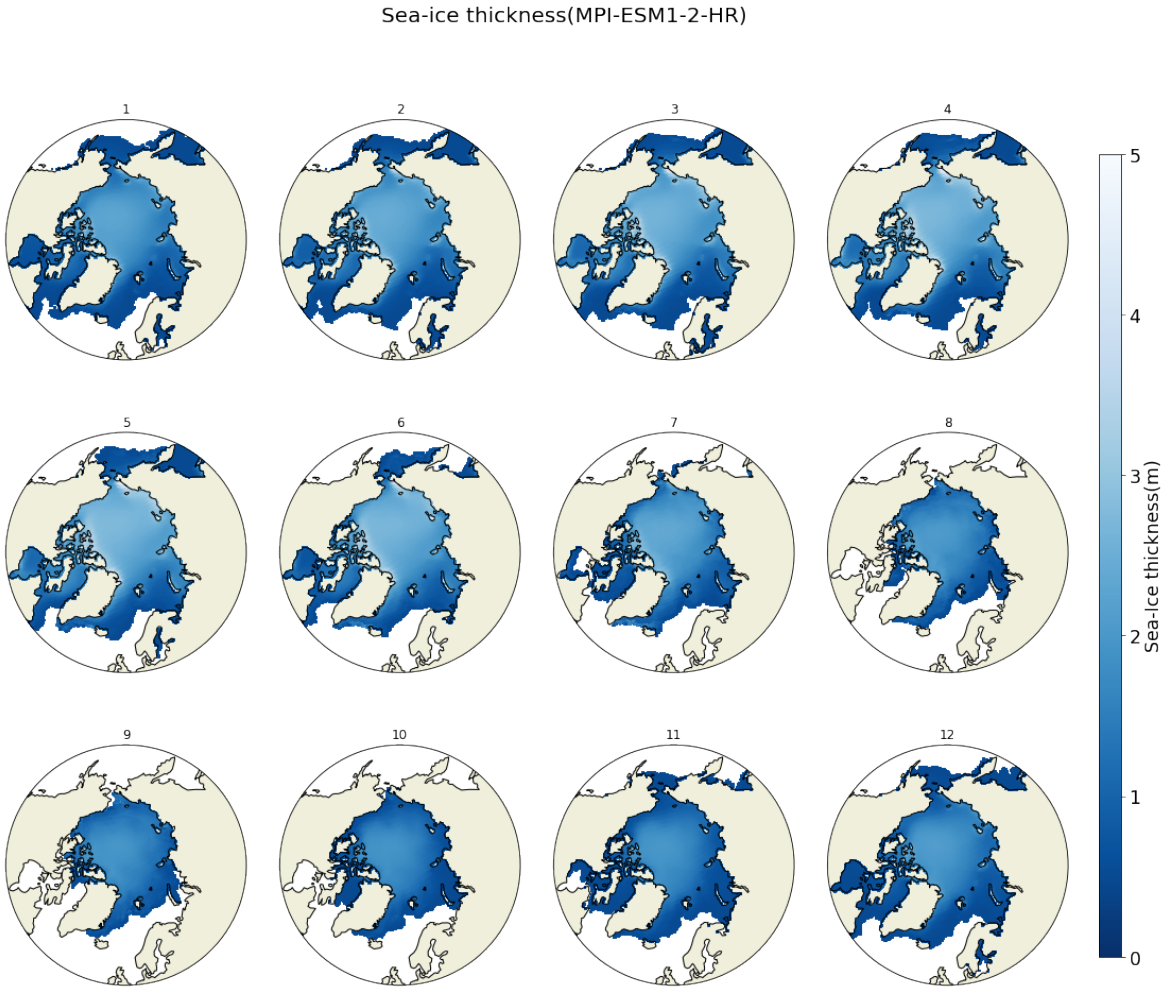

Figure 4.55: MPI-ESM1-2-HR output monthly average sea-ice thickness distribution from 1979-2014

Figure 4.68 shows the monthly average sea-ice thickness distribution of the MPI-ESM1-2-HR model's output. Seasonal variation and regional differences are not significant. The central Arctic and Canadian Archipelago generally have thicker sea ice than the peripheral Arctic. From March to June, the Beaufort Sea, Chukchi Sea, East Siberian Sea, and the Laptev Sea also have slightly higher sea-ice thickness.

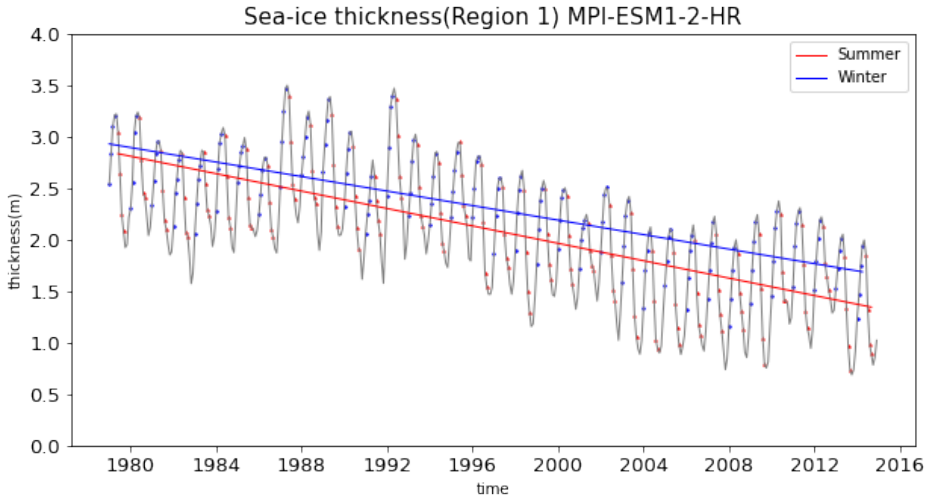

Figure 4.56: MPI-ESM1-2-HR output inter-annual variability of regional average sea-ice thickness from 1979-2014 in region1

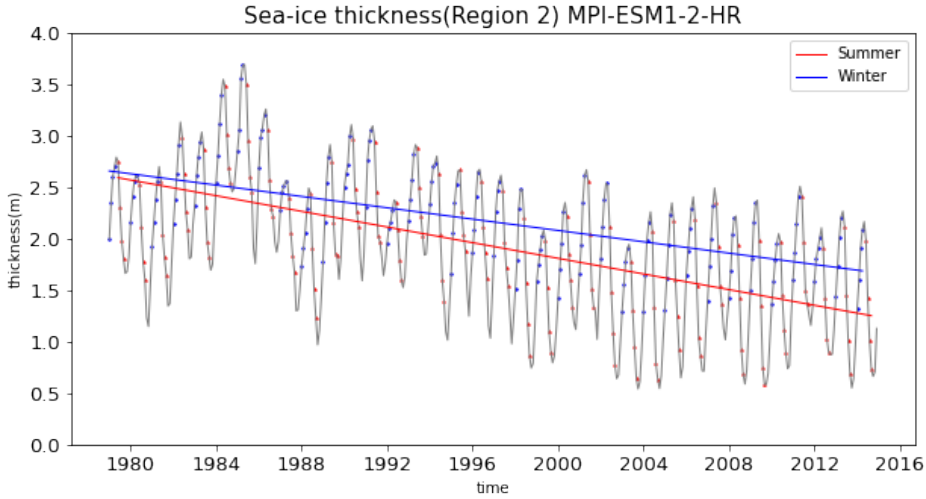

Figure 4.57: MPI-ESM1-2-HR output inter-annual variability of regional average sea-ice thickness from 1979-2014 in region2

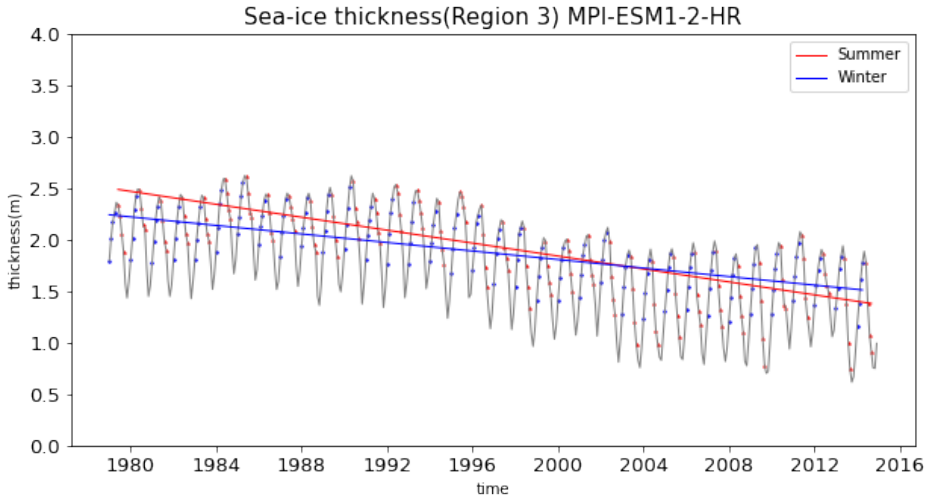

Figure 4.58: MPI-ESM1-2-HR output inter-annual variability of regional average sea-ice thickness from 1979-2014 in region3

MPI-ESM1-2-HR model output result indicates a decreasing trend of sea-ice thickness in the whole Arctic region. Figure 4.56-4.58 show annual variation and trend of sea-ice thickness by MPI-ESM1-2-HR model projection in summer and winter seasons in three different regions, respectively. In regions 1 and 2, winter had higher sea-ice thickness than summer; in region3, before 2002, summer had thicker sea ice; after then, winter sea-ice thickness exceeded summer due to a faster rate of sea-ice thinning in summer. In region1, in summer, sea-ice thickness decreased by 52.56%, and winter decreased by 42.38%. In region2, in summer,sea-ice thickness decreased by 51.69%, and winter decreased by 46.38%. In region3, summer sea-ice thickness decreased by 44.51%; winter sea-ice thickness decreased by 32.55%. Summer has a faster sea-ice thickness decreasing rate than winter, while both summer and winter season's sea-ice thickness decrease rapidly. In regions 1 and 2 in the summer season, there is an apparent sea-ice thinning effect: sea-ice thickness decreased by more than half.

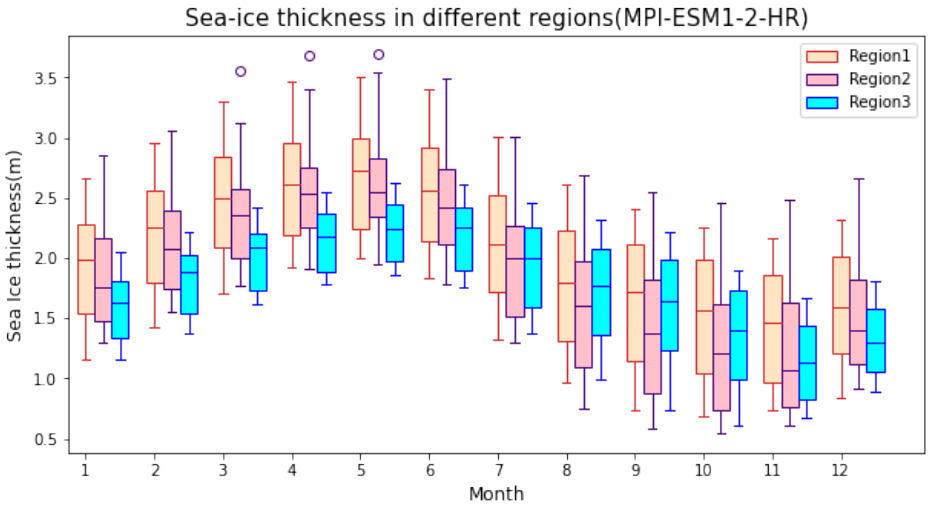

Figure 4.59: Regional comparison of MPI-ESM1-2-HR output sea-ice thickness

Figure 4.59 compares three regions each month for MPI-ESM1-2-HR output sea-ice thickness. There is a simultaneous seasonal cycle shown in the box plot. Maximum sea-ice thickness occurs in May, and minimum sea-ice thickness occurs in November. When comparing sea-ice thickness between regions, from December to June, the ranking order of sea-ice thickness is region1>region2>region3. In July, region1 has thicker sea ice than region2 and 3, region2 and 3 has almost equal sea-ice thickness, while region2 has a more comprehensive annual range. From August to November, the ranking order of sea-ice thickness is region1>region3>region2(referring to average sea-ice thickness).

4.5.3 Sea-ice motion

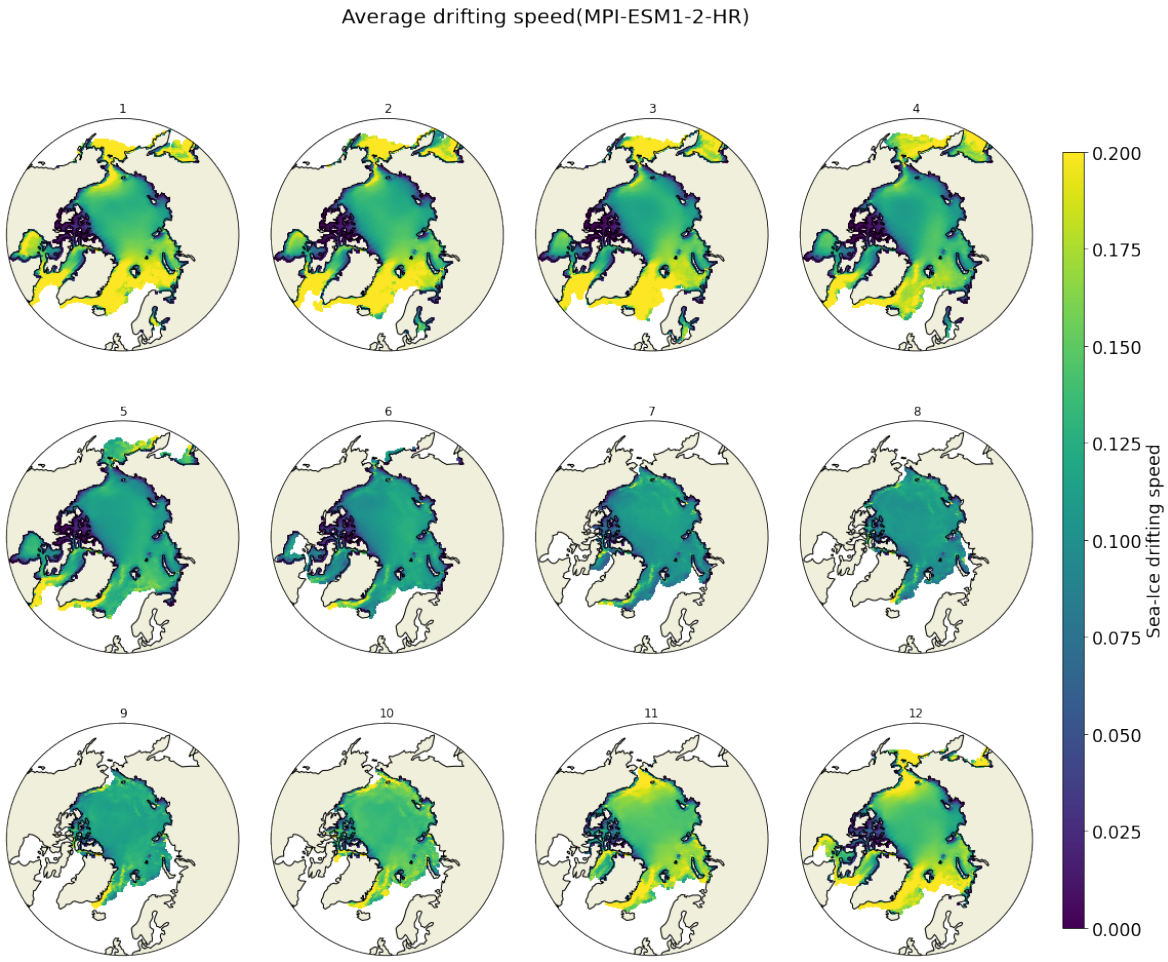

Figure 4.60: MPI-ESM1-2-HR output monthly average sea-ice drifting speed distribution from 1979-2014

Peripheral Arctic has much faster sea-ice motion than the central Arctic, especially on the Atlantic side. Figure 4.60 shows the monthly average sea-ice drifting speed from 1979-2014. From November to April, In the Greenland sea, Barents sea, Chukchi sea, and Bering sea, sea ice has a faster motion than in the central Arctic; in other months, the regional difference in sea-ice motion is not very strong.

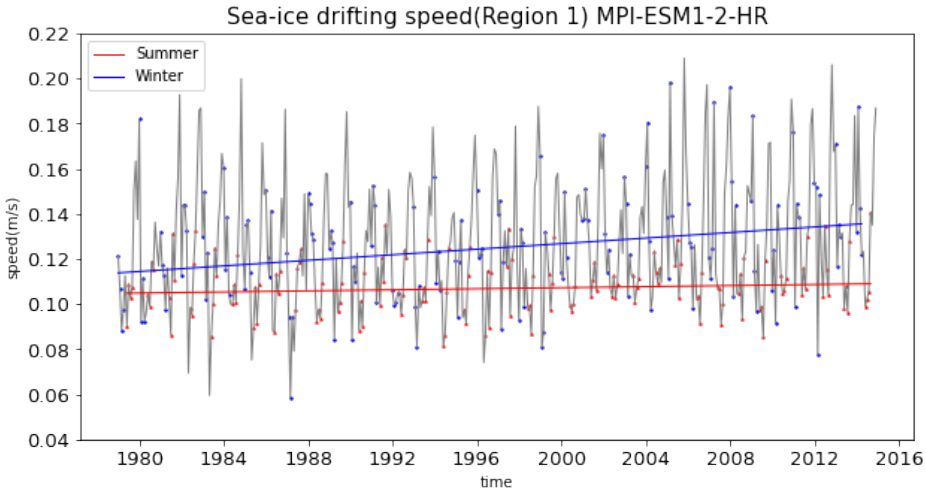

Figure 4.61: MPI-ESM1-2-HR output time series of sea ice drifting speed from 1979-2014 in region1

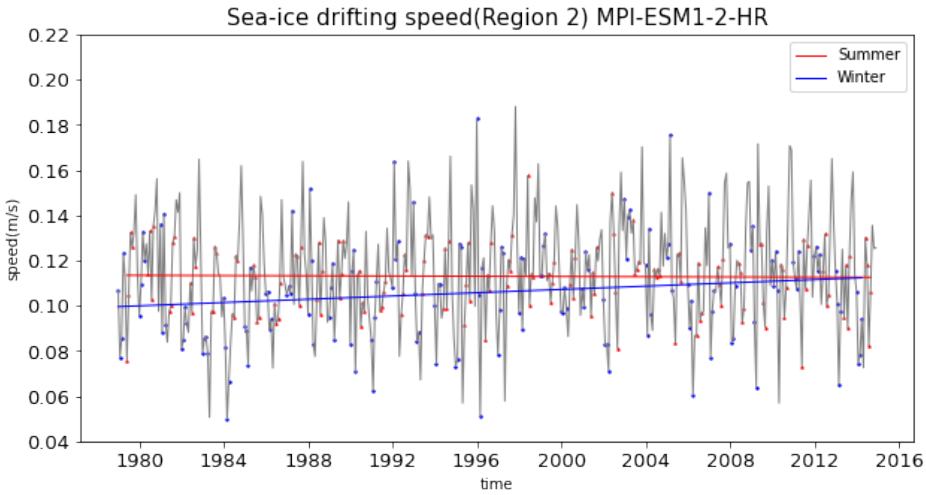

Figure 4.62: MPI-ESM1-2-HR output time series of sea ice drifting speed from 1979-2014 in region2

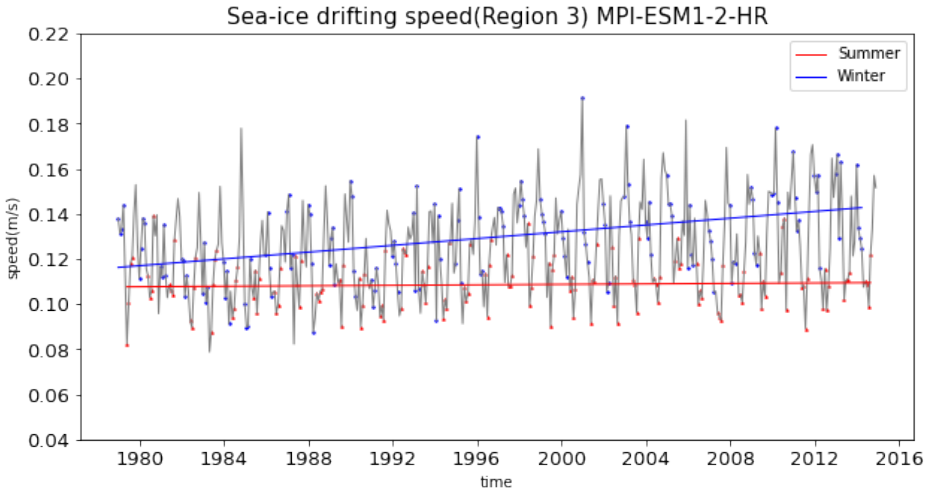

Figure 4.63: MPI-ESM1-2-HR output time series of sea ice drifting speed from 1979-2014 in region3

Figure 4.61-4.63 shows the annual variation and summer, winter trend of MPI-ESM1-2-HR output sea-ice drifting speed in region1,2 and 3 respectively. In winter,

there is a clear increasing trend of sea-ice drifting speed in the Arctic region, while in summer, no clear trend is visible. In regions 1, 2and 3, winter sea-ice drifting speed is higher than summer. Due to the faster increasing rate in winter in region2, the seasonal difference almost disappeared at the end of our studying period.

Winter sea-ice motion increases significantly, while summer sea-ice motion is projected to be stable. In region1, in summer, sea-ice drifting speed increased by 3.96%, in winter increased by 19.09%, and at the end of the studying period, winter speed slightly exceeded summer speed. In region2, in summer, sea-ice drifting speed decreased by 0.79%, and winter increased by 12.83%. In region3, in summer, sea-ice drifting speed increased by 1.72%, and winter increased by 22.78%.

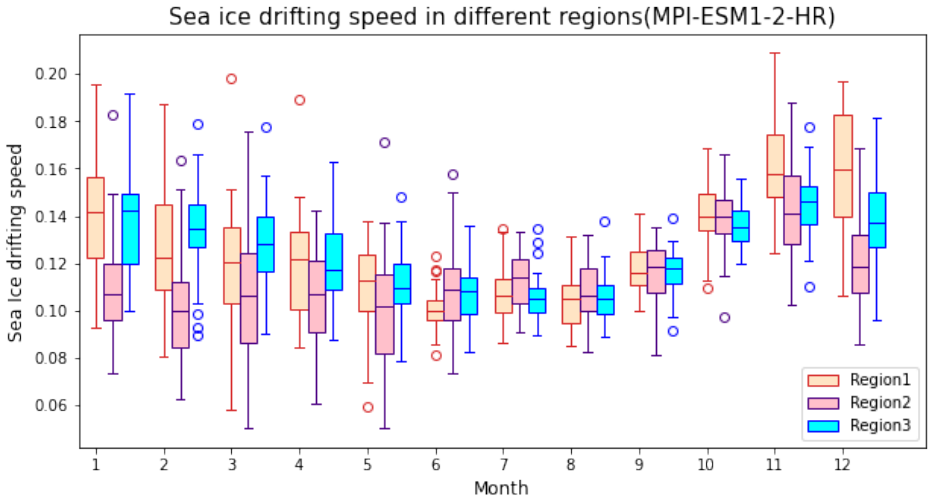

Figure 4.64: Regional comparison of MPI-ESM1-2-HR output sea-ice drifting speed

Figure 4.64 compares the MPI-ESM1-2-HR output sea-ice drifting speed between three regions for each month. The result is quite scattered. There is not a clear united seasonal cycle in the three regions. From November to May, a significant regional difference is noticeable, and from June to October, there is no significant seasonal difference. Winter seasons also have wider annual variation, while sea-ice motion in summer seasons does not have a large variety.

4.6 NorESM2-LM

NorESM2-LM is one version of the Norwegian Earth System Model. It has a horizontal resolution of 1 for the ocean and sea ice components. The sea ice model component is based upon version 5.1.2 of the CICE sea ice model. A NorESM2 specific change includes the effect of wind drift of snow into the ocean following Lecomte et al., 2013. For the CMIP6 configuration of NorESM, the BLOM grid resolution is one zonally and 1/4Â° meridionally at the equator, gradually approaching more isotropic grid cells at higher latitudes. The discretization of the sea ice thickness distribution uses five

thickness categories. The dynamics used in the model are Elastic viscoplastic dynamics. The thermodynamic model is Mushy layer thermodynamics with prognostic internal energy and salinity within the sea ice (Turner and Hunke, 2015). Melt ponds are allowed to form on undeformed ice (Hunke et al., 2013). The freezing point of seawater is salinity-dependent (Assur, 1960).

4.6.1 Sea-ice extent

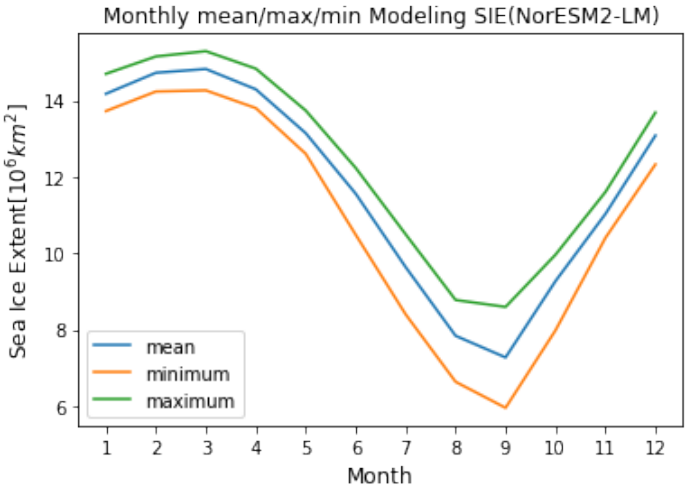

Figure 4.65: NorESM2-LM output sea-ice extent mean, maximum and minimum

Figure 4.65 shows the sea-ice extent seasonal cycle in the NorESM2-LM model projection. In NorESM2-LM model output, March has the maximum sea-ice extent up to $15.29 \times 10^6 km^2$, and September has the minimum sea-ice extent down to $5.95 \times 10^6 km^2$. The amplitude of the seasonal cycle is approximately $3.78 \times 10^6 km^2$. From May to August, sea-ice extent rapidly decreases; after September, sea-ice extent recovers quickly.

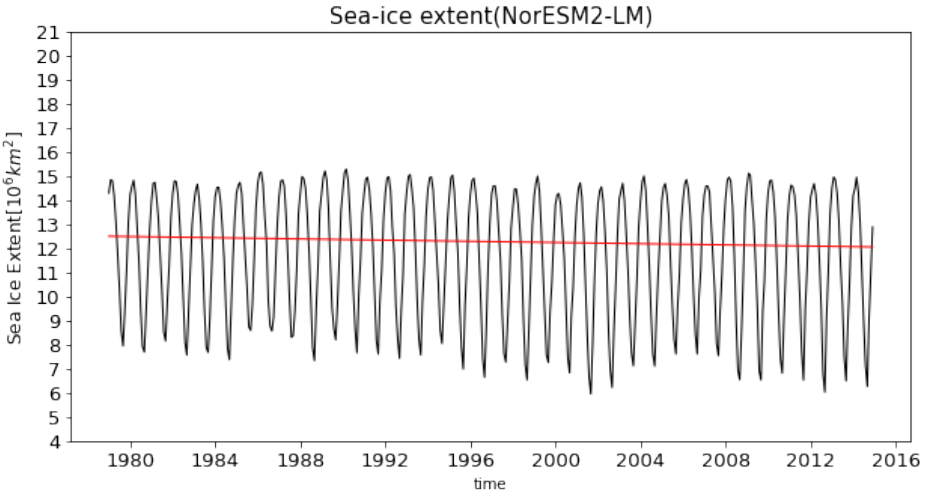

Figure 4.66: NorESM2-LM output sea ice extent trend

Figure 4.66 shows the annual variation and trend between 1979-2014 by NorESM2-LM model output. There is a slight decreasing trend of sea-ice extent from 1979-2014, which decreased by 3.56%. In March, sea-ice extent remains steady for 36 years; in September, there is a slight fluctuation in sea-ice extent.

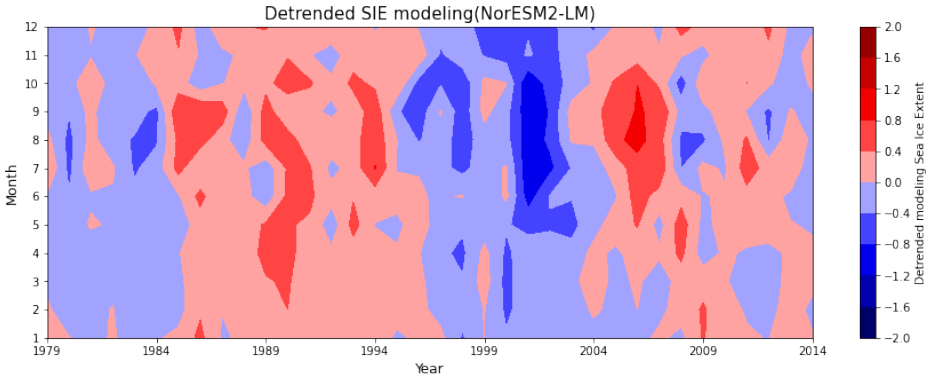

Figure 4.67: NorESM2-LM output detrended sea ice extent

Figure 4.67 shows the detrended sea-ice extent for each month between 1979-2014. There's decadal variation of sea-ice extent.

4.6.2 Sea-ice thickness

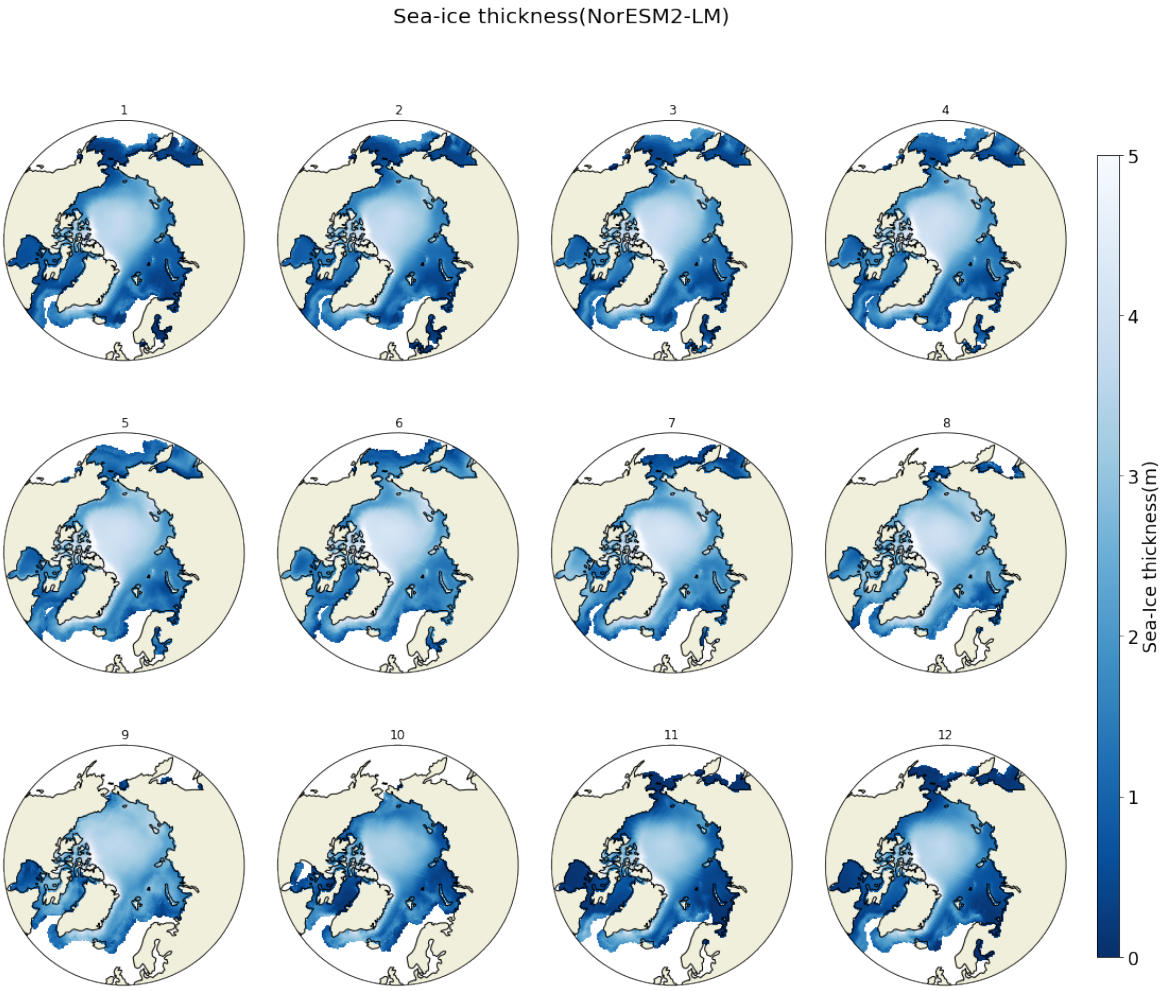

Figure 4.68: NorESM2-LM output monthly average sea-ice thickness distribution from 1979-2014

Figure 4.68 shows the monthly average sea-ice thickness distribution of the NorESM2-LM model's output. NorESM2-LM model's output indicates a generally thicker sea-ice condition than other models. Even though there is a seasonal variation of sea-ice thickness each month, sea-ice thickness distribution follows almost the same rule that there is thicker sea-ice in the central Arctic region, Canadian Archipelago, and on the east coast of the Greenland continent. Peripheral Arctic usually has a thinner sea-ice condition.

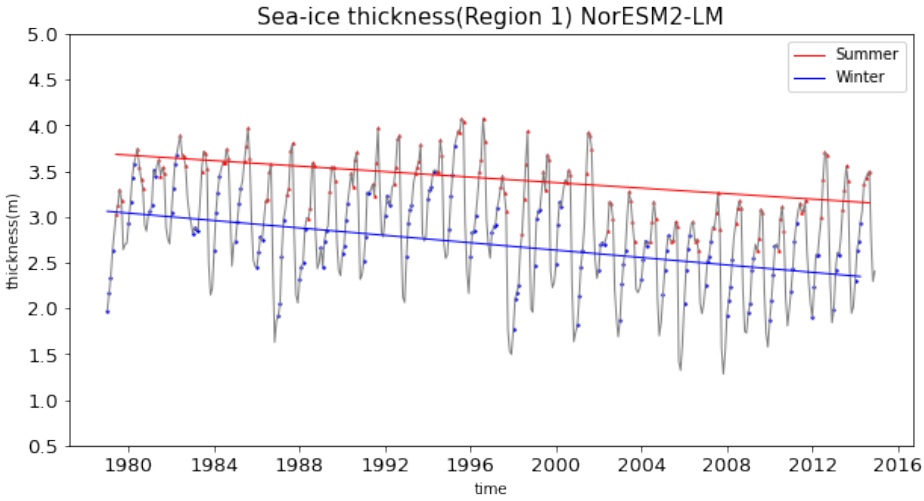

Figure 4.69: NorESM2-LM output inter-annual variability of regional average sea-ice thickness from 1979-2014 in region1

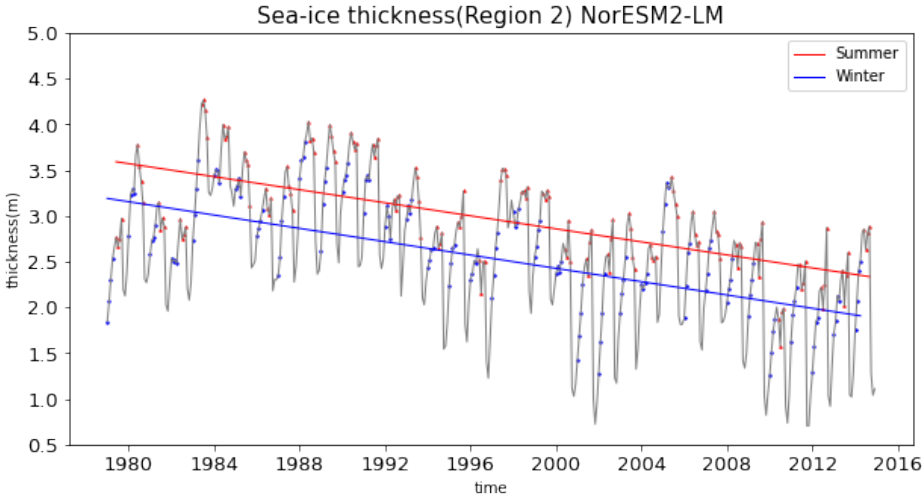

Figure 4.70: NorESM2-LM output inter-annual variability of regional average sea-ice thickness from 1979-2014 in region2

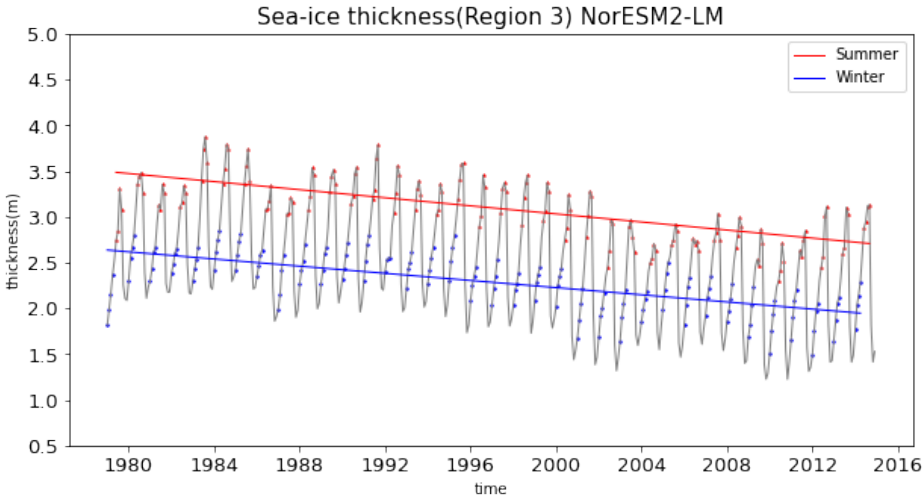

Figure 4.71: NorESM2-LM output inter-annual variability of regional average sea-ice thickness from 1979-2014 in region3

Figure 4.69-4.71 show annual variation and trend of sea-ice thickness by NorESM2-LM model projection in summer and winter seasons in three different regions, respectively. NorESM2-LM model output result indicates a decreasing trend of sea-ice thickness in the whole Arctic region. In the Arctic region, summer seasons have higher sea-ice thickness than winter seasons. In region1, in summer, sea-ice thickness decreased by 14.37%, and winter decreased by 32.28%. In region2, in summer,sea-ice thickness decreased by 34.97%, and winter decreased by 40.21%. In region3, summer sea-ice thickness decreased by 22.31%, and winter sea-ice thickness decreased by 26.14%. Winter has a faster sea-ice thickness decreasing rate than summer, and sea-ice thickness in region2 decreased most rapidly. In all three regions, there is a noticeable seasonal difference.

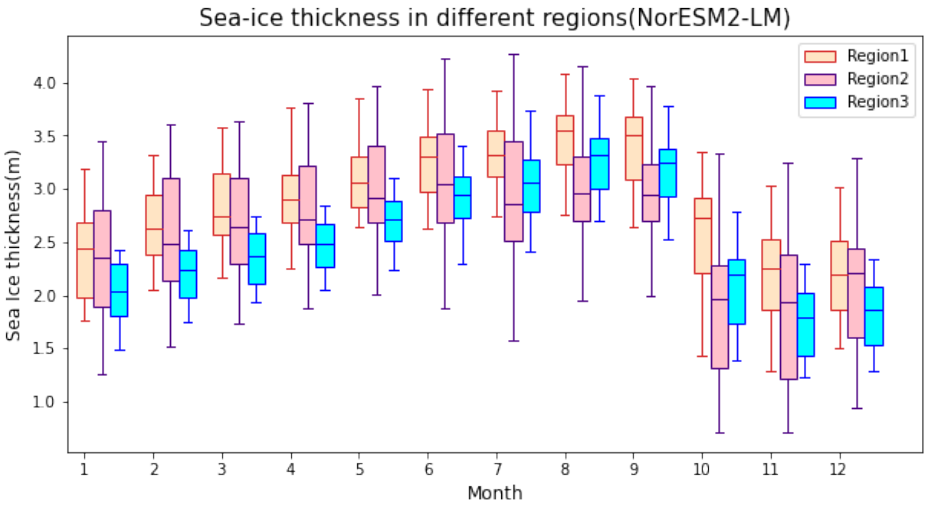

Figure 4.72: Regional comparison of NorESM2-LM output sea-ice thickness

Figure 4.72 compares three regions each month for NorESM2-LM output sea-ice thickness. The box plot shows a simultaneous seasonal cycle for all three regions. For region1 and region3, maximum sea-ice thickness occurs in August, and for region2 in June. Minimum sea-ice thickness occurs in August for all regions. For region1, sea-ice thickness gradually increases from December to August, keeping stable in September, and then decreases sharply from September to November. For region2, sea-ice thickness increase from November to June, become steady until September, then suddenly decrease; in October and November, sea-ice thickness is stable. For region3, the sea-ice thickness increases from November to August, keeping stable in September and suddenly dropping in October. Overall, there was a rapid decrease in sea-ice thickness from September to October.

4.6.3 Sea-ice motion

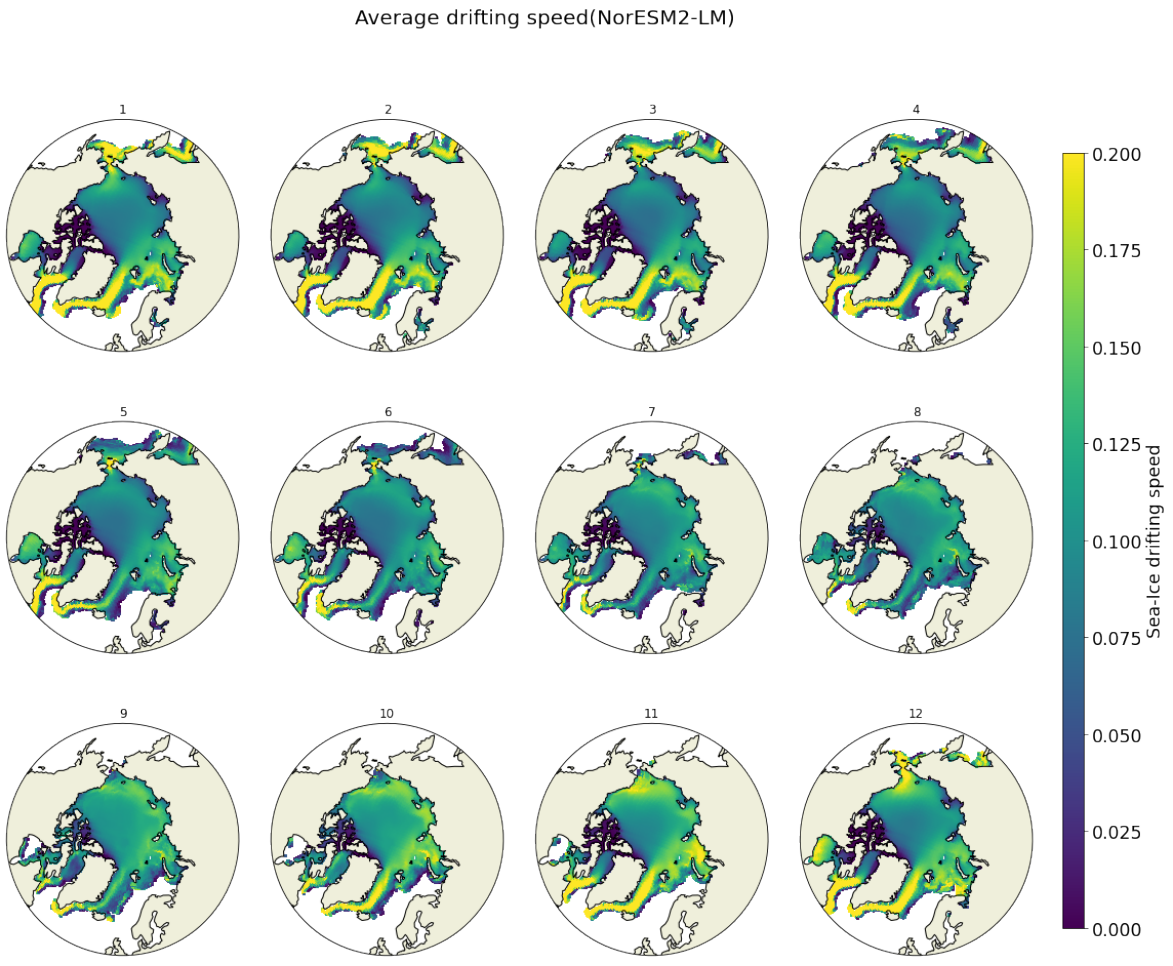

Figure 4.73: NorESM2-LM output monthly average sea-ice drifting speed distribution from 1979-2014

Figure 4.73 shows the monthly average sea-ice drifting speed from 1979-2014. Peripheral Arctic has much faster sea-ice motion than the central Arctic, especially on the Atlantic side. The Greenland Sea has much faster sea-ice motion from October to April than the central Arctic. In November and December, Chukchi has a higher sea-ice drifting speed. The Bering Sea has a higher sea-ice drifting speed from January to April. In the summer, from June to September, sea-ice motion in the Arctic region is generally in a low state.

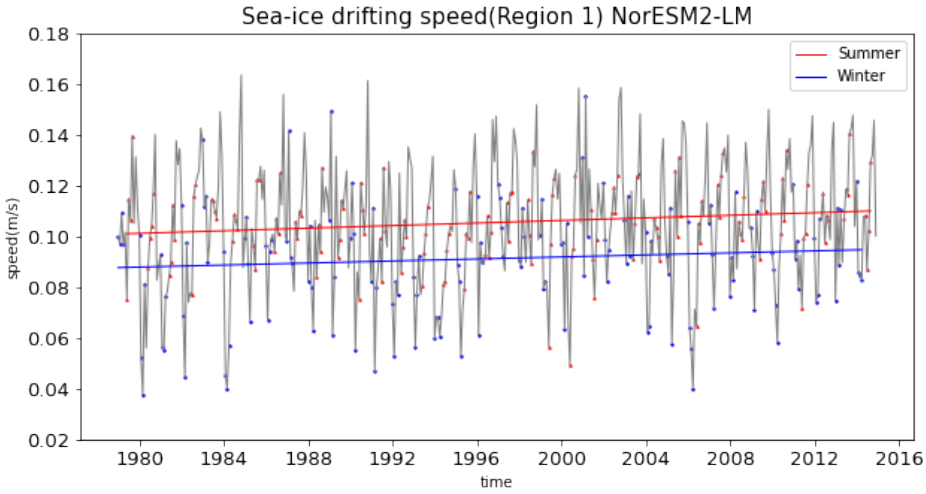

Figure 4.74: NorESM2-LM output time series of sea ice drifting speed from 1979-2014 in region1

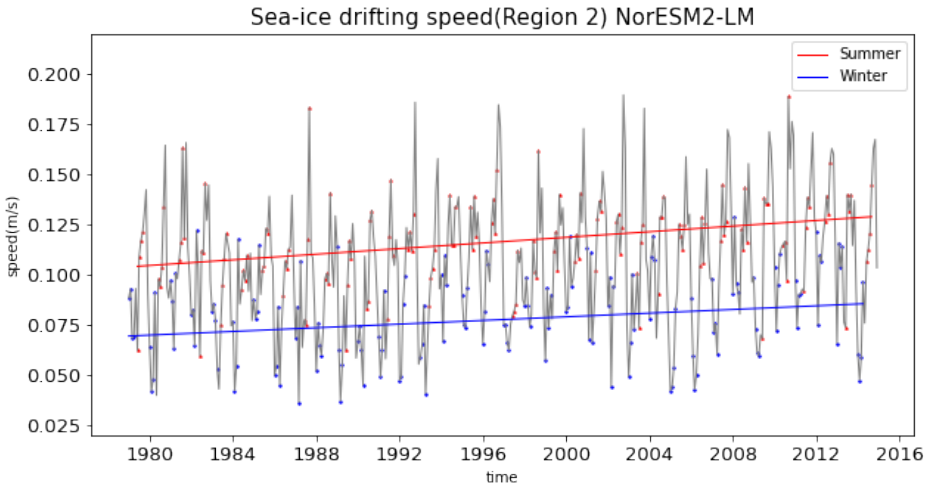

Figure 4.75: NorESM2-LM output time series of sea ice drifting speed from 1979-2014 in region2

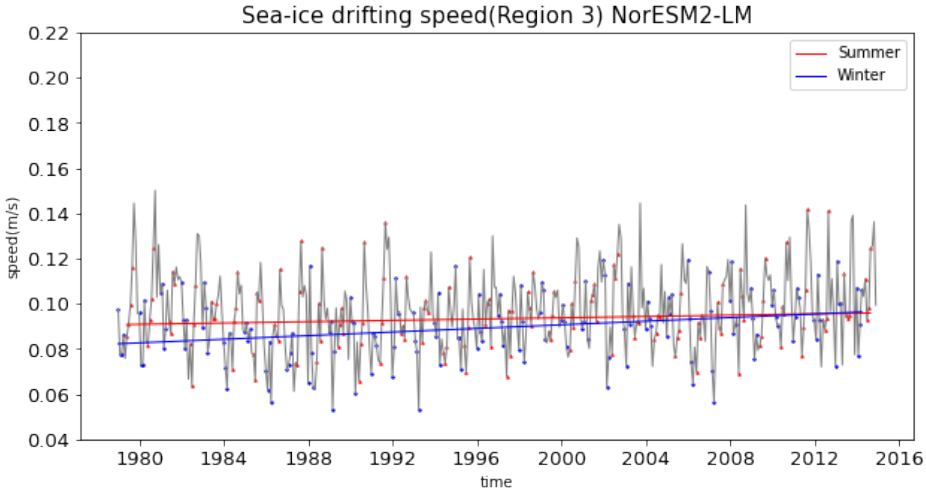

Figure 4.76: NorESM2-LM output time series of sea ice drifting speed from 1979-2014 in region3

Figure 4.74-4.76 shows the annual variation and summer, winter trend of NorESM2-LM output sea-ice drifting speed in region1,2 and 3 respectively. In re-

gion1, in summer, sea-ice drifting speed increased by 8.86%, in winter increased by 8.02%, In region2, in summer, sea-ice drifting speed increased by 23.71%, in winter increased by 23.16%. In region3, in summer, sea-ice drifting speed increased by 5.62%, and winter increased by 17.11%. Winter seasons significantly increase sea-ice motion, while summer sea-ice motion is projected to be stable. In regions 1 and 2, the increasing rate of sea-ice drifting speed in the summer and winter seasons has no big difference; in region3, winter sea-ice drifting speed increased much faster than in summer. Summer has faster sea-ice motion than winter. region2 has the biggest seasonal difference; region3 has the smallest.

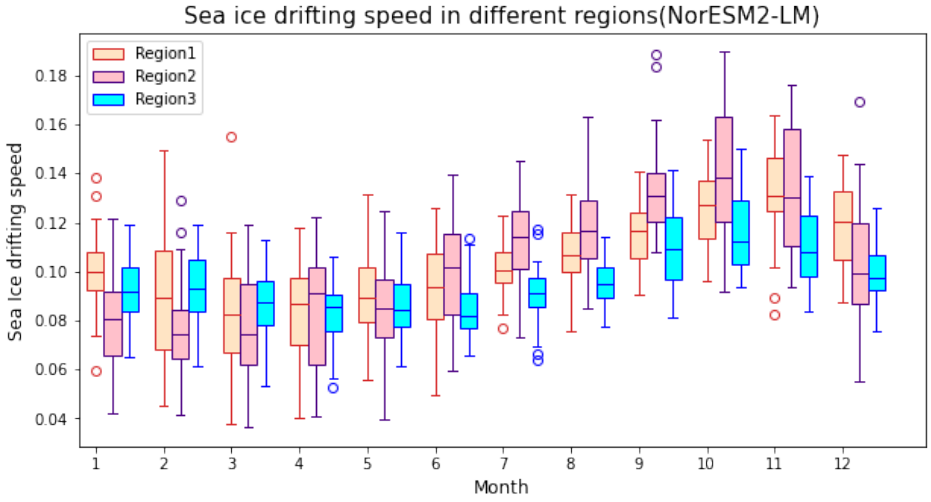

Figure 4.77: Regional comparison of NorESM2-LM output sea-ice drifting speed

Figure 4.77 compares NorESM2-LM output sea-ice drifting speed between three regions for each month. region1 reached the highest sea-ice drifting speed in November, while region2 and region3 reached the maximum sea-ice drifting speed in October, in Arctic, minimum sea-ice motion occurs in March. From January to May, sea-ice motion is steadily in a low state; from June to October, it increases, and sea-ice drifting speed decreases after November. In the case of seasonal cycle amplitude, region2 > region1> region3.

5. Comparison of CMIP6 models to observations

We use independent samples t-test to determine if the observation result and model result have equal mean. Our null assumption is that they have equal population variance, and we set $\alpha = 0.05$. If the P value>0.05, we accept the null assumption, meaning the difference between the model and observation is insignificant. We do t-tests for all twelve months between observation and each model. Each data group has 36 samples, referred to as sea-ice extent data from 1979-2014. Table 5.1-Table 5.6 shows P values in t-test results for EC-Earth3 model, ACCESS-CM2 model, BCC-CSM2-MR model, MPI-ESM1-2-HR model, Nor-ESM2-LM model and GFDL-ESM4 model, respectively. Those values larger than 0.05 mean that model and observation has equal mean.

5.1 Sea-ice extent

5.1.1 Observation sea-ice extent

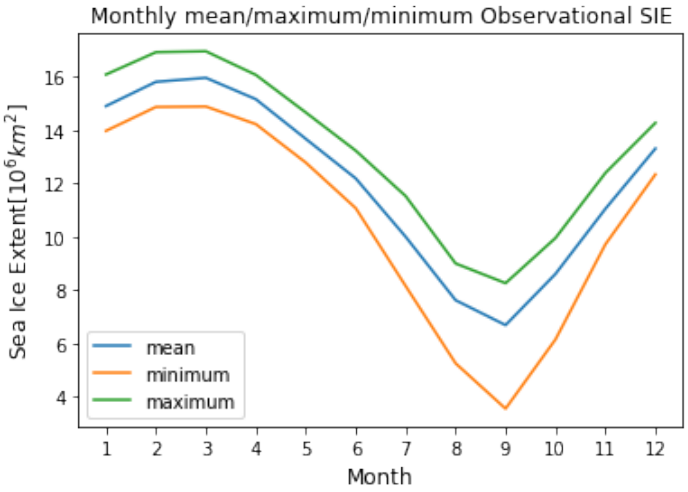

Figure 5.1: Observation sea-ice extent mean,maximum and minimum

Figure 5.1 shows the seasonal cycle of sea-ice extent in the observation result. March has the maximum sea-ice extent up to $16.95 \times 10^6 km^2$, and September has the

Table 5.1: P value in t-test result comparing EC-Earth3 model with observation

EC-Earth3	P value					
	Sea-ice extent	Sea-ice thickness		Sea-ice motion		
	Whole Arctic	1	2	1	2	3
January	0.00	0.00	0.00	0.20	0.65	0.20
February	0.00	0.00	0.00	0.04	0.87	0.04
March	0.00	0.00	0.00	0.00	0.28	0.00
April	0.00	0.00	0.00	0.93	0.62	0.93
May	0.00	0	0	0.23	0.83	0.23
June	0.00	0	0	0.26	0.01	0.26
July	0.00	0	0	0.67	0.62	0.67
August	0.00	0	0	0.06	0.01	0.06
September	0.00	0	0	0.00	0.20	0.00
October	0.00	0.00	0.00	0.41	0.00	0.41
November	0.00	0.00	0.00	0.31	0.16	0.31
December	0.00	0.00	0.00	0.24	091	0.24

Table 5.2: P value in t-test result comparing ACCESS-CM2 model with observation

ACCESS-CM2	P value					
	Sea-ice extent	Sea-ice thickness		Sea-ice motion		
	Whole Arctic	1	2	1	2	3
January	0.01	0.00	0.00	0.18	0.21	0.18
February	0.00	0.00	0.00	0.95	0.34	0.00
March	0.00	0.00	0.00	0.06	0.46	0.00
April	0.00	0.00	0.00	0.00	0.94	0.00
May	0.00	0	0	0.12	0.93	0.01
June	0.00	0	0	0.00	0.00	0.00
July	0.03	0	0	0.01	0.02	0.00
August	0.61	0	0	0.44	0.75	0.00
September	0.48	0	0	0.59	0.95	0.00
October	0.63	0.00	0.00	0.48	0.29	0.33
November	0.46	0.00	0.00	0.60	0.32	0.13
December	0.49	0.00	0.00	0.78	0.20	0.55

Table 5.3: P value in t-test result comparing BCC-CSM2-MR model with observation

BCC-CSM2-MR	P value					
	Sea-ice extent	Sea-ice thickness		Sea-ice motion		
	Whole Arctic	1	2	1	2	3
January	0.00	0.00	0.01	0.76	0.88	0.03
February	0.00	0.00	0.24	0.13	0.54	0.00
March	0.00	0.00	0.01	0.00	0.47	0.01
April	0.00	0.00	0.00	0.41	0.71	0.00
May	0.00	0	0	0.01	0.58	0.59
June	0.00	0	0	0.68	0.96	0.01
July	0.00	0	0	0.26	0.06	0.00
August	0.00	0	0	0.93	0.01	0.00
September	0.00	0	0	0.05	0.02	0.31
October	0.00	0.00	0.00	0.98	0.00	0.66
November	0.00	0.00	0.00	0.47	0.01	0.84
December	0.00	0.00	0.00	0.99	0.52	0.48

Table 5.4: P value in t-test result comparing MPI-ESM1-2-HR model with observation

MPI-ESM1-2-HR	P value					
	Sea-ice extent	Sea-ice thickness		Sea-ice motion		
	Whole Arctic	1	2	1	2	3
January	0.00	0.41	0.00	0.00	0.02	0.00
February	0.01	0.17	0.00	0.00	0.01	0.00
March	0.14	0.05	0.00	0.00	0.00	0.00
April	0.44	0.01	0.00	0.00	0.00	0.00
May	0.00	0	0	0.00	0.38	0.00
June	0.47	0	0	0.30	0.05	0.00
July	0.74	0	0	0.73	0.94	0.00
August	0.00	0	0	0.90	0.00	0.00
September	0.12	0	0	0.00	0.01	0.01
October	0.00	0.24	0.57	0.44	0.36	0.00
November	0.00	0.01	0.03	0.00	0.04	0.00
December	0.00	0.02	0.78	0.00	0.01	0.00

Table 5.5: P value in t-test result comparing Nor-ESM2-LM model with observation

Nor-ESM2-LM	P value					
	Sea-ice extent	Sea-ice thickness		Sea-ice motion		
	Whole Arctic	1	2	1	2	3
January	0.00	0.00	0.00	0.28	0.23	0.39
February	0.00	0.00	0.00	0.99	0.57	0.22
March	0.00	0.00	0.00	0.03	0.40	0.65
April	0.00	0.00	0.00	0.13	0.34	0.18
May	0.00	0	0	0.71	0.88	0.27
June	0.00	0	0	0.63	0.06	0.37
July	0.05	0	0	0.51	0.94	0.79
August	0.27	0	0	0.00	0.00	0.68
September	0.01	0	0	0.00	0.42	0.21
October	0.00	0.00	0.00	0.19	0.52	0.12
November	0.87	0.00	0.01	0.65	0.25	0.14
December	0.04	0.00	0.00	0.92	0.76	0.16

Table 5.6: P value in t-test result comparing GFDL-ESM4 model with observation

GFDL-ESM4	P value		
	Sea-ice extent	Sea-ice thickness	
	Whole Arctic	1	2
January	0.00	0.09	0.04
February	0.00	0.05	0.00
March	0.00	0.02	0.00
April	0.00	0.00	0.00
May	0.00	0	0
June	0.00	0	0
July	0.00	0	0
August	0.00	0	0
September	0.13	0	0
October	0.22	0.87	0.00
November	0.01	0.00	0.07
December	0.00	0.10	0.64

minimum sea-ice extent down to $3.56 \times 10^6 km^2$. The amplitude of the seasonal cycle is approximately $4.63 \times 10^6 km^2$. From April to September, sea-ice extent decreases rapidly; after September, sea-ice extent recovers quickly.

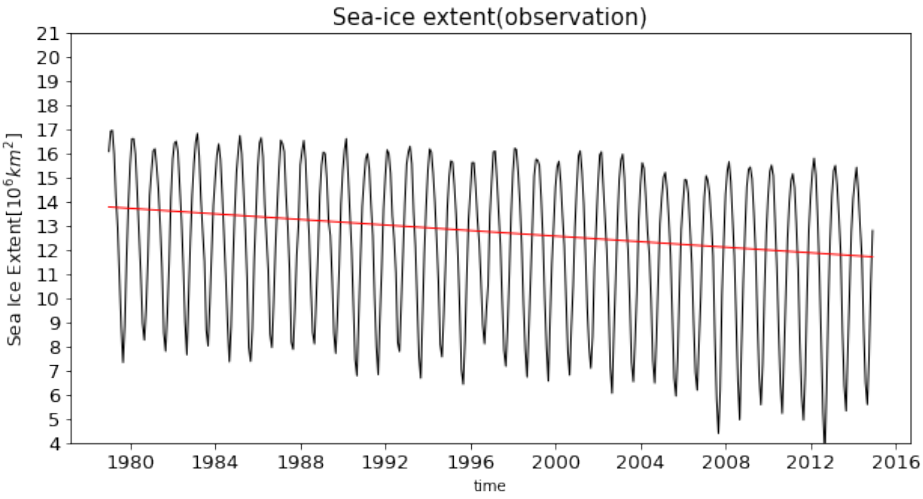

Figure 5.2: Observation sea ice extent trend

Figure 5.2 shows the annual variation and trend between 1979-2014 by observation. There is a decreasing trend of sea-ice extent from 1979-2014 that sea-ice extent decreased by 15.00%. Before 2000, the decreasing trend of sea-ice extent was not prominent enough; in the first decade of the 21st-century sea-ice extent, sea-ice extent decreased most rapidly.

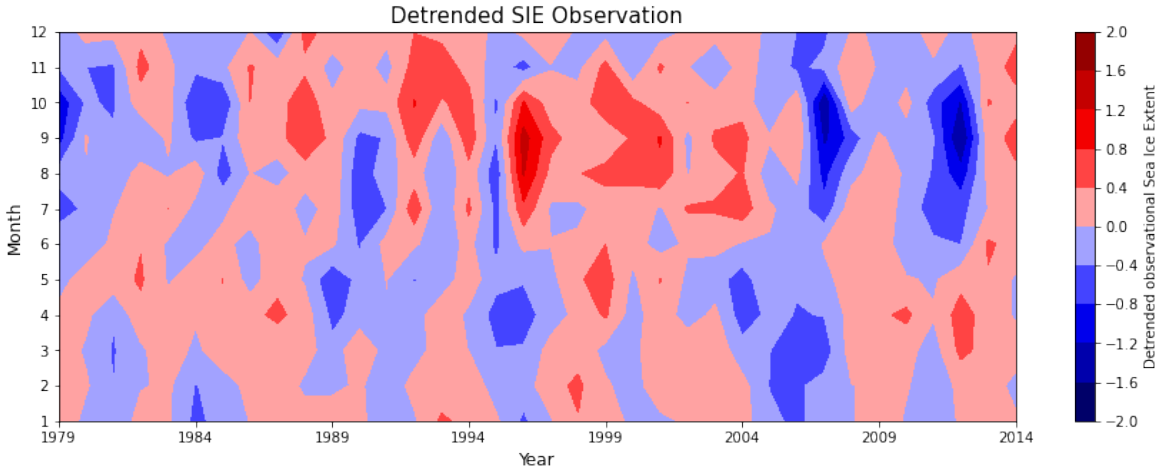

Figure 5.3: Observation detrended sea ice extent

Figure 5.3 shows the detrended sea-ice extent for each month between 1979-2014 from observation result. There's more frequent variation of sea-ice extent.

5.1.2 Comparison of Sea ice extent between CMIP6 and observation

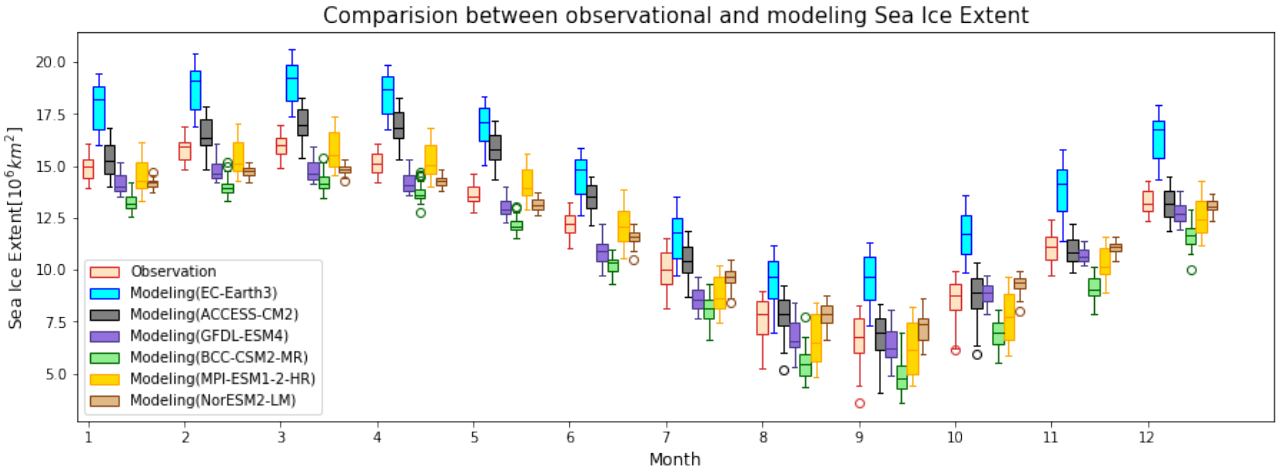

Figure 5.4: Comparison of Sea ice extent between CMIP6 and observation

Figure 5.4 compared 5 CMIP6 models' result with observation result of sea-ice extent. EC-Earth3 has the highest deviation among all the models: sea-ice extent is much greater than the observation result, especially in winter. According to Table 5.1, EC-Earth3 model output sea-ice extent is significantly different from observation.
For ACCESS-CM2 model, according to Table 5.2, from August to December it has a good estimation result, while from January to July it overestimate sea-ice extent.
For GFDL-ESM4 model, according to Table 5.6, in most cases it is underestimating sea-ice extent, except from September to October when GFDL-ESM4 model provides an plausible estimation.
For BCC-CSM2-MR model, according to Table 5.3, all of them is much lower than 0.05, means BCC-CSM2-MR model is constantly underestimating sea-ice extent and has a significant deviation compared with observation
For MPI-ESM1-2-HR model, according to Table 5.4, it provides an almost perfect estimation for March, April, June, and September. It underestimates sea-ice extent in January, February, July, August, October, November, and December. In May, it is overestimating sea-ice extent.
For NorESM2-LM model, according to Table 5.5, from January to June, the NorESM2-LM model underestimates sea-ice extent; In July, August, November, and December, it reasonably estimates sea-ice extent. In September and October, it overestimates sea-ice extent.NorESM2-LM model shows a much smaller annual range than any other model result or observation result.

To summarize the evaluation of CMIP6 models, EC-Earth3 is overestimating sea

ice extent, BCC-CSM2-MR model underestimates all year round. Other models more or less have some months when they reasonably estimate sea-ice extent. ACCESS-CM2 overestimates sea-ice extent in the first half of the year, GFDL-ESM4 underestimates except autumn, MPI-ESM1-2-HR and NorESM2-LM model have either underestimation or overestimation

5.2 Sea-ice thickness

5.2.1 Observation sea-ice thickness

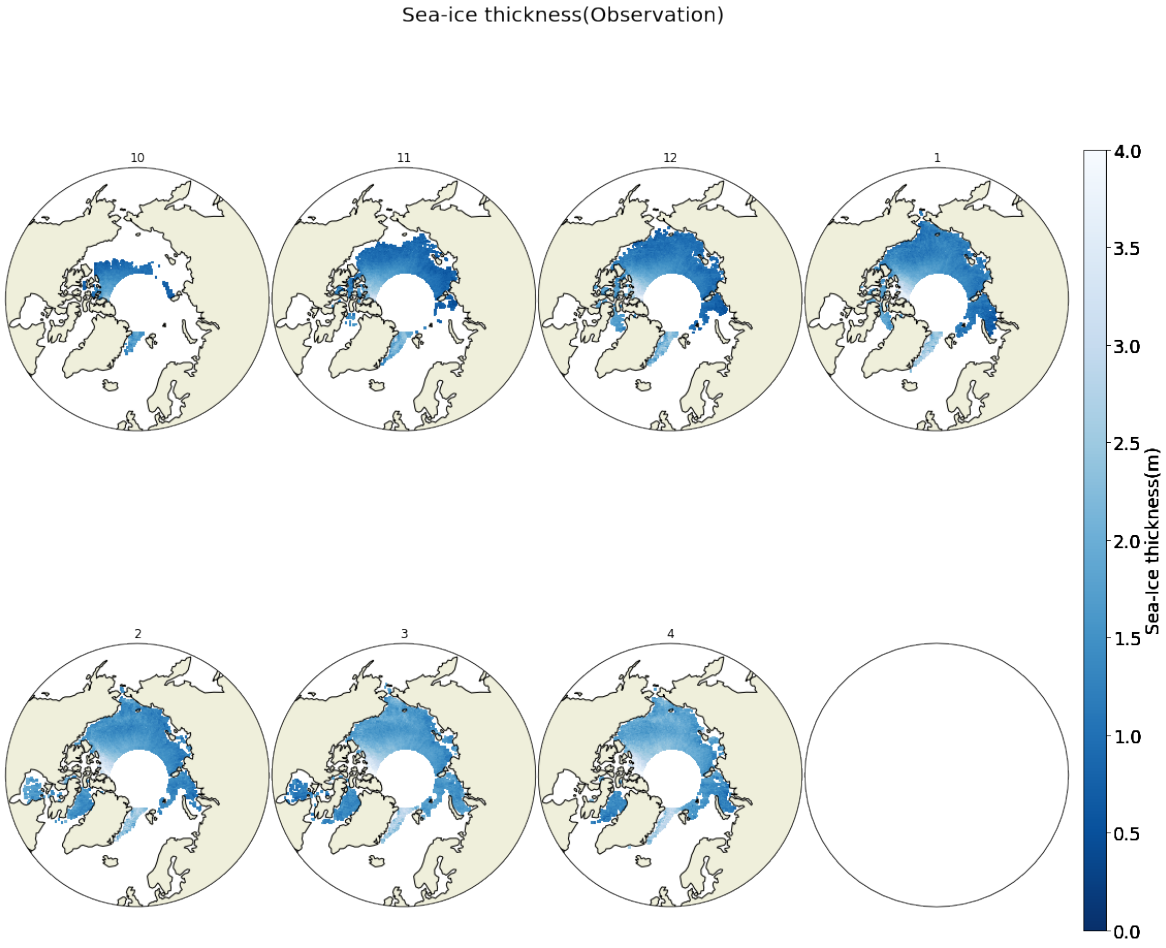

Figure 5.5: Observation winter season monthly average sea-ice thickness distribution from

Figure 5.5 shows the monthly average sea-ice thickness distribution from October to April from Envisat and CryoSat-2 satellite radar altimetry observation results. Data cannot cover the whole time and spatial range, same as CMIP6 model simulation, so only limited results can be obtained. From Figure 5.5, we can only see a generally even sea-ice thickness distribution. Sea ice becomes slightly thicker in the direction from the peripheral Arctic to Central Arctic. Canadian Archipelago usually has thicker sea

ice.

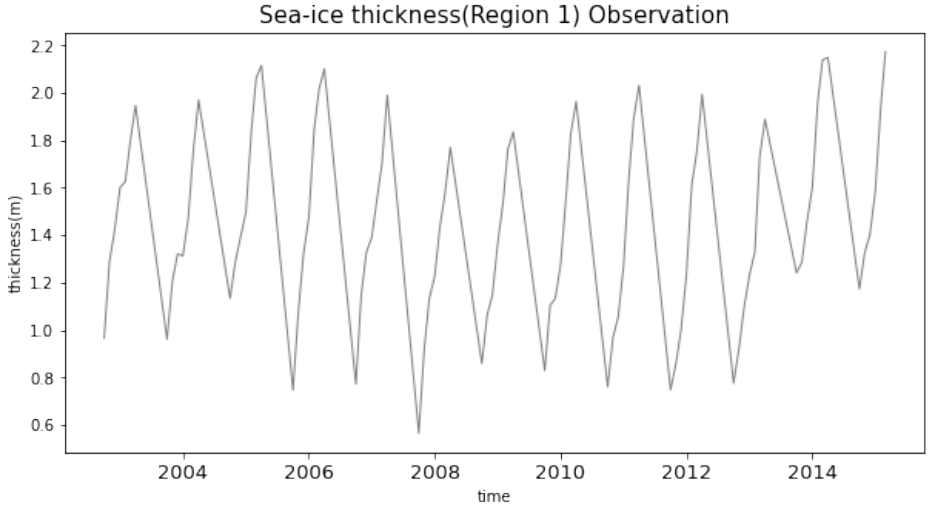

Figure 5.6: Observational inter-annual variability of regional average sea-ice thickness from 2002-2014 in region1

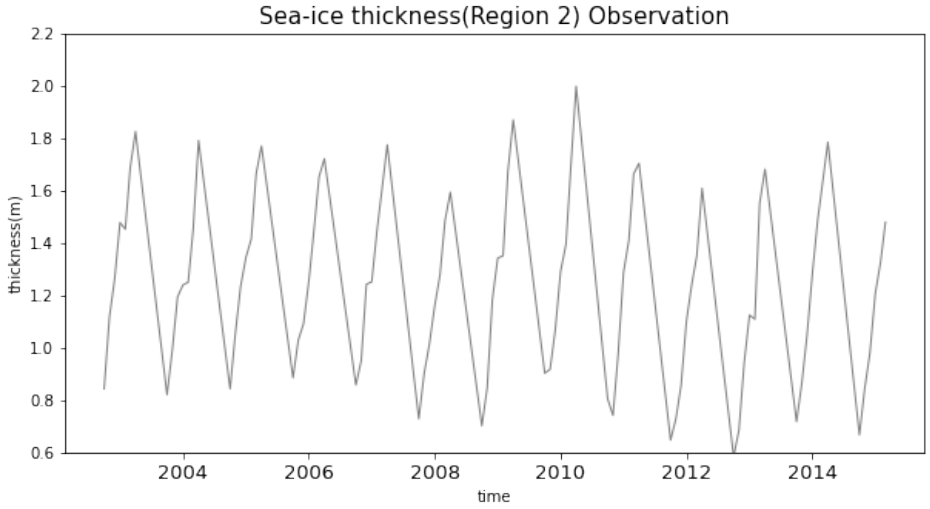

Figure 5.7: Observational inter-annual variability of regional average sea-ice thickness from 2002-2014 in region2

Figure 5.6-5.7 show annual variation of observation sea-ice thickness in region1 and region2. Regular seasonal fluctuation is visible, but there's no significant trend of winter months' sea-ice thickness. Observational sea-ice thickness is slightly higher in region1 than in region2.

5.2.2 Comparison of Sea ice thickness between CMIP6 and observation

Like the comparison between observation and modeling sea-ice extent, we use an independent samples T-test and aim to find months in which model sea-ice thickness has no significant difference from observation in all three regions, which is reflected

when the P value is larger than 0.05. Sea-ice thickness observation data range from 10/2002-12/2014, and we only have observation data from October to April for seven months; for October, November, and December, we have 13 data samples. For the other months, we only have 12 data samples. To make the t-test accurate, we select those with the same time spot in all model thickness data.

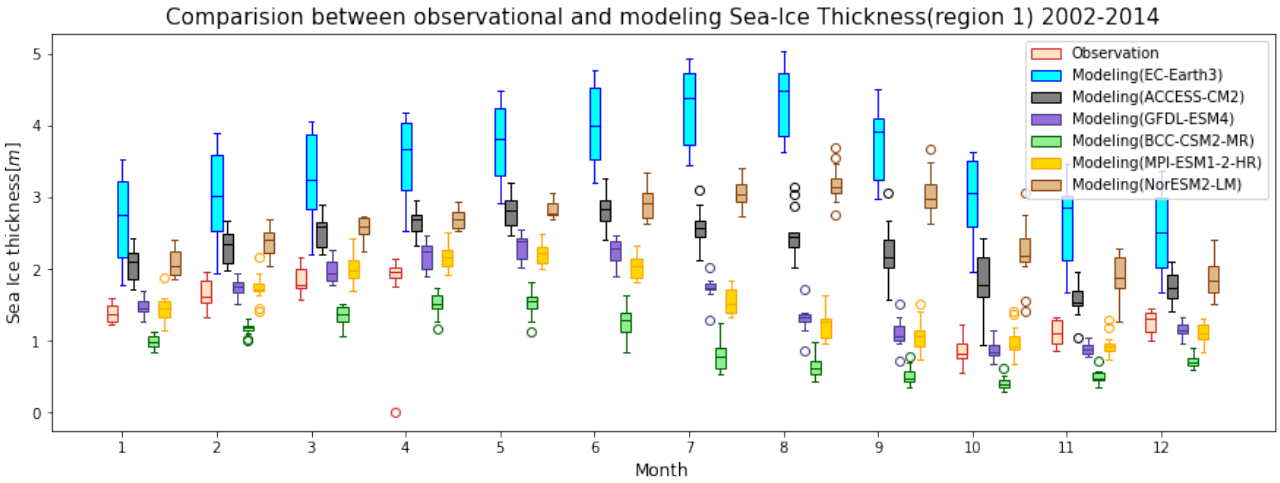

Figure 5.8: Comparison of Sea ice thickness between CMIP6 and observation in region1

Figure 5.8 compared 5 CMIP6 models' result with observation result of sea-ice thickness in region1. Due to the lack of summer months sea-ice thickness observation data, we only compare CMIP6 models with the observation from October to April. The modeling result is scattered, especially in summer.

In the observation result, April has the highest sea-ice thickness of 1.97m(median), and October has the lowest sea-ice thickness of 0.83m(median). Sea-ice thickness increases from October to April.

EC-Earth3 model has a maximum sea-ice thickness in August(4.48m) and minimum sea-ice thickness in December(2.51m). For the EC-Earth3 model, according to Table 5.1, in all the months, EC-Earth3 is significantly overestimating sea-ice thickness in region1. ACCESS-CM2 model output sea-ice thickness reaches the maximum in June(2.83m) and minimum in November(1.53m). For ACCESS-CM2 model, according to Table 5.2, in all the months, ACCESS-CM2 is significantly overestimating sea-ice thickness in region1. GFDL-ESM4 model output sea-ice thickness reaches the maximum in May(2.40m) and minimum in October(0.84m). according to Table 5.6, in October, January, February model output has no significantly different from observation, in November it is underestimating sea-ice thickness, in March and April it is overestimating sea-ice thickness. BCC-CSM2-MR model has a maximum sea-ice thickness in May(1.55m) and minimum sea-ice thickness in October(0.41m). For the BCC-CSM2-MR model, according to Table 5.3, model output is significantly different from observation. All the time BCC-CSM2-MR model underestimates sea-ice thickness.

MPI-ESM1-2-HR model output sea-ice thickness reaches the maximum in May(2.22m) and minimum in November(0.92m). According to Table 5.3, in October, January, February, and March MPI-ESM1-2-HR sea-ice thickness has no significant difference from observation. In November and December, the MPI-ESM1-2-HR model underestimates sea-ice thickness, and in April, it underestimates sea-ice thickness. NorESM2-LM model output sea-ice thickness reaches the maximum in August(3.14m) and minimum in December(1.85m). For the NorESM2-LM model, according to Table 5.5, model output is significantly different from observation. Nor-ESM-LM model overestimates sea-ice thickness all the time.

Only the BCC-CSM2-MR model and GFDL-ESM4 model have a similar seasonal cycle as observation, which has a minimum sea-ice thickness in October and constantly increases until April. Other models' minimum thickness occurs 1 or 2 months (s), lagging behind the observation. For the magnitude of sea-ice thickness, only the GFDL-ESM4 model and MPI-ESM1-2-HR model numerical results in most months fall into the credible range compared with observation according to the t-test result. EC-Earth3 model, ACCESS-CM2 model, and NorESM2-LM model have a higher value than observation, and the BCC-CSM2-MR model has a constantly lower value than observation.

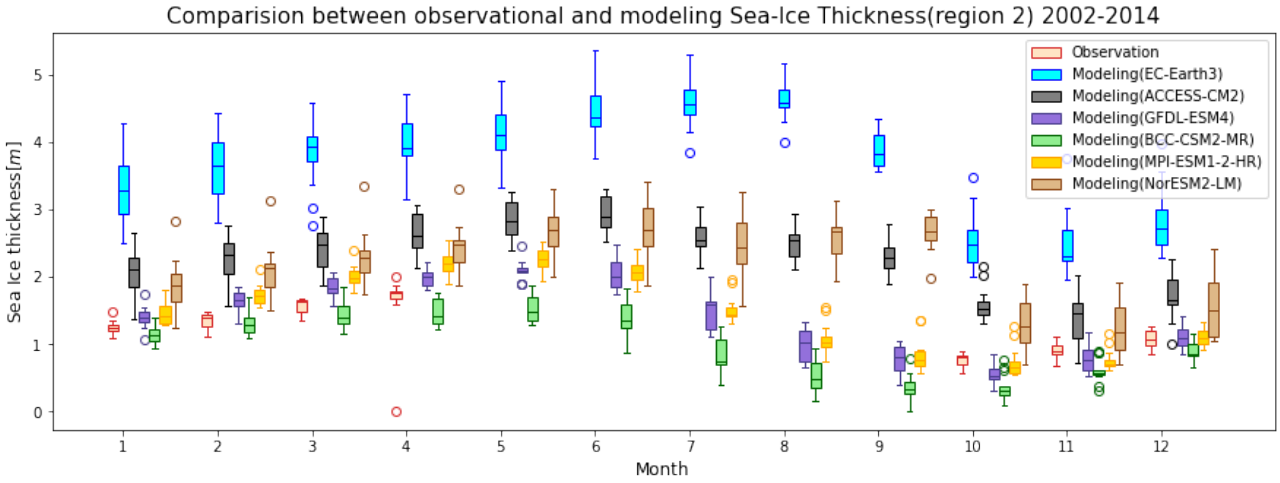

Figure 5.9: Comparison of Sea ice thickness between CMIP6 and observation in region2

Figure 5.9 compared 5 CMIP6 models' results with observation results of sea-ice thickness in the region2 from October to April. Similar to region1, in the observation result, sea-ice thickness increases from October(0.80m) to April(1.77m). GFDL-ESM4 model, BCC-CSM2-MR model, and MPI-ESM1-2-HR model have a similar seasonal cycle to observation result that sea-ice thickness is increasing from October to April. EC-Earth3 model has a maximum sea-ice thickness in August(4.59m) and minimum sea-ice thickness in December(2.31m). For the EC-Earth3 model, according to Table 5.1, in all the months, EC-Earth3 is significantly overestimating sea-ice thickness in region2. ACCESS-CM2 model output sea-ice thickness reaches the maximum in

June(2.88m) and minimum in November(1.46m). For ACCESS-CM2 model, P value for each months comparing model and observation from October to April is respectively $1.07 \times 10^{-10}, 0.00, 2.98 \times 10^{-6}, 1.08 \times 10^{-7}, 2.38 \times 10^{-8}, 2.55 \times 10^{-8}, 8.02 \times 10^{-9}$, all of them is much lower than 0.05 too. In all the months, ACCESS-CM2 is significantly overestimating sea-ice thickness in region2. GFDL-ESM4 model output sea-ice thickness reaches the maximum in May(2.10m) and minimum in October(0.53m). According to Table 5.6, in November and December, model output has no significant difference from observation, in October it underestimate sea-ice thickness, from January to April it overestimates sea-ice thickness.

BCC-CSM2-MR model has a maximum sea-ice thickness in May(1.48m) and minimum sea-ice thickness in October(0.30m). According to Table 5.3, model has plausible result only in February, in other months it is underestimating sea-ice thickness.

MPI-ESM1-2-HR model output sea-ice thickness reaches the maximum in May(2.27m) and minimum in November(0.71m). According to Table 5.4, in October and December, MPI-ESM1-2-HR model output has no significant difference compared with observation, in November, it is underestimating sea-ice thickness, from January to April, it is overestimating sea-ice thickness.

NorESM2-LM model output sea-ice thickness reaches the maximum in May(2.71m) and minimum in November(1.17m). According to Table 5.5, NorESM2-LM model output is significantly different from observation. NorESM2-LM model is overestimating sea-ice thickness in all available months.

Considering the magnitude of model simulation results, EC-Earth3, ACCESS-CM2 model, and NorESM2-LM model output are constantly higher than observation result, BCC-CSM2-MR model is mainly underestimating sea-ice thickness. GFDL-ESM4 and MPI-ESM1-2-HR perform best for simulating sea-ice thickness in region2. However, their common problem is overestimation from January to April. During summer seasons, modeling results are more scattered than during winter seasons.

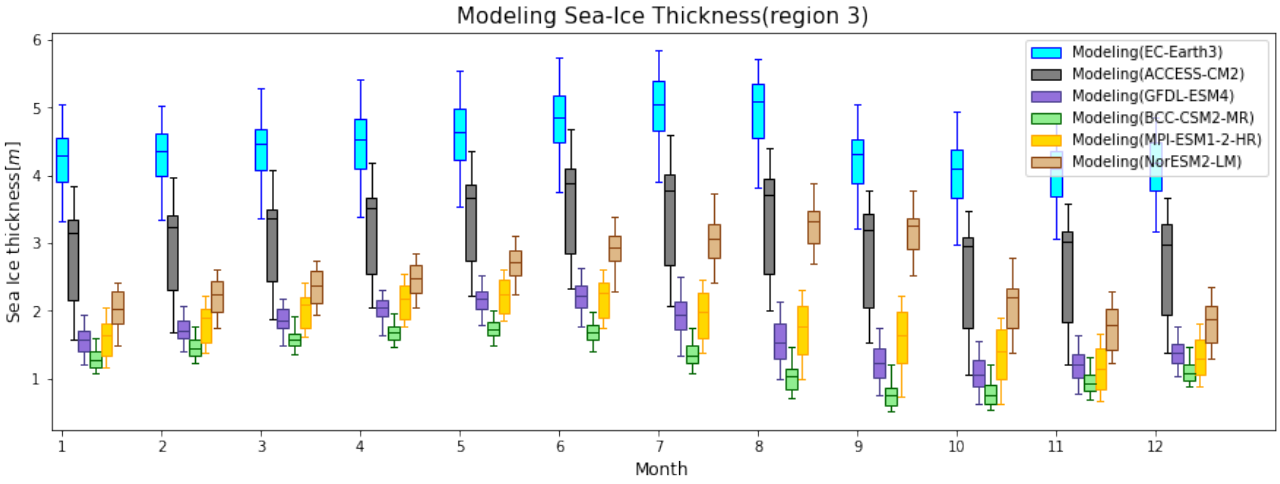

Figure 5.10: Comparison of Sea ice thickness between CMIP6 and observation in region3

Figure 5.10 compared 5 CMIP6 models' results of sea-ice thickness in the region3 from October to April. We only do model inter-comparison in region3 since there is no central Arctic data available in observation data. The model outputs are quite scattered since the EC-Earth3 model and ACCESS-CM2 model is two models much higher than the four other models in most of the months. In the summer seasons, the NorESM2-LM model is noticeably higher than the other three models from July to September. GFDL-ESM4 and MPI-ESM1-2-HR models have similar seasonal cycles and magnitudes. For all the model results, the EC-Earth3 model has a maximum sea-ice thickness in July(4.43m) and minimum sea-ice thickness in October(3.42m), ACCESS-CM2 model output sea-ice thickness reaches the maximum in June(2.77m), and minimum in October(1.64m). GFDL-ESM4 model output sea-ice thickness reaches the maximum in June(2.04m) and minimum in October(0.80m). BCC-CSM2-MR model has a maximum sea-ice thickness in May(1.63m) and minimum sea-ice thickness in September(0.61m). MPI-ESM1-2-HR model output sea-ice thickness reaches the maximum in May(1.94m) and minimum in November(0.81m). NorESM2-LM model output sea-ice thickness reaches the maximum in August(2.91m) and minimum in November(1.42m). From the modeling result, we can see that maximum sea-ice thickness usually happens in May and July, and minimum sea-ice thickness usually happens around October and November.

5.3 Sea-ice motion

5.3.1 Observation sea-ice motion

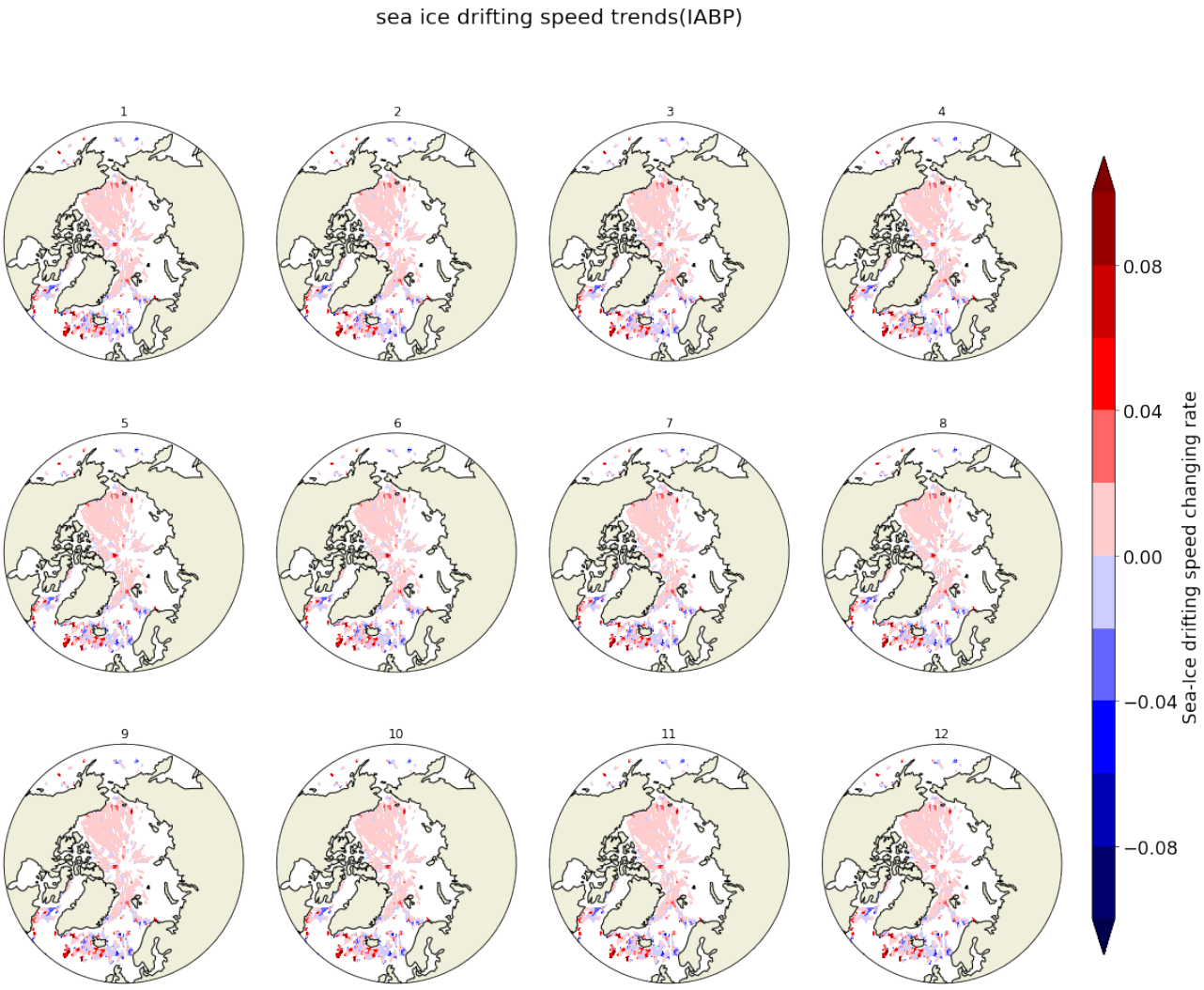

Figure 5.11: Distribution of IABP data sea-ice drifting speed changing rate from 1979-2014

Figure 5.11 shows the changing rate of sea-ice drifting speed produced by IABP data from 1979-2014. The red color means in this spot sea-ice drifting speed is increasing, blue color means in this spot sea-ice drifting speed is decreasing. A widely distributed positive trend can be found in all months. In the south Greenland Sea, there are several negative spots, but there is a high possibility because the buoy is in open water rather than sea ice.

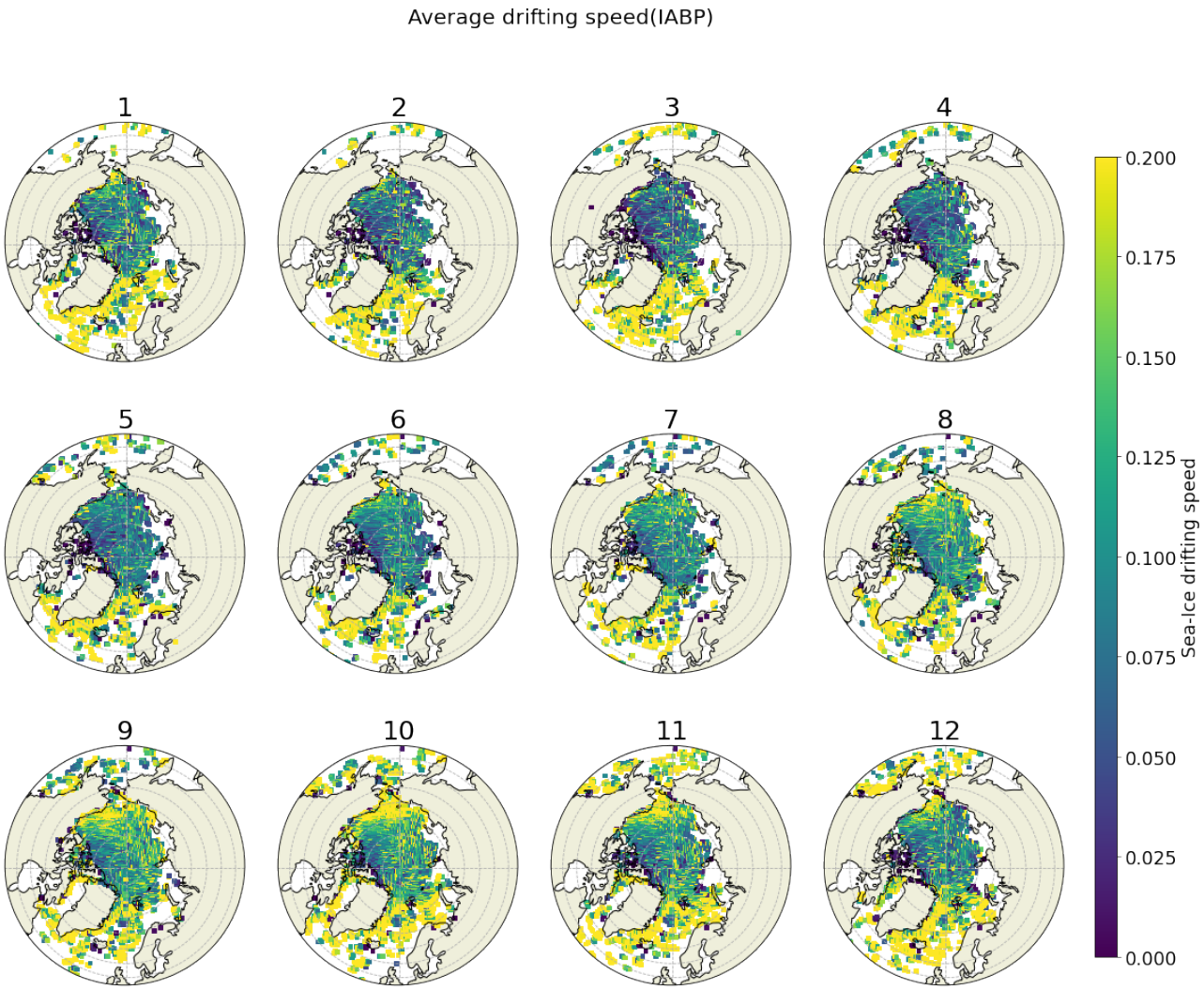

Figure 5.12: Distribution of IABP data averaged sea-ice drifting speed from 1979-2014

Figure 5.12 shows the monthly average sea-ice drifting speed distribution from 1979-2014. the central Arctic and Canadian Archipelago region always has comparatively low sea-ice drifting speed all year round. The Arctic on the Pacific Ocean side has less active sea-ice motion than the Atlantic Ocean side. From January to July, the Beaufort Sea, Chukchi Sea, and the East Siberian Sea are in a steady low sea-ice emotion state, while from August to December, there is faster sea-ice motion.

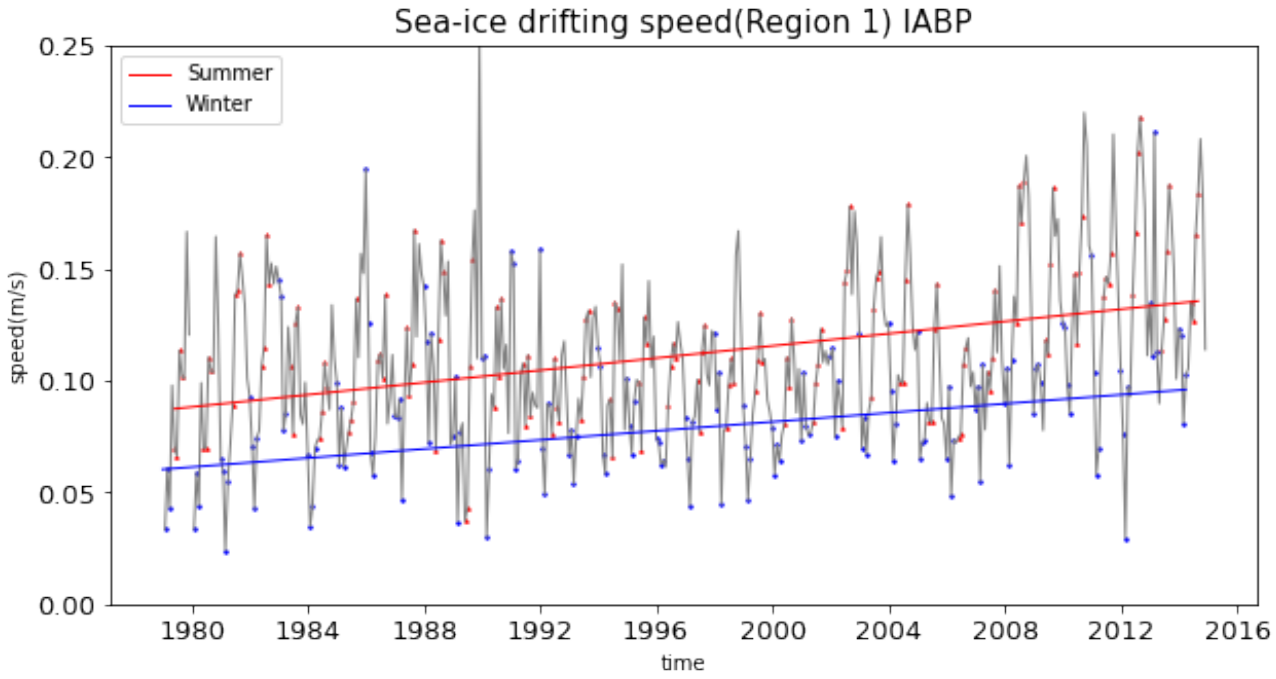

Figure 5.13: Annual variation and trend of IABP sea-ice drifting speed between 1979-2021 in region1

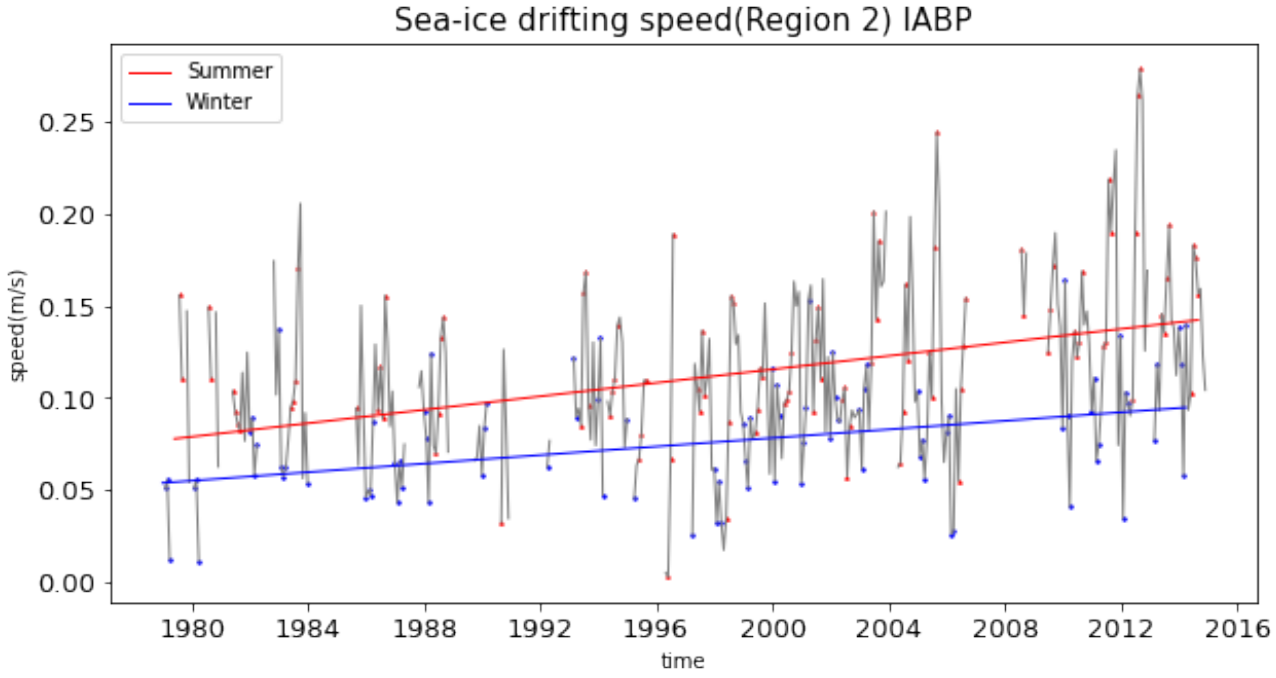

Figure 5.14: Annual variation and trend of IABP sea-ice drifting speed between 1979-2021 in region2

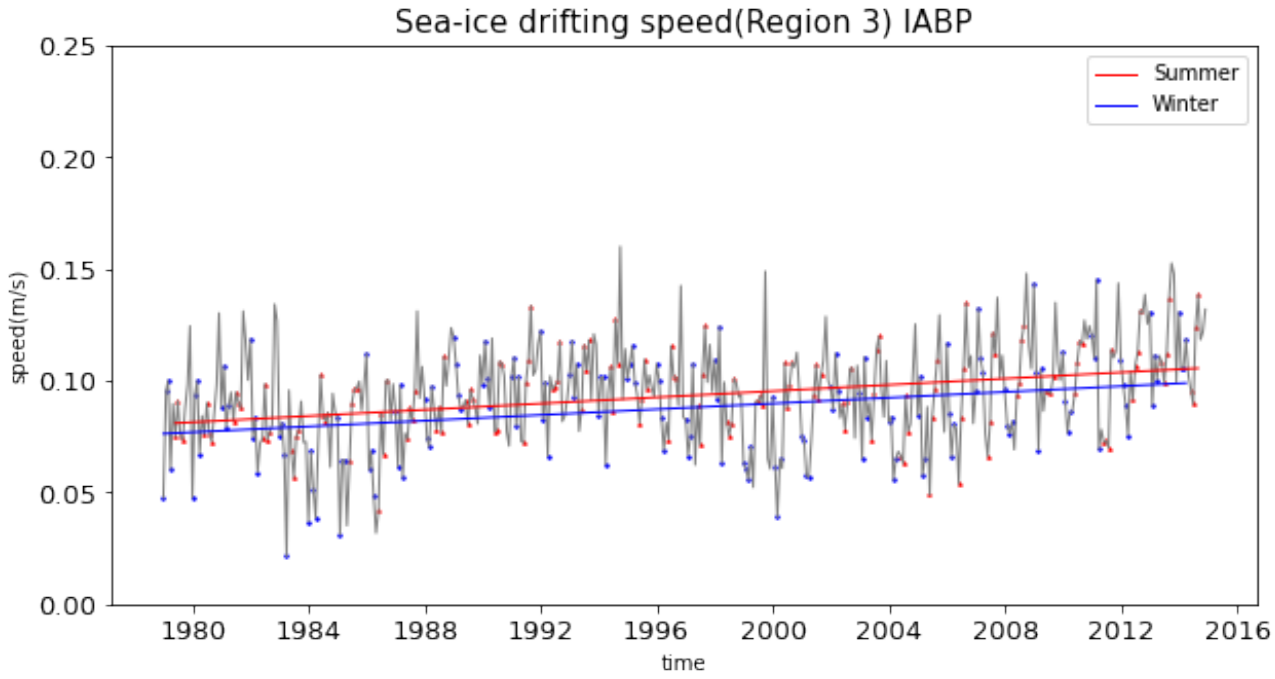

Figure 5.15: Annual variation and trend of IABP sea-ice drifting speed between 1979-2021 in region3

Figures 5.13-5.15 show annual variation of observation sea-ice drifting speed in region1, region2 and region3 between 1979-2014. In the IABP buoy data result, sea-ice drifting speed has an increasing trend. Summer monthsâ sea-ice motion is always faster than winter monthsâ sea-ice motion; while seasonal differences can be observed in region1 and region2, in region3, the seasonal gap is not clear. In region1, in summer, sea-ice drifting speed increased by 55.07%, in winter increased by 59.07%, In region2, in summer, sea-ice drifting speed increased by 82.92%, in winter increased by 72.04%. In region3, in summer, sea-ice drifting speed increased by 30.32%, and winter increased by 26.70%. Summer sea ice motion increase faster than winter. The variation rate of sea-ice motion in buoy observation results is exceedingly high, even though most models projected an increasing trend of sea-ice motion, the rate is far below reality.

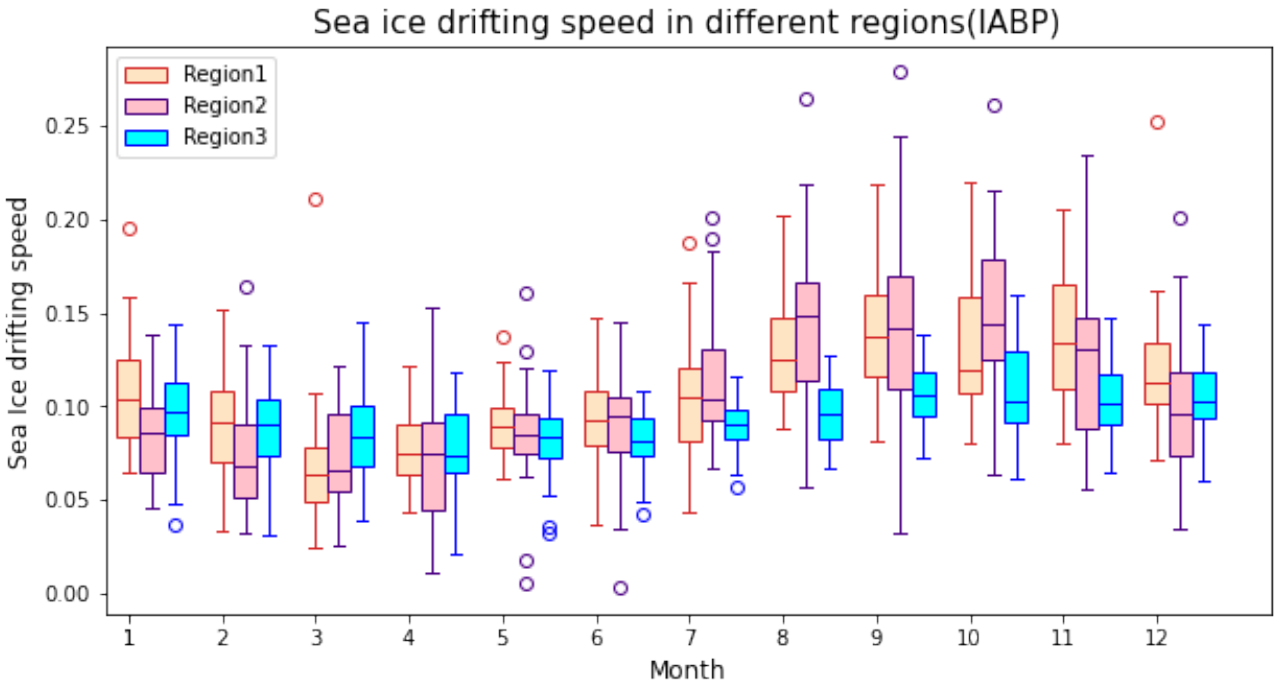

Figure 5.16: Regional comparison of sea-ice drifting speed monthly

Figure 5.16 shows box plot comparing IABP data sea-ice drifting speed in region1,2 and 3 in each months from 1979-2014. region1 has a maximum sea-ice drifting speed in September and a minimum in March. region2 has a minimum sea-ice drifting speed in March and August, region3 has the maximum sea-ice drifting speed in September, and the minimum sea-ice drifting speed is in April. Region3 has the slightest seasonal cycle.

5.3.2 Comparison of sea-ice motion between CMIP6 and observation

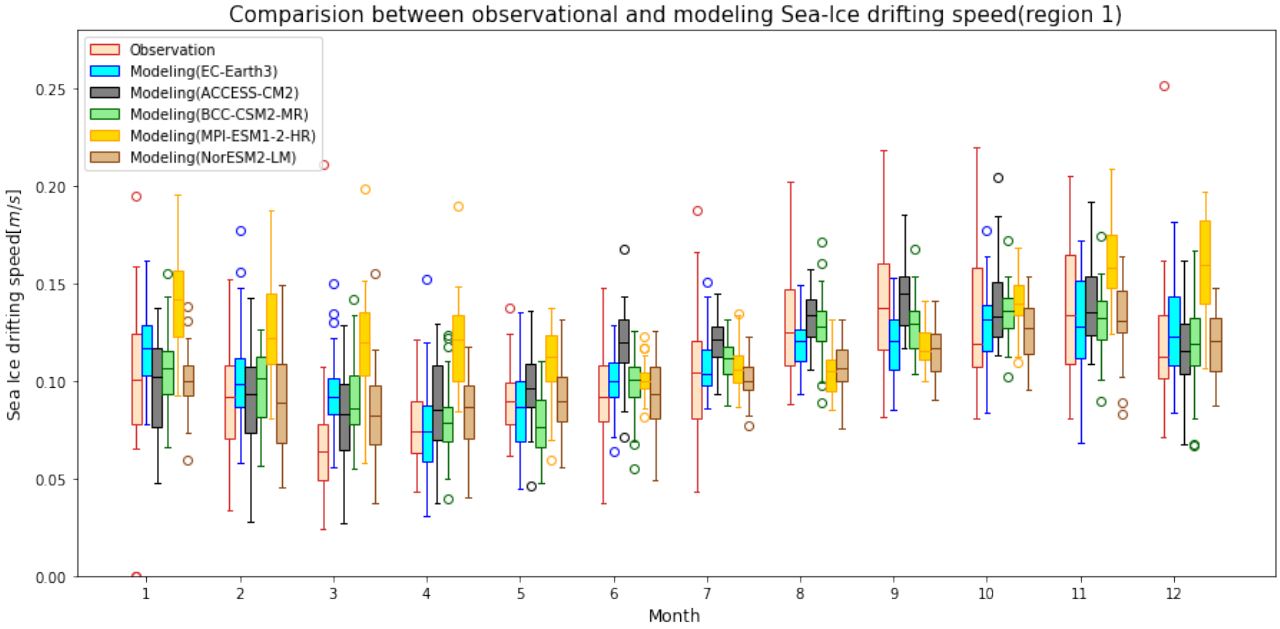

Figure 5.17: Comparison of sea-ice drifting speed between CMIP6 and observation in region1

Figure 5.17 compares 5 CMIP6 model outputs sea-ice drifting speed with buoy data calculated sea-ice drifting speed in region1. Despite scattered sea-ice thickness model output, sea-ice drifting speed result is comparatively unified. Slowest sea-ice motion in buoy data result occurs in March(0.06m/s), and fastest sea-ice motion happens in September(0.14mm/s).For model outputs, EC-Earth3 model output has fastest sea-ice motion in October(0.13m/s) and slowest sea-ice motion in April(0.07m/s). ACCESS-CM2 model output has fastest sea-ice motion in September(0.15m/s) and slowest sea-ice motion happens in March(0.08m/s). BCC-CSM2-MR model output has fastest sea-ice motion in November(0.13m/s) and slowest sea-ice motion in May(0.08m/s). MPI-ESM1-2-HR model output has fastest sea-ice motion in December(0.16m/s), and slowest sea-ice motion in June(0.10m/s). NorESM2-LM model output has fastest sea-ice motion in November(0.13m/s), and slowest sea-ice motion in March(0.08m/s).

We did independent samples t-test for each month between observation and model output sea-ice speed. For EC-Earth3 model, according to Table 5.1, EC-Earth3 has good simulation for sea-ice speed in January, April, May, June, July, August, October, November and December, in which P value from t-test result is larger than 0.05. It overestimated in February and March and underestimated in September.

For ACCESS-CM2 model, according to Table 5.2, except for June and July, in other months, ACCESS-CM2 provides plausible simulation. ACCESS-CM2 model overesti-

mates sea-ice motion in June and July.

For BCC-CSM2-MR model, according to Table 5.3, BCC-CSM2-MR simulates sea-ice drifting speed well in whole year except March, where the P value is lower than 0.05. In March, it overestimated sea-ice speed.

For MPI-ESM1-2-HR model, according to Table 5.4, MPI-ESM1-2-HR model only provides good simulation in June and July, and in October when P values are greater than 0,05. During August and September, the MPI-ESM1-2-HR model underestimates, while it overestimates from November to May.

For NorESM2-LM model, according to Table 5.5, NorESM2-LM model provides a good estimation of sea-ice drifting speed in most months, except March, August, and September, where the P value is smaller than 0.05. It overestimates in March and underestimates in August and September. To summarize the model performance, except in March, when all of the models are overestimating sea-ice drifting speed, in other months, most of the model outputs do not have a high deviation compared with the observation result. The most noticeable model deviation is in the Winter months, MPI-ESM1-2-HR model output is higher than observation and other models. During summer seasons, there is a overestimate in ACCESS-CM2 model output. From July to September, there was an underestimate in BCC-CSM2-MR model output. Sea-ice thickness model results cope with sea-ice motion observation and model results in region1.

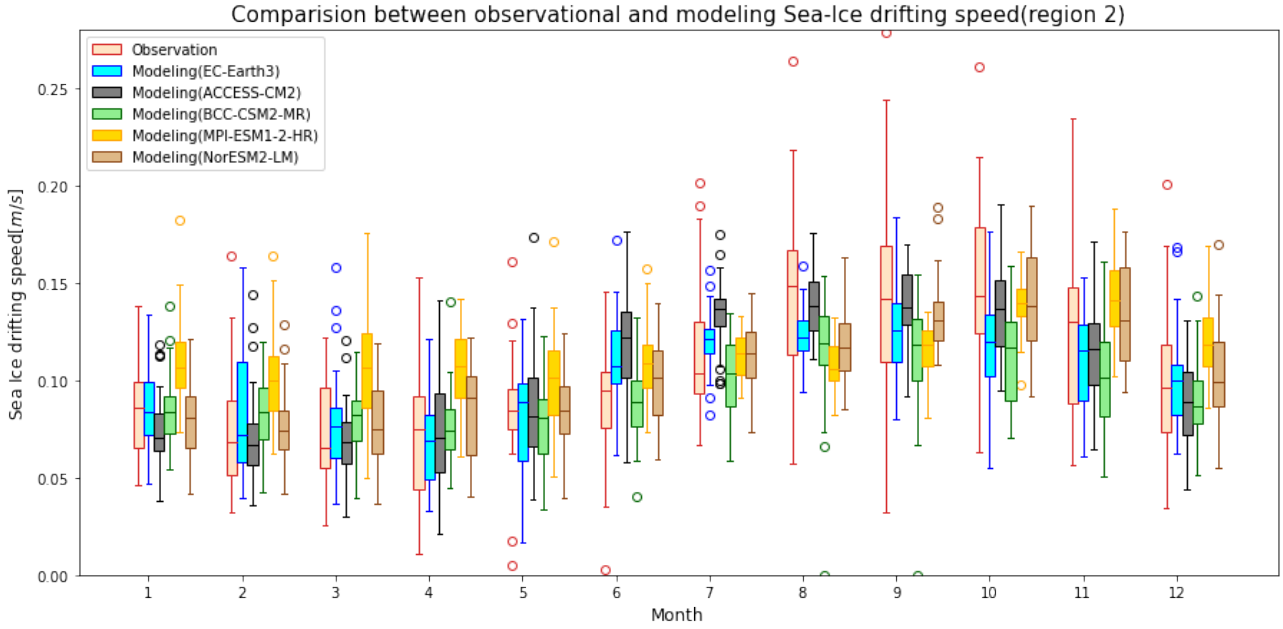

Figure 5.18: Comparison of sea-ice drifting speed between CMIP6 and observation in region2

Figure 5.18 compares 5 CMIP6 model outputs sea-ice drifting speed with buoy data calculated sea-ice drifting speed in region2. In region2, there is a larger seasonal cycle amplitude compared with region1. Furthermore, buoy observation data

show a larger seasonal cycle amplitude and a wider annual variation range, especially in summer. For observation output, maximum sea-ice drifting speed occurs in August(0.145m/s), and minimum sea-ice drifting speed happens in March (0.072m/s). For model outputs, EC-Earth3 model has maximum sea-ice drifting speed in September(0.126m/s) and minimum in April (0.169m/s). ACCESS-CM2 model has maximum sea-ice drifting speed in August (0.138m/s), and minimum sea-ice drifting speed in February (0.066m/s). BCC-CSM2-MR model output has maximum sea-ice drifting speed in Augustc(0.104m/s), and minimum sea-ice drifting speed in Aprilc(0.074m/s). MPI-ESM1-2-HR model output has a maximum sea-ice drifting speed in Novembercc(0.141m/s) and minimum sea-ice drifting speed in Februaryc(0.100m/s). NorESM2-LM model output has maximum sea-ice drifting speed in October(0.138m/s), and minimum sea-ice drifting speed in Februaryc(0.075m/s).

In region2, for EC-Earth3 model, according to Table 5.1, the EC-Earth3 model works well in most months, except June, August, and October, when the P value is smaller than 0.05. It is overestimating in June and underestimating in August and October.

For ACCESS-CM2 model, according to Table 5.2, in most months ACCESS-CM2 model has good simulation except June and July when P value is smaller than 0.05. It overestimates sea-ice drifting speed in June and July.

For BCC-CSM2-MR model, according to Table 5.3, from December to July, the BCC-CSM2-MR model has a P value larger than 0.05, which means it has good simulation results in those months, while from August to November in summer, the model result is significantly different from the observation that it underestimates sea-ice drifting speed.

For MPI-ESM1-2-HR model, according to Table 5.4, MPI-ESM1-2-HR has accurate simulation of sea-ice motion in May, June, July and October, since P values for those months are greater than 0.05. From November to April, it overestimates sea-ice motion; in August and September, it underestimates sea-ice thickness.

For the NorESM2-LM model, according to Table 5.5, most months has P value greater than 0.05, except August, it means in August sea-ice speed is significantly different from observation. In August, the NorESM2-LM model underestimated sea-ice motion.

ACCESS-CM2 overestimates summer sea-ice speed, MPI-ESM1-2-HR overestimates winter sea-ice motion and underestimates summer. BCC-CSM2-MR model underestimates ice motion in summer. EC-Earth3 and NorESM-LM generally have good simulations.

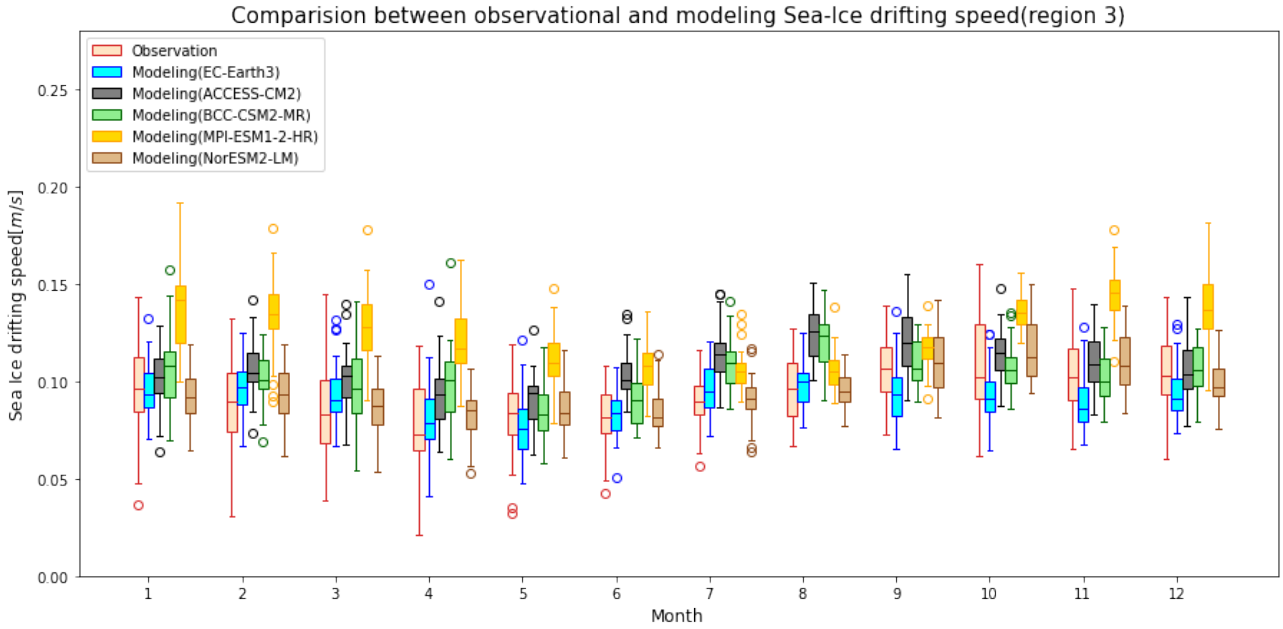

Figure 5.19: Comparison of sea-ice drifting speed between CMIP6 and observation in region3

Figure 5.19 compares 5 CMIP6 model outputs sea-ice drifting speed with buoy data calculated sea-ice drifting speed in region3. Compared with region1 and region2, region3 has minimal seasonal cycle amplitude. In region3, in observation result, maximum sea-ice drifting speed occurs in September(0.106m/s), and minimum occurs in April(0.073m/s). For model outputs, the EC-Earth3 model output has the maximum sea-ice drifting speed in August(0.100m/s) and the minimum sea-ice drifting speed in May(0.075m/s). ACCESS-CM2 model output ha maximum sea-ice drifting speed in August(0.125m/s), and minimum sea-ice drifting speed in April(0.094m/s). BCC-CSM2-MR model output has maximum sea-ice drifting speed in August(0.123m/s) and minimum sea-ice drifting speed in May(0.083m/s). MPI-ESM1-2-HR model output has a maximum sea-ice drifting speed in November(0.146m/s) and minimum sea-ice drifting speed in July(0.105m/s). NorESM2-LM model has maximum sea-ice drifting speed in October(0.112m/s), and minimum sea-ice drifting speed in June(0.081m/s). For EC-Earth3, according to Table 5.1, from January to June and August, EC-Earth3 has accurate simulation. However, it overestimates in July and underestimates ice motion from September to December.

For ACCESS-CM2 model, according to Table 5.2, in January, October, November, and December, model output and observation have no significant difference as the P value is larger than 0.05. From February to October ACCESS-CM2 model overestimates sea-ice motion.

For BCC-CSM2-MR model, according to Table 5.3, in May and from September to December, model output has no significant difference from observation, as P value is greater than 0.05. BCC-CSM2-MR model overestimates sea-ice drifting speed from

January to April and in June, July, and August.
For MPI-ESM1-2-HR model, according to Table 5.4, the model output is significantly different from observation. MPI-ESM1-2-HR model is overestimating sea-ice drifting speed all year round. MPI-ESM1-2-HR model has a higher deviation in winter than in summer. For NorESM2-LM model, according to Table 5.5, model has good simulation all year round.
To briefly summarize the model performance in three regions for sea-ice motion, we can see NorESM2-LM model has the best performance among all the models, and ACCESS-CM2 has a good simulation for regions 1 and 2. EC-Earth3 also has satisfying performance in simulating sea-ice motion for the whole Arctic, that it has good simulation in more than eight months for each region. A few models have common problems: BCC-CSM2-MR model tends to underestimate sea-ice drifting speed in summer seasons in region1 and region2 while overestimating in many months in region3. MPI-ESM1-2-HR model tends to overestimate sea-ice drifting speed, especially in winter months. ACCESS-CM2 model overestimates sea-ice drifting speed in summer for regions 1 and 2. In region3, the ACCESS-CM2 model mostly overestimates sea-ice motion except in winter months.

6. Discussion

6.1 Strengths and weakness of the models

Koenigk and Dekker, 2020 already indicate EC-Earth-VEG has the trend of sea ice extent in similar time series as in this thesis, it also points out the seasonal cycle that minimum in August. EC-Earth3 model has a minimum sea-ice extent one month earlier than the observation result, so one of the weaknesses of the EC-Earth3 model is simulating the seasonal cycle of sea-ice extent. EC-Earth3 model also overestimates sea-ice extent vastly. Koenigk and Dekker, 2020 shows and overestimation in Sea-ice thickness in East Greenland, while our study also point out the overestimation of sea-ice thickness in Chukchi, Beaufort and Laptev, East Siberian Sea. So another weakness of the EC-Earth3 model is that it overestimates sea-ice thickness to a large extent compared with observation and all other models. The advantage of the EC-Earth3 model includes it having a reasonable estimation of the annual variation and decreasing trend of sea-ice extent, and also it simulates plausible regional distribution and magnitude of sea-ice drifting speed.

Shu et al., 2020 demonstrate a lower trend of sea-ice extent compared with observatiobn in ACCESS-CM2 model. However, in over study, ACCESS-CM2 model has the strength that it indicates a similar seasonal cycle of the sea-ice extent to observation result, and it accurately estimates the decreasing rate of sea-ice extent is very close to observation. Problems of the ACCESS-CM2 model are that it tends to overestimate sea-ice extent when sea-ice extent is in a high state. Shu et al., 2020 got the result that the ice thickness is lower than in PIOMAS, however, in our study, ACCESS-CM2 model has generally overestimated sea-ice thickness in whole Arctic region, and it fails to simulate a correct seasonal cycle of sea-ice thickness in winter months.

[Bing ZHOU, 2021 model indicates a faster decreasing trend in September than in March, but it not yet point out other sea-ice extent properties. In our study, BCC-CSM2-MR model simulates the seasonal cycle and its amplitude perfectly for sea-ice extent and indicates its decreasing trend. And in the winter months, the BCC-CSM2-MR model shows a correct seasonal cycle of sea-ice thickness. The weakness of the BCC-CSM2-MR model is that it underestimates sea-ice extent, sea-ice thickness, and

sea-ice motion(in region 2). It is not good at describing the regional distribution of sea-ice drifting speed, and it has an inaccurate projection of peripheral sea-ice drifting speed. BCC-CSM2-MR model well captured the warming trend of surface air temperature and evaluated tropical climate variability compared with other models, and it probably relates to smaller sea-ice coverage and thinner sea-ice in model output.
Watts et al., 2021 points out GFDL-ESM4 model underestimate sea ice edge for the Barents and Kara Seas. In our study, the strength of the GFDL-ESM4 model is its ability to simulate the decreasing trend of sea-ice extent, it is good at presenting periodical features of sea-ice extent, and the magnitude of the GFDL-ESM4 model projected sea-ice extent is comparatively close to observation. Watts et al., 2021 also does not think GFDL-ESM4 model provides satisfactory result in September, but our study shows GFDL-ESM4 model provides correct estimation for sea-ice thickness in the seasonal cycle and the magnitude of sea-ice thickness. In the GFDL-ESM4 model, its weakness is the deviation in simulating the seasonal cycle. MPI-ESM1-2-HR model simulate the sea ice thickness distribution similar to the PIOMAS reanalysis (Gutjahr et al., 2019b) and in our study MPI model also has good performance in sea-ice thickness study. MPI model also has the advantage that it shows a similar regional distribution for sea-ice drifting speed in the winter months. The weakness of the MPI-ESM1-2-HR model is that it underestimates sea-ice extent almost all year round except the spring season. And in the summer months, sea-ice drifting speed distribution and the regional difference in sea-ice motion between the three regions are not clearly shown. The most apparent problem of the MPI-ESM1-2-HR model is that it hardly simulates the increasing rate of sea-ice motion in summer and has a severe estimation of summer sea-ice motion. Seland et al., 2020 indicates that NorESM2-LM model and observation has a good match, and summer trend of sea ice area is well captured. It said the sea ice decreasing March is well captured by NorESM2-LM, but September trend is underestimated. In our study, NorESM2-LM can show a correct seasonal cycle of sea-ice extent, and the magnitude of sea-ice extent in the model is plausible. But the decreasing rate of sea-ice extent in the model result is too low that it can't show an evident annual variation of sea-ice extent. NorESM2-LM model also failed to simulate the correct seasonal cycle of sea-ice thickness in winter months and overestimated sea-ice thickness. Despite no good performance in sea-ice extent and sea-ice thickness, in the case of sea-ice motion, it has the best performance among all models. It shows proper sea-ice drifting speed distribution in all seasons, and it clearly presents the seasonal cycle of sea-ice drifting speed in three regions, and the magnitude of sea-ice motion is pretty close to the buoy data result. However, it still has the problem that the increasing rate of sea-ice motion is much lower than reality. Its primary disadvantage is bad at simulating the annual variation of sea ice. Most models' increasing rate of modeled

sea-ice drifting speed is far below IABP buoy data result, especially the NorESM2-LM model and MPI-ESM1-2-HR model in summer months. The scattered result of model output sea-ice thickness is because sea-ice thickness model data and even observation data have uncertainties around or under 1 meter, which increases the difficulties verifying model sea-ice thickness.
We can attribute some model output features to the physical description of sea ice. For example, the overestimation(underestimation) of sea-ice extent physically corresponds with the overestimation(underestimation) of sea-ice thickness in EC-Earth3 and BCC-CSM2-MR. However, most times, sea-ice properties vary systematically in a model.

6.2 New findings

Even though the periodical signal in sea-ice extent has disappeared in the 21^{st} century, many models' projection result still has a vital periodical sign which is probably due to the original input of sea-ice extent in the 20^{th} century. All selected CMIP6 models indicate a negative trend in sea-ice thickness and a clear positive trend in sea-ice drifting speed in the central Arctic region, which means the zero ice motion zone is gradually reducing and drifting of sea-ice in the central Arctic becomes inevitable. In CMIP6 models, sea-ice thickness uncertainties still failed to be reduced, which can we can see in the scattered modeling result in sea-ice thickness. In CMIP6, some models are already able to catch up with the observational sea-ice coverage decreasing rate, but there are still a few models underestimating the decrease of sea-ice coverage.
When comparing CMIP6 sea-ice thickness results with previous studies, many CMIP6 models can simulate the appropriate sea-ice thinning process. In CMIP6 model results, generally, summer sea-ice thickness has a much sharper decrease than in winter, but different from previous decades and what we observed in winter sea-ice thickness, future sea-ice thickness will no longer be in a steady state, and winter half-year will start to have contributed to the sea-ice thinning process.
Smedsrud et al., 2011 demonstrated that the increasing trend in sea-ice drift start in 1992. Rampal et al., 2009b shows that between 1979-2007, sea-ice drifting speed increased by $0.05km \cdot day^{-1}year^{-1}$ on average in Arctic region. While cold months from December to May has a faster increase trend of $0.06km \cdot day^{-1}year^{-1}$, compared to the trend ($0.05km \cdot day^{-1}year^{-1}$) during the warm month from June to September. CMIP6 model projections of sea ice motion increasing rate is already higher than ealier period, but the main weakness of the CMIP6 model is that none of the selected models can catch up with the IABP buoy data sea-ice drifting decreasing rate. It is still mainly underestimating the sea-ice motion, which we need to improve in future model development.

We have also studied the regional difference in the thesis, models generally can distinguish different features of sea-ice properties in peripheral and central Arctic, but the difference between the Chukchi Sea, the Beaufort Sea, and Laptev sea, East Siberian in some models are still not demonstrated by models.
Regional biases of sea-ice thickness and motion distribution are most likely due to persistent oceanic and atmospheric circulation preferences. The sea-ice extent decreasing rate bias is due to inter-annual variability in each model. The bias of sea-ice thickness in the model might be due to the snow insulation effect and bias in albedo. The bias of regional sea-ice might be related to ocean model bias cause sea-ice coverage is related to ocean surface water temperature Etc.

7. Conclusions

In the thesis, we looked at 6 CMIP6 models, which are EC-Earth3, ACCESS-CM2, BCC-CSM2-MR, GFDL-ESM4, MPI-ESM1-2-HR, NORESM2-LM, and compared their simulation result of sea-ice extent, sea-ice thickness and sea-ice motion with observation. There are common features of sea ice that models agreed upon, and each model has its simulation result.

Most models(except EC-Earth3 and GFDL-ESM4) and observation agreed on a seasonal cycle for the sea-ice extent that maximum sea-ice extent occurs in March, and minimum sea-ice extent occurs in September. All models successfully simulated a decreasing trend which copes with observation. Only the decreasing rate of sea-ice extent in each model varies.

Most selected models have agreed upon the distribution of sea-ice thickness: Central Arctic and Canadian Archipelago always have the thickest sea ice, followed by the East Siberian Sea, Laptev Sea, and Chukchi Sea, Beaufort Sea. East Greenland Sea, Barents Sea, Buffin Bay, and the Kara Sea always have the thinnest sea ice. Generally, the central Arctic has thicker sea ice than the peripheral sea; the peripheral sea on the Pacific side has thicker sea ice than the Atlantic. From all the model results, there's a noticeable decreasing trend for sea-ice thickness even though there's no significant trend in observation. EC-Earth3, ACCESS-CM2, and NorESM-LM model indicate that summer sea-ice thickness is higher than winter, while BCC-CSM2-MR, GFDL-ESM4, MPI-ESM1-2-HR agreed that winter sea-ice thickness is higher than summer. As we compared model output sea-ice thickness with observation winter sea-ice thickness, GFDL-ESM4, MPI-ESM1-2-HR have plausible simulation. According to these two models, sea-ice thickness has a more rapid decreasing rate in summer than in winter, and among all the regions that we study, region2, which refers to Laptev and the East Siberian Sea, has the most rapid sea-ice thinning process than all other regions. And these models show that maximum sea-ice thickness usually occurs in May, and minimum sea-ice thickness happens in October. Observation results and GFDL-ESM4, MPI-ESM1-2-HR, and NorESM2-LM model agreed that in region1, sea ice is thicker than in region2. All models demonstrate a minor seasonal fluctuation of sea ice in the central Arctic.

sea-ice drifting speed distribution is also agreed by most models and observation, that Peripheral Arctic sea-ice on Atlantic side has the fastest sea-ice motion, followed by Peripheral Arctic sea-ice at Pacific side, Canadian Archipelago and Central Arctic always have the slowest sea-ice motion.

Compared with the scattered model output in sea-ice thickness, sea-ice motion model outputs generally have much closer simulation to observation. Most of the selected models show an increasing trend of sea-ice motion, and summer sea-ice motion has faster than winter, which copes with observation. However, most models have a quicker increasing rate of sea-ice motion in winter than in summer, which is different from observation. All selected models severely underestimate the increasing rate of sea-ice motion. Corresponding with the comparatively faster thinning process in the region2 simulated by models, there's also a faster increasing rate in region2 in the observation result, and it's supported by BCC-CSM2-MR and NorESM2-LM models' output. However, all models and observations also agreed that region1 has faster sea-ice motion in winter than region2. And same as sea-ice thickness, sea-ice motion also has the slightest seasonal variation in the Central Arctic region. Each model has individual features too.

EC-Earth3 model's decreasing rate of sea-ice extent is similar to observation. In the seasonal cycle, the EC-Earth3 model's minimum sea-ice extent occurs in August, one month earlier than observation. EC-Earth3 model also has a larger sea ice extent seasonal cycle amplitude.

The EC-Earth3 model simulates that regions 1 and 2 have a similar sea-ice thickness in summer, while in winter, region2 has thicker sea ice than region1; it is different from the observation where region1 has slightly higher sea-ice thickness. Correspondingly, region1 has much faster ice motion in winter than region2, while in summer, their motion magnitude is similar. ACCESS-CM2 model tends to overestimate sea-ice extent too, but its decreasing rate of sea-ice extent is similar to observation. ACCESS-CM2 model also overestimates sea-ice thickness. In ACCESS-CM2 model output, Central Arctic ice thickness> the Chukchi Sea and the Beaufort Sea> Laptev and the East Siberian Sea, which copes with observation. In the ACCESS-CM2 model, seasonal variation of sea-ice thickness is reduced because of a more rapid decrease of thickness in summer. Maximum ice thickness happens in June and minimum ice thickness in October and November. In the ACCESS-CM2 model, the annual variation of ice thickness is substantial, but the regional difference is slight. ACCESS-CM2 model indicates the largest seasonal cycle amplitude in region2, and maximum sea-ice motion for region1,2 occurs in September, minimum occurs in March; for the central Arctic, maximum sea-ice motion occurs in August and minimum in May, its error is controlled within one month.

BCC-CSM2-MR constantly underestimates sea-ice thickness, but it has a good simulation of the ice thickness seasonal cycle. For sea-ice thickness, the BCC-CSM2-MR model indicates that Central Arctic > Laptev and the East Siberian Sea > Chukchi, and the Beaufort Sea, it doesn't cope with observation. For sea-ice motion, in summer, it simulates a slight regional difference, while in winter, there's an enormous regional difference. In the BCC-CSM2-MR model, the summer regional difference is more prominent than the winter. Maximum sea-ice thickness occurs in May, and minimum sea-ice thickness occurs in September and October. BCC-CSM2-MR model is an exception when simulating the trend of sea-ice motion, and there are slightly decreasing trend in region1 in summer which is far different from observation. In the GFDL-ESM4 model, the maximum sea-ice extent occurs in February, which is one month earlier than observation, and it slightly underestimates sea-ice extent except in autumn. GFDL-ESM4 model has a good simulation of sea-ice thickness. It indicates that peripheral sea ice melts faster than central Arctic ice, and ice thickness is higher in region1 than region2, which copes with observation.

MPI-ESM1-2-HR model is slightly overestimating sea-ice extent in May and June and underestimating sea-ice extent from July to December, and it is overestimating the decreasing trend of sea-ice extent. Before 2002, summer ice thickness is higher than winter; afterward, winter is higher than summer because of the rapid decrease in summer ice thickness. MPI-ESM1-2-HR model also shows higher ice thickness in region1 than region2, which comes with observation. MPI-ESM1-2-HR model vastly underestimates summer sea-ice motion, so in regions 1 and 3, winter sea-ice motion is higher than summer. In the winter months, there's a big regional difference. In the summer months, there's a slight regional difference.

Nor-ESM2-LM model has a good estimation for the magnitude of sea-ice extent, but it has a smaller seasonal cycle amplitude and a much lower decreasing rate. It also overestimated sea-ice thickness to a large extent and failed to simulate the correct seasonal cycle amplitude of sea-ice thickness. It has a maximum sea-ice thickness in August and a minimum sea-ice thickness in December. Summer has faster ice motion and is increasing faster than winter. region2 has the most rapidly increasing rate in sea-ice motion, and it has the biggest seasonal cycle amplitude.

To evaluate the simulation of selected CMIP6 models for sea-ice extent, Most of the selected models managed to simulate seasonal cycle and decreasing trend for sea-ice extent, while the NorESM2-LM model shows a way too slight decrease for sea-ice extent. For the magnitude of sea-ice extent, EC-Earth3 is generally overestimating sea-ice extent greatly, especially in winter; the BCC-CSM2-MR model underestimates sea-ice extent all year round. ACCESS-CM2, MPI-ESM1-2-HR, and NorESM2-LM models perform the best for at least four months when there's no significant difference

between the model and observation.

CMIP6 provides scattered model outputs for sea-ice thickness due to the high error of sea-ice thickness. Only GFDL-ESM4 and MPI-ESM1-2-HR models have no significant difference from observation in a certain amount of months. BCC-CSM2-MR underestimates sea-ice thickness, EC-Earth3, ACCESS-CM2, and NORESM2-LM models are highly overestimating sea-ice thickness, especially in summer. GFDL-ESM4 and MPI-ESM1-2-HR have the best performance at sea-ice thickness simulation.

For sea-ice motion, ACCESS-CM2 has a good simulation for regions 1 and 2. EC-Earth3 also has satisfying performance for the whole Arctic. BCC-CSM2-MR model underestimates sea-ice drifting speed in summer seasons in region1 and region2 while overestimating in many months in region3. MPI-ESM1-2-HR model overestimates sea-ice drifting speed all year round. ACCESS-CM2 model overestimates sea-ice drifting speed in summer for regions 1 and 2. In region3, the ACCESS-CM2 model mostly overestimates sea-ice motion except in winter months. NorESM2-LM model has the best performance overall, and ACCESS-CM2 has the second-best simulation for regions 1 and 2. EC-Earth3 also has a good simulation for sea-ice motion.

Bibliography

A. Adcroft, W. Anderson, V. Balaji, C. Blanton, M. Bushuk, C. O. Dufour, J. P. Dunne, S. M. Griffies, R. Hallberg, M. J. Harrison, I. M. Held, M. F. Jansen, J. G. John, J. P. Krasting, A. R. Langenhorst, S. Legg, Z. Liang, C. McHugh, A. Radhakrishnan, B. G. Reichl, T. Rosati, B. L. Samuels, A. Shao, R. Stouffer, M. Winton, A. T. Wittenberg, B. Xiang, N. Zadeh, and R. Zhang. The gfdl global ocean and sea ice model om4.0: Model description and simulation features. *Journal of Advances in Modeling Earth Systems*, 11(10):3167–3211, 2019. doi: https://doi.org/10.1029/2019MS001726. URL https://agupubs.onlinelibrary.wiley.com/doi/abs/10.1029/2019MS001726.

M. Ananicheva, T. Callaghan, D. Dahl-Jensen, S. Gerland, M. Granskog, G. Hovelsrud, M. Johansson, J. Key, W. Meier, M. Olsen, et al. Snow, water, ice and permafrost in the arctic (swipa): Climate change and the cryosphere. 2011.

A. Assur. *Composition of sea ice and its tensile strength*, volume 44. US Army Snow, Ice and Permafrost Research Establishment, 1960.

D. Bi, M. Dix, S. Marsland, S. Oâfarrell, A. Sullivan, R. Bodman, R. Law, I. Harman, J. Srbinovsky, H. A. Rashid, et al. Configuration and spin-up of access-cm2, the new generation australian community climate and earth system simulator coupled model. *Journal of Southern Hemisphere Earth Systems Science*, 70(1):225–251, 2020.

Y.-J. R. [Bing ZHOU, Ying XIAO. Simulation and projection of arctic sea ice and climate by bcc-csm2-mr. *Advances in Climate Change Research*, 17(1):58, 2021.

M. Dix, D. Bi, P. Dobrohotoff, R. Fiedler, I. Harman, R. Law, C. Mackallah, S. Marsland, S. O'Farrell, H. Rashid, J. Srbinovsky, A. Sullivan, C. Trenham, P. Vohralik, I. Watterson, G. Williams, M. Woodhouse, R. Bodman, F. B. Dias, C. M. Domingues, N. Hannah, A. Heerdegen, A. Savita, S. Wales, C. Allen, K. Druken, B. Evans, C. Richards, S. M. Ridzwan, D. Roberts, J. Smillie, K. Snow, M. Ward, and R. Yang. Csiro-arccss access-cm2 model output prepared for cmip6 cmip historical, 2019. URL https://doi.org/10.22033/ESGF/CMIP6.4271.

R. Döscher, M. Acosta, A. Alessandri, P. Anthoni, T. Arsouze, T. Bergman, R. Bernardello, S. Boussetta, L.-P. Caron, G. Carver, M. Castrillo, F. Catalano, I. Cvijanovic, P. Davini, E. Dekker, F. J. Doblas-Reyes, D. Docquier, P. Echevarria, U. Fladrich, R. Fuentes-Franco, M. Gröger, J. v. Hardenberg, J. Hieronymus, M. P. Karami, J.-P. Keskinen, T. Koenigk, R. Makkonen, F. Massonnet, M. Ménégoz, P. A. Miller, E. Moreno-Chamarro, L. Nieradzik, T. van Noije, P. Nolan, D. O'Donnell, P. Ollinaho, G. van den Oord, P. Ortega, O. T. Prims, A. Ramos, T. Reerink, C. Rousset, Y. Ruprich-Robert, P. Le Sager, T. Schmith, R. Schrödner, F. Serva, V. Sicardi, M. Sloth Madsen, B. Smith, T. Tian, E. Tourigny, P. Uotila, M. Vancoppenolle, S. Wang, D. Wårlind, U. Willén, K. Wyser, S. Yang, X. Yepes-Arbós, and Q. Zhang. The ec-earth3 earth system model for the coupled model intercomparison project 6. *Geoscientific Model Development*, 15(7):2973–3020, 2022a. doi: 10.5194/gmd-15-2973-2022. URL https://gmd.copernicus.org/articles/15/2973/2022/.

R. Döscher, M. Acosta, A. Alessandri, P. Anthoni, T. Arsouze, T. Bergman, R. Bernardello, S. Boussetta, L.-P. Caron, G. Carver, M. Castrillo, F. Catalano, I. Cvijanovic, P. Davini, E. Dekker, F. J. Doblas-Reyes, D. Docquier, P. Echevarria, U. Fladrich, R. Fuentes-Franco, M. Gröger, J. v. Hardenberg, J. Hieronymus, M. P. Karami, J.-P. Keskinen, T. Koenigk, R. Makkonen, F. Massonnet, M. Ménégoz, P. A. Miller, E. Moreno-Chamarro, L. Nieradzik, T. van Noije, P. Nolan, D. O'Donnell, P. Ollinaho, G. van den Oord, P. Ortega, O. T. Prims, A. Ramos, T. Reerink, C. Rousset, Y. Ruprich-Robert, P. Le Sager, T. Schmith, R. Schrödner, F. Serva, V. Sicardi, M. Sloth Madsen, B. Smith, T. Tian, E. Tourigny, P. Uotila, M. Vancoppenolle, S. Wang, D. Wårlind, U. Willén, K. Wyser, S. Yang, X. Yepes-Arbós, and Q. Zhang. The ec-earth3 earth system model for the coupled model intercomparison project 6. *Geoscientific Model Development*, 15(7):2973–3020, 2022b. doi: 10.5194/gmd-15-2973-2022. URL https://gmd.copernicus.org/articles/15/2973/2022/.

ECMWF. Sea ice thickness climate data record (cdr), 2015. URL DOI:10.24381/cds.6679a99a. sea ice thickness observation data.

ESGF. arth system grid federation), 2022. URL https://esgf-node.llnl.gov/projects/cmip6/. ESGF.

S. Forsstrom, S. Gerland, and C. A. Pedersen. Thickness and density of snow-covered sea ice and hydrostatic equilibrium assumption from in situ measurements in fram strait, the barents sea and the svalbard coast. *Annals of Glaciology*, 52(57):261â270, 2011. doi: 10.3189/172756411795931598.

O. Gutjahr, D. Putrasahan, K. Lohmann, J. H. Jungclaus, J.-S. von Storch, N. Brüggemann, H. Haak, and A. Stössel. Max planck institute earth system model (mpi-esm1.2) for the high-resolution model intercomparison project (high-resmip). *Geoscientific Model Development*, 12(7):3241–3281, 2019a. doi: 10.5194/gmd-12-3241-2019. URL https://gmd.copernicus.org/articles/12/3241/2019/.

O. Gutjahr, D. Putrasahan, K. Lohmann, J. H. Jungclaus, J.-S. von Storch, N. Brüggemann, H. Haak, and A. Stössel. Max planck institute earth system model (mpi-esm1.2) for the high-resolution model intercomparison project (high-resmip). *Geoscientific Model Development*, 12(7):3241–3281, 2019b. doi: 10.5194/gmd-12-3241-2019. URL https://gmd.copernicus.org/articles/12/3241/2019/.

C. Haas. *Sea ice thickness distribution*, chapter 2, pages 42–64. John Wiley Sons, Ltd, 2017. ISBN 9781118778371. doi: https://doi.org/10.1002/9781118778371.ch2. URL https://onlinelibrary.wiley.com/doi/abs/10.1002/9781118778371.ch2.

E. Hansen, S. Gerland, M. A. Granskog, O. Pavlova, A. H. H. Renner, J. Haapala, T. B. LÃžyning, and M. Tschudi. Thinning of arctic sea ice observed in fram strait: 1990â2011. *Journal of Geophysical Research: Oceans*, 118(10):5202–5221, 2013. doi: https://doi.org/10.1002/jgrc.20393. URL https://agupubs.onlinelibrary.wiley.com/doi/abs/10.1002/jgrc.20393.

E. C. Hunke, D. A. Hebert, and O. Lecomte. Level-ice melt ponds in the los alamos sea ice model, cice. *Ocean Modelling*, 71:26–42, 2013. ISSN 1463-5003. doi: https://doi.org/10.1016/j.ocemod.2012.11.008. URL https://www.sciencedirect.com/science/article/pii/S1463500312001680. Arctic Ocean.

W. III. A dynamic thermodynamic sea ice model. *Journal of Physical Oceanography - J PHYS OCEANOGR*, 9:815–846, 07 1979. doi: 10.1175/1520-0485(1979)009<0815:ADTSIM>2.0.CO;2.

J. Jungclaus, M. Bittner, K.-H. Wieners, F. Wachsmann, M. Schupfner, S. Legutke, M. Giorgetta, C. Reick, V. Gayler, H. Haak, P. de Vrese, T. Raddatz, M. Esch, T. Mauritsen, J.-S. von Storch, J. Behrens, V. Brovkin, M. Claussen, T. Crueger, I. Fast, S. Fiedler, S. Hagemann, C. Hohenegger, T. Jahns, S. Kloster, S. Kinne, G. Lasslop, L. Kornblueh, J. Marotzke, D. Matei, K. Meraner, U. Mikolajewicz, K. Modali, W. Müller, J. Nabel, D. Notz, K. Peters-von Gehlen, R. Pincus, H. Pohlmann, J. Pongratz, S. Rast, H. Schmidt, R. Schnur, U. Schulzweida, K. Six,

B. Stevens, A. Voigt, and E. Roeckner. Mpi-m mpi-esm1.2-hr model output prepared for cmip6 cmip historical, 2019. URL https://doi.org/10.22033/ESGF/CMIP6.6594.

S. Kern, T. Lavergne, D. Notz, L. T. Pedersen, R. T. Tonboe, R. Saldo, and A. M. Sørensen. Satellite passive microwave sea-ice concentration data set intercomparison: closed ice and ship-based observations. *The Cryosphere*, 13(12):3261–3307, 2019.

T. Koenigk and E. Dekker. Sea ice representation in CMIP6 simulations with EC-Earth3-Veg. In *EGU General Assembly Conference Abstracts*, EGU General Assembly Conference Abstracts, page 20372, May 2020. doi: 10.5194/egusphere-egu2020-20372.

J. P. Krasting, J. G. John, C. Blanton, C. McHugh, S. Nikonov, A. Radhakrishnan, K. Rand, N. T. Zadeh, V. Balaji, J. Durachta, C. Dupuis, R. Menzel, T. Robinson, S. Underwood, H. Vahlenkamp, K. A. Dunne, P. P. Gauthier, P. Ginoux, S. M. Griffies, R. Hallberg, M. Harrison, W. Hurlin, S. Malyshev, V. Naik, F. Paulot, D. J. Paynter, J. Ploshay, B. G. Reichl, D. M. Schwarzkopf, C. J. Seman, L. Silvers, B. Wyman, Y. Zeng, A. Adcroft, J. P. Dunne, R. Dussin, H. Guo, J. He, I. M. Held, L. W. Horowitz, P. Lin, P. Milly, E. Shevliakova, C. Stock, M. Winton, A. T. Wittenberg, Y. Xie, and M. Zhao. Noaa-gfdl gfdl-esm4 model output prepared for cmip6 cmip historical, 2018. URL https://doi.org/10.22033/ESGF/CMIP6.8597.

R. Kwok, G. Spreen, and S. Pang. Arctic sea ice circulation and drift speed: Decadal trends and ocean currents. *Journal of Geophysical Research: Oceans*, 118(5):2408–2425, 2013. doi: https://doi.org/10.1002/jgrc.20191. URL https://agupubs.onlinelibrary.wiley.com/doi/abs/10.1002/jgrc.20191.

S. Laxon, N. Peacock, and D. Smith. High interannual variability of sea ice thickness in the arctic region. *Nature*, 425(6961):947–950, 2003.

O. Lecomte, T. Fichefet, M. Vancoppenolle, F. Domine, F. Massonnet, P. Mathiot, S. Morin, and P. Barriat. On the formulation of snow thermal conductivity in large-scale sea ice models. *Journal of Advances in Modeling Earth Systems*, 5(3):542–557, 2013. doi: https://doi.org/10.1002/jame.20039. URL https://agupubs.onlinelibrary.wiley.com/doi/abs/10.1002/jame.20039.

M. Lepparanta. *The Drift of Sea Ice*. Geophysical Sciences. Springer Berlin Heidelberg, Berlin, Heidelberg, 2nd ed. 2011. edition, 2011. ISBN 1-283-08281-0.

K. Maeda, N. Kimura, and H. Yamaguchi. Temporal and spatial change in the relationship between sea-ice motion and wind in the arctic. *Polar Research*, 39, Nov.

2020. doi: 10.33265/polar.v39.3370. URL https://polarresearch.net/index.php/polar/article/view/3370.

W. N. Meier, J. Stroeve, and F. Fetterer. Whither arctic sea ice? a clear signal of decline regionally, seasonally and extending beyond the satellite record. *Annals of Glaciology*, 46:428â434, 2007. doi: 10.3189/172756407782871170.

W. N. Meier, G. K. Hovelsrud, B. E. van Oort, J. R. Key, K. M. Kovacs, C. Michel, C. Haas, M. A. Granskog, S. Gerland, D. K. Perovich, A. Makshtas, and J. D. Reist. Arctic sea ice in transformation: A review of recent observed changes and impacts on biology and human activity. *Reviews of Geophysics*, 52(3):185–217, 2014. doi: https://doi.org/10.1002/2013RG000431. URL https://agupubs.onlinelibrary.wiley.com/doi/abs/10.1002/2013RG000431.

J. Mingle. Ipcc special report on the ocean and cryosphere in a changing climate, 2020.

D. Notz and S. Community. Arctic sea ice in cmip6. *Geophysical Research Letters*, 47(10):e2019GL086749, 2020. doi: https://doi.org/10.1029/2019GL086749. URL https://agupubs.onlinelibrary.wiley.com/doi/abs/10.1029/2019GL086749. e2019GL086749 10.1029/2019GL086749.

A. Oikkonen and J. Haapala. Variability and changes of arctic sea ice draft distribution ndash; submarine sonar measurements revisited. *The Cryosphere*, 5(4):917–929, 2011. doi: 10.5194/tc-5-917-2011. URL https://tc.copernicus.org/articles/5/917/2011/.

R. G. J. M. Parodi-Perdomo, Jose Antonio. Ec-earth-consortium ec-earth3 model output prepared for cmip6 cmip historical, 2019. URL https://doi.org/10.22033/ESGF/CMIP6.4700.

C. A. Pedersen, E. Roeckner, M. LÃŒthje, and J.-G. Winther. A new sea ice albedo scheme including melt ponds for echam5 general circulation model. *Journal of Geophysical Research: Atmospheres*, 114(D8), 2009. doi: https://doi.org/10.1029/2008JD010440. URL https://agupubs.onlinelibrary.wiley.com/doi/abs/10.1029/2008JD010440.

D. Perovich, W. Meier, M. Tschudi, S. Hendricks, A. Petty, D. Divine, S. Farrell, S. Gerland, C. Haas, L. Kaleschke, et al. Arctic report card 2020: Sea ice. 2020.

P. Rampal, J. Weiss, and D. Marsan. Evidence for significant acceleration of arctic sea ice drift over the last 25 years. *AGU Fall Meeting Abstracts*, 12 2007.

P. Rampal, J. Weiss, and D. Marsan. Positive trend in the mean speed and deformation rate of arctic sea ice, 1979â2007. *Journal of Geophysical Research: Oceans*, 114 (C5), 2009a. doi: https://doi.org/10.1029/2008JC005066. URL https://agupubs.onlinelibrary.wiley.com/doi/abs/10.1029/2008JC005066.

P. Rampal, J. Weiss, and D. Marsan. Positive trend in the mean speed and deformation rate of arctic sea ice, 1979–2007. *Journal of Geophysical Research: Oceans*, 114(C5), 2009b.

I. Rigor. Iabp drifting buoy pressure, temperature, position, and interpolated ice velocity, version 1 (g00791), 2017. URL ftp://iabp.apl.washington.edu/pub/IABP/C. IABP.

Ø. Seland, M. Bentsen, D. Olivié, T. Toniazzo, A. Gjermundsen, L. S. Graff, J. B. Debernard, A. K. Gupta, Y.-C. He, A. Kirkevåg, J. Schwinger, J. Tjiputra, K. S. Aas, I. Bethke, Y. Fan, J. Griesfeller, A. Grini, C. Guo, M. Ilicak, I. H. H. Karset, O. Landgren, J. Liakka, K. O. Moseid, A. Nummelin, C. Spensberger, H. Tang, Z. Zhang, C. Heinze, T. Iversen, and M. Schulz. Overview of the norwegian earth system model (noresm2) and key climate response of cmip6 deck, historical, and scenario simulations. *Geoscientific Model Development*, 13(12):6165–6200, 2020. doi: 10.5194/gmd-13-6165-2020. URL https://gmd.copernicus.org/articles/13/6165/2020/.

y. Seland, M. Bentsen, D. J. L. Oliviè, T. Toniazzo, A. Gjermundsen, L. S. Graff, J. B. Debernard, A. K. Gupta, Y. He, A. Kirkevåg, J. Schwinger, J. Tjiputra, K. S. Aas, I. Bethke, Y. Fan, J. Griesfeller, A. Grini, C. Guo, M. Ilicak, I. H. H. Karset, O. A. Landgren, J. Liakka, K. O. Moseid, A. Nummelin, C. Spensberger, H. Tang, Z. Zhang, C. Heinze, T. Iversen, and M. Schulz. Ncc noresm2-lm model output prepared for cmip6 cmip historical, 2019. URL https://doi.org/10.22033/ESGF/CMIP6.8036.

A. J. Semtner Jr. A model for the thermodynamic growth of sea ice in numerical investigations of climate. *Journal of Physical Oceanography*, 6(3):379–389, 1976.

Q. Shu, Q. Wang, Z. Song, F. Qiao, J. Zhao, M. Chu, and X. Li. Assessment of sea ice extent in cmip6 with comparison to observations and cmip5. *Geophysical Research Letters*, 47(9):e2020GL087965, 2020. doi: https://doi.org/10.1029/2020GL087965. URL https://agupubs.onlinelibrary.wiley.com/doi/abs/10.1029/2020GL087965. e2020GL087965 2020GL087965.

L. H. Smedsrud, A. Sirevaag, K. Kloster, A. Sorteberg, and S. Sandven. Recent wind driven high sea ice area export in the fram strait contributes to arctic sea ice decline.

The Cryosphere, 5(4):821–829, 2011. doi: 10.5194/tc-5-821-2011. URL https://tc.copernicus.org/articles/5/821/2011/.

D. Thomas. The quality of sea ice velocity estimates. *Journal of Geophysical Research: Oceans*, 104(C6):13627–13652, 1999. doi: https://doi.org/10.1029/1999JC900086. URL https://agupubs.onlinelibrary.wiley.com/doi/abs/10.1029/1999JC900086.

A. K. Turner and E. C. Hunke. Impacts of a mushy-layer thermodynamic approach in global sea-ice simulations using the cice sea-ice model. *Journal of Geophysical Research: Oceans*, 120(2):1253–1275, 2015. doi: https://doi.org/10.1002/2014JC010358. URL https://agupubs.onlinelibrary.wiley.com/doi/abs/10.1002/2014JC010358.

T. Vihma and J. Haapala. Geophysics of sea ice in the baltic sea: A review. *Progress in Oceanography*, 80(3-4):129–148, 2009.

J. E. Walsh, F. Fetterer, J. S. stewart, and W. L. Chapman. A database for depicting arctic sea ice variations back to 1850. *Geographical Review*, 107(1):89–107, 2017. doi: 10.1111/j.1931-0846.2016.12195.x. URL https://doi.org/10.1111/j.1931-0846.2016.12195.x.

M. Watts, W. Maslowski, Y. J. Lee, J. C. Kinney, and R. Osinski. A spatial evaluation of arctic sea ice and regional limitations in cmip6 historical simulations. *Journal of Climate*, 34(15):6399 – 6420, 2021. doi: 10.1175/JCLI-D-20-0491.1. URL https://journals.ametsoc.org/view/journals/clim/34/15/JCLI-D-20-0491.1.xml.

T. Wu, M. Chu, M. Dong, Y. Fang, W. Jie, J. Li, W. Li, Q. Liu, X. Shi, X. Xin, J. Yan, F. Zhang, J. Zhang, L. Zhang, and Y. Zhang. Bcc bcc-csm2mr model output prepared for cmip6 cmip historical, 2018. URL https://doi.org/10.22033/ESGF/CMIP6.2948.

F. Zhang, X. Pang, R. Lei, M. Zhai, X. Zhao, and Q. Cai. Arctic sea ice motion change and response to atmospheric forcing between 1979 and 2019. *International Journal of Climatology*, 42(3):1854–1876, 2022. doi: https://doi.org/10.1002/joc.7340. URL https://rmets.onlinelibrary.wiley.com/doi/abs/10.1002/joc.7340.

M. Zygmuntowska, P. Rampal, N. Ivanova, and L. H. Smedsrud. Uncertainties in arctic sea ice thickness and volume: new estimates and implications for trends. *The Cryosphere*, 8(2):705–720, 2014. doi: 10.5194/tc-8-705-2014. URL https://tc.copernicus.org/articles/8/705/2014/.